SOL-GEL PROCESSING OF BIOACTIVE GLASS POWDERS

BY

ROUNAN LI

A DISSERTATION PRESENTED TO THE GRADUATE SCHOOL
OF THE UNIVERSITY OF FLORIDA IN PARTIAL FULFILLMENT
OF THE REQUIREMENTS FOR THE DEGREE OF
DOCTOR OF PHILOSOPHY

UNIVERSITY OF FLORIDA

1991

Dedicated to My Family

ACKNOWLEDGMENTS

The author wishes to express her sincere gratitude to Dr. Larry L. Hench, supervisory committee chairman and teacher, for his encouragement and assistance through the course of this study. A special thank you as well goes to Dr. A.E. Clark for his advice and support.

She also wishes to extend thanks to the members of her committee, Dr. R.T. DeHoff, Dr. E.D. Whitney, Dr. C.J. Vierck and Dr. P.H. Holloway, for their patience and useful comments. Special thanks goes to Dr. J.K. West for his cheerfulness and motivation during this research. In addition, thanks are extended to Guy P. Latorre and A. Barrett for their assistance in the laboratory.

TABLE OF CONTENTS

LIST OF TABLES

LIST OF FIGURES

SOL-GEL PROCESSING OF BIOACTIVE GLASS POWDERS

BY

Rounan Li

August 1991

A series of glass powders in the $CaO-P_2O_5-SiO_2$ system were successfully produced by sol-gel processing, an alternative to the conventional melt processing of bioactive glass and glass-ceramics with remarkable advantages of high purity and high homogeneity as well as low processing temperature.

Characterization of gel-derived powders before and after in-vitro testing was conducted using FTIR reflection spectroscopy, X-ray diffraction analysis, inductively coupled plasma (ICP) analysis, thermal analysis and nitrogen absorption BET.

Most gel-derived powders before in-vitro testing were amorphous and porous with a large surface area, ranging from 200 to 650 m^2/g. Surface area increased with increasing SiO_2 content (50 mol.% to 90 mol.%) in the compositions and could also be controlled by heat treatment temperature.

By defining bioactivity as the ability of materials to

form a surface hydroxyapatite (HA) layer in a simulated body environment, the in-vitro tests indicated that all the gel-derived powders with different compositions were bioactive. Compositions with up to 70 mol.% SiO_2 showed higher rates of formation of HA in the tris-buffered in-vitro solutions than melt-derived Bioglasses®. The bioactivity generally increased with decreasing SiO_2 content. However, gel-derived powders containing as high as 90 mol.% SiO_2 in composition still showed the formation of a hydroxyapatite surface layer within 7 days at 37°C, whereas the SiO_2 compositional boundary of bioactivity of conventional melt-derived bioactive glass and glass-ceramics never exceeds 60 mol.%. Thus, the SiO_2 compositional boundary for bioactivity is extended significantly from 60 mol.% up to 90 mol.% by using sol-gel technology.

The texture, especially the surface area, has an important role in developing the bioactive surface HA layer. The enhanced bioactivity and the extended compositional region of bioactivity appears to be due to the increased density of nucleation sites for crystallization of hydroxyapatite on the SiO_2-rich surface of the sol-gel derived bioactive glass powders.

CHAPTER I
INTRODUCTION

1.1 Implant Materials

A biomaterial is a nonviable material used in or as a medical device, intended to interact with biological systems [1]. Biomaterials may be distinguished from other materials in that they possess a combination of properties, including chemical, mechanical, physical and biological properties that render them suitable for safe, effective and reliable use within a physiological environment, an environment that is both extremely hostile and sensitive to foreign bodies. At present, there are as many as 50 different materials used in the 40 different medical and dental devices developed for replacement or repair of tissues or organs of the body [2].

Biomaterials used in implantable devices are metals, polymers and glass, glass-ceramics or ceramics [3-4]. Even though metals and polymers are widely used in maxillofacial and orthopaedic applications, success with these types of the materials has limits, especially in long-term, >20 years, applications. It is not only because these materials may elicit certain undesirable responses, such as metal sensitivity, but also some degree of motion may occur at the

1

nonadherent implant-tissue interface, which will eventually lead to interface deterioration. The resulting pain can force surgical removal. Sufficient movement can lead to implant failure or bone fracture. As a result of this situation, numerous investigations have been initiated to find a material which will firmly adhere to bone.

One approach has involved the use of porous metallic implants. The concept involves bone ingrowth into a porous surface which could provide mechanical interlocking. The mechanical load is distributed over a wide area, reducing the chance of bone necrosis due to stress concentration at local sites [5-8]. The use of porous metal surfaces to anchor prosthetic devices to bone seems promising. One of the major points which remains to be shown is the effect of the increase in surface area associated with a porous surface and the resulting corrosion which could occur over long periods of time.

Another approach to improve stability of the biomaterial-tissue interface involves the use of inert porous ceramic materials. Due to their highly oxidized state, ceramics are inert materials capable of resisting degradation in severe environments [9]. The concept behind inert porous ceramics is the ingrowth of tissue into pores on the surface or throughout the implant [10]. The interface is established by the living tissue in the pores. The increased interfacial

area between the implant and the tissue results in an increased inertial resistance to movement of the device in the tissue. One of these attempts involved the use of a slip cast mixture of alumina, calcium carbonate, silica and magnesium carbonate, so-called Cerosium [11]. Evaluation of this material revealed little bone ingrowth into the pores. This was attributed to a small pore size. Studies show that when pore sizes exceed 100 μm, bone will grow within the interconnecting pore channels near the surface and maintain its vascularity and long-term viability [12-13]. In this manner, the implant serves as a structural bridge and model or scaffold for bone formation. The microstructure of certain corals makes an almost ideal investment material for the casting of structures with highly controlled pore sizes. A replamineform process to duplicate the porous microstructure of corals that have a high degree of uniform pore size and interconnection was developed [14]. The first step is to machine the coral with proper microstructure into the desired shape. The machined coral shape is then fired to remove CO_2 from the limestone, forming CaO while maintaining the microstructure of the original coral. The CaO structure serves as an investment material for forming the porous material. After the desired material is cast into the pores, the CaO is easily removed from the material by dissolving in dilute HCl. The most promising coral genus, Porites, has

pores with a size range of 140-160 μm, with all the pores interconnected [12]. Replamineform porous materials of $\alpha-Al_2O_3$, TiO_2 and calcium phosphates have been used as bone implants with the calcium phosphates being the most acceptable [15].

Materials such as Al_2O_3 may also be made by using suitable foaming agent that evolves gases during heating. Porous alumina and calcium aluminates were produced by mixing powdered $CaCO_3$ with fine Al_2O_3 powder, firing at 1450-1500°C for about 20 hours. In this manner, a foamed material with pore size determined by the original $CaCO_3$ particles was produced [16].

Porous materials are weaker than the equivalent bulk form in proportion to the percentage of porosity. As the porosity increases, the strength of the material decreases rapidly. Much surface area is also exposed so that the effects of the environment on decreasing strength become more important. Aging of porous materials, with their subsequent decrease in strength, poses problems as to the long-term application of porous materials unless they are designed to be resorbable.

Resorbable biomaterials are designed to degrade gradually over a period of time and be replaced by the natural host tissue [17]. Because large quantities of material may be replaced, it is also essential that a

resorbable biomaterial consists only of metabolically acceptable substances. This criterion imposes considerable limitations on the compositional design of resorbable materials. Successful materials are porous or particulate calcium phosphate ceramic materials for hard tissue replacement [18].

A completely unique approach to the problem of permanent fixation is the use of bioactive materials. A bioactive material is one that elicits a specific biological response at the interface of the material which results in the formation of a bond between the tissues and the material. This subject was initiated by L.L. Hench and colleagues in the late 1960s and early 1970s [19-27]. They discovered that certain compositions of glasses (Bioglasses®) could bond with bone when implanted. Later work by Wilson and Nolletti showed that certain compositions of the bioactive glasses also bond to soft tissues [28]. The concept of bioactive bonding involves the use of controlled surface reactions to achieve a chemical attachment to tissues. This material shows 1) no local or systemic toxicity, 2) no long-term inflammatory or foreign body response, 3) bonding to hard and soft tissue without an intervening fibrous capsule, and 4) a good surgical handling ability.

® Registered trademark, University of Florida, Gainesville, FL 32611.

The mechanism of tissue attachment is directly related to the type of tissue response at the implant interface. It is now well established that no implant material is truly inert in the living body; all materials elicit a response from host tissues. If the material is toxic, the surrounding tissue dies; if the material is nontoxic and dissolves, tissue replaces it; if the material is nontoxic and biologically inactive, a fibrous tissue capsule of variable thickness forms; and if the material is nontoxic and biologically active, an interfacial bond can form between the material and the surrounding tissues [29-30]. Bioglass$^{®}$ implants falls into the last category. The controlled surface reactivity of these Bioglass$^{®}$ implants allows the bonding of the materials to living bone.

The bonding to bone has been associated with the formation of a hydroxyapatite (HA) layer on the surface of the glasses. It has also been shown that an even narrower range of glass compositions can bond to soft tissues [31-32]. A characteristic of the soft-tissue bonding compositions is a very rapid rate of HA formation. This has been previously attributed to the presence of Na_2O in the glass composition which increases the solution pH at the implant-tissue interface and thereby enhances the precipitation and crystallization of HA [33]. The rate of HA formation has also been shown to be very strongly dependent on the ratio of

SiO_2, glass network former, to Na_2O, network modifier, in the glass [34]. When the glass composition contains 60% SiO_2, or more, bonding to tissues is no longer observed [35].

Further experiments revealed a considerable range of chemical composition of glasses or glass-ceramics which allow bone-bonding to the implant interface. These include a Ceravital®-type glass-ceramics which contain only apatite as the crystalline phase [36-37] and A-W bioactive glass-ceramics which contain apatite and wollastonite crystalline phases in a $MgO-CaO-SiO_2-P_2O_5$ system [38-40]. Figure 1.1 shows the bone-bonding boundaries of all the bioactive glasses and glass-ceramics in the $Na_2O-CaO-SiO_2$ system (with a constant 6 wt% P_2O_5). Inside the bioactive boundary (region A), the glass and glass-ceramics develop HA on the surface both in-vitro and in-vivo and bond with bone. Outside the boundary, the materials are either inert (region B) or of a resorbable type (region C). Region D is a non-glass-forming and nonbonding region. Bioactive glass-ceramics Ceravital® and A-W glass-ceramics are shown in Figure 1.1. However, note that the Ceravital® and A-W contain crystalline phases and a glassy matrix. Also, the A-W contains more P_2O_5 than the other compositions in the figure. The relationships illustrated   in   the   figure   are   only

---

® Trademark, Leitz Corp. West Germany.
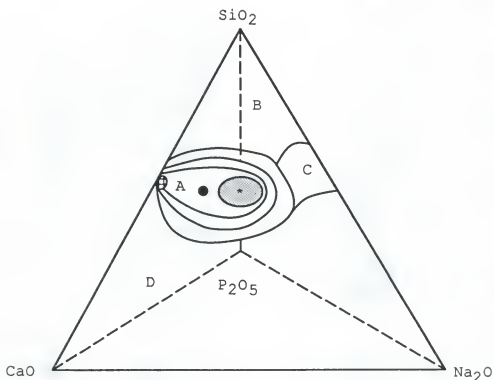
Bioactive Bonding Boundaries

A Bonding at 30 days or less
B Nonbonding, reactivity is too low
C Nonbonding, reactivity is too high
D Nonbonding, nonglass forming

*   Bioglass ® 45S5
●   Ceravital ®
⊕   A/W Glass-ceramics
     (Larger P_2O_5 content)
▨   Soft Tissue Bonding

Figure 1.1 Bioglass bone bonding composition diagram
       (with 6 wt % P_2O_5).

qualitative comparisons. It has to be emphasized that all these bioactive glasses or glass-ceramics have a SiO_2 content less than 60%. The bone-bonding mechanism on the Ceravital®-type material was explained on the basis of dissolution of the apatite and phagocytosis of the glassy matrix by macrophages [41-42], while the A-W bioactive glass-ceramics form a thin layer of carbonate containing hydroxyapatite on their surface [43]. However, specific features of bone-bonding mechanisms of bioactive glasses and glass-ceramics are not yet clear.

Since the discovery of Bioglass®, many different bioglass applications have been explored. These include many in hard tissues, such as coatings of Bioglass® on orthopaedic devices (total hip arthroplasties), devices for use in maxillofacial and middle ear applications and dental ridge maintenance applications [44-46].

The bioactive glass, in powder or paste form, has a very large potential use as well. These powders in particle range of 100 to 500 μm can be used not only to augment, but also regenerate the body's hard tissues. They can be directly placed in bone-deficient areas and can be also mixed with various types of collagen or resorbable polymer carrier system to form pastes that can be then molded into the deficiency. These powders and pastes can fill in irregular bony wounds and spaces as a putty or by injection, whereas

bulk materials would need to be either clinically shaped or preclinically shaped with the aid of a computer [47-49]. These powders can fill irregular shaped bony defects caused by local or systemic disease, congenital malformations or trauma. Several clinical applications, such as treatment of periodontal lesions [50] or urinary incontinence [51], of bioactive glass powders are already in trial.

1.2 Melt Processing and Sol-Gel Processing

Up to present time, bioactive glass powders have been produced using conventional glass technology. The glass components in the form of grains of oxides or carbonates are mixed in a platinum crucible and then melted and homogenized at high temperatures, 1250°C-1400°C. Powders are made by pouring glass into a liquid medium, such as water, fracturing the frozen glass into small fragments, called a frit. Subsequent grinding and size separation steps are necessary to achieve powders with a specific size range, such as 90μm to 710μm, required for periodontal treatment. The flowchart of melting method is schematically illustrated in Figure 1.2, column A.

There are several disadvantages of these conventional glass processing methods for bioactive glasses:

(A)   (B)

TRADITIONAL MELT PROCESSING   SOL-GEL PROCESSING
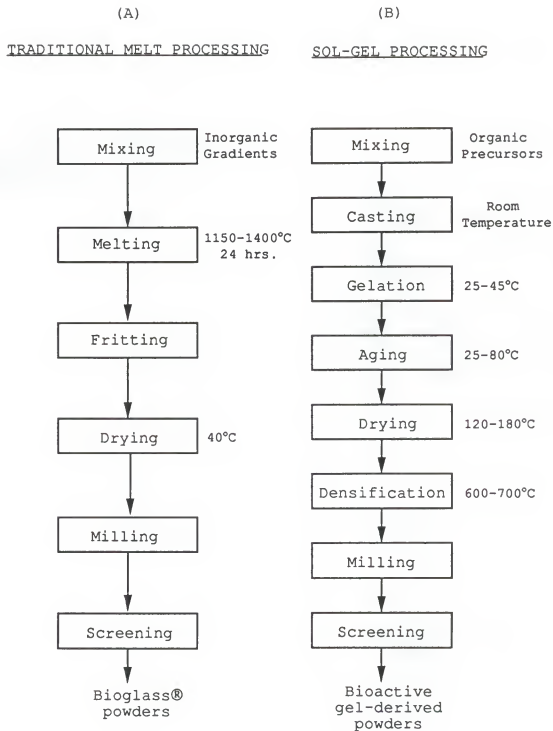
Figure 1.2   Schematic illustration of melting
             method and sol-gel method of preparing
             bioactive glasses

1) It is difficult to maintain the very high purity required for optimal bioactivity. This is primarily because of the high temperatures associated with melting and homogenization, but is also related to the low silica and high alkali content of the traditional bioactive glass compositions. These compositions are very reactive chemically and tend to dissolve even platinum and can easily pick up other multiple valence cations as impurities. It has been shown that impurities could reduce or totally eliminate the bioactivity of the bioceramics. Gross and Strunz [52] have shown how sensitive tissue bonding is to M^{+3}, M^{+4}, and M^{+5} impurity cations in bioactive glass-ceramics. Greenspan and Hench [53] have shown that a small amount of Al^{+3} can completely eliminate bone bonding for bioactive glasses. Recently Kitsugi and colleagues [54] and Kokubo and coworkers [39] have shown similar compositional sensitivities in other bioactive glass and glass-ceramic systems.

2) Process steps of grinding, polishing, fritting, sieving, etc. all expose a bioactive powder to potential contaminants and the negative effects on bioactivity described above.

3) There is a compositional limitation imposed on bioactive glasses and glass-ceramics made by conventional high temperature processes. This is due to the extremely high equilibrium liquidus temperature of SiO_2, $1713^{\circ}C$, and the

extremely high viscosity of silicate melts with high SiO_2 content.

4) High temperature processing in platinum crucibles and multiple handling steps also increase production costs considerably. The additional costs are not only in energy, but also in capital equipment, labor, maintenance, quality assurance and quality control etc. Lowering the processing temperature lowers such costs considerably.

Low temperature sol-gel processing offers an alternative to conventional glass and glass-ceramic processing with the potential advantages indicated above. There is also the exciting possibility of achieving new compositional ranges of bioactive glass or glass-ceramics by use of this low temperature chemical processing.

Research of the sol-gel process has become a widely spread field during the last decade [55-57]. The scientific understanding of this chemical processing of ceramics, glasses and composites has matured and several applications have reached commercialization. Sol-gel processing is now successfully used for films, powders, fibers, and even for as-cast net shape precision optical components [58]. These new materials take advantage of the intermediate ultraporous state of gel processing. As summarized in Figure 1.2, column B, the chemical processing schedule used has six processing steps which lead to ultraporous materials, without going to

the seventh, full densification stage. Stabilization temperatures of pure silica components used for optics range from 650°C to 1000°C depending on pore size. In contrast, the multicomponent biogel-glass systems are stabilized at lower temperatures of 600°C to 700°C.

Basically, the sol-gel process involves the synthesis of an inorganic network by mixing the metal alkoxides in solution, followed by hydrolysis, gelation and low temperature firing to produce a material. The sequences of sol-gel processing and melt processing are in the Figure 1.3. In sol-gel processing, the alkoxides are mixed in water, followed by casting, gelation, aging, drying and densification at a relatively low temperatures. Inherent in this process is the ability to modify the network structure through controlled hydrolysis and polycondensation reactions [59-60]. Thus, structural variation can be produced without compositional changes. Since the material can be prepared from gels by sintering at relatively low temperatures (600°C-700°C), most of the disadvantages of high temperature processing can be eliminated with much higher control over purity. Also, sol-gel processing offers potential advantages of ease of powder production, a broader range of bioactivity, and a better control of bioactivity by changing either the composition or the microstructure through processing parameters.

Relative Time
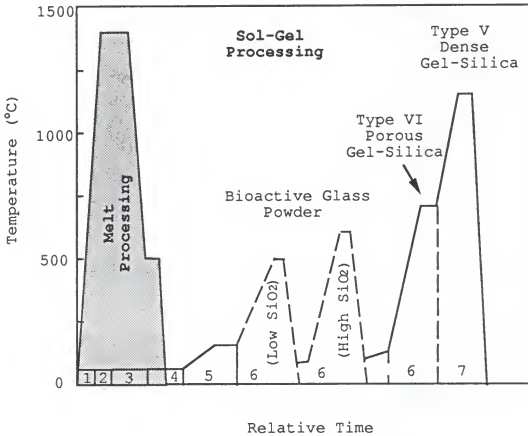
Figure 1.3 Sol-gel processing sequence.
            1.mixing, 2.casting,3.gelation, 4.aging,
            5.drying, 6.stabilization 7.densification.

1.3 Objectives

The purpose of this work is to develop a reliable method for preparing the bioactive gel-glass powders in the $CaO-P_2O_5-SiO_2$ system via a sol-gel route and to study a series of gel-derived powders with the intent of developing an understanding of the characteristic features that control rate of hydroxyapatite formation in-vitro and thereby bioactivity of the powders.

A general overview of implant materials and the sol-gel method has been described in the previous section. Chapter II reviews the literature of bioactive glasses and glass-ceramics, their bioactivities, both in-vitro and in-vivo studies and their compositional range in bonding with tissues. The literature reviews also include sol-gel processing in more detail. The methods employed in this study for the preparation of the bioactive gel-derived powders, the in-vitro testing and the experimental technique used for characterization are described in Chapter III. The measured features of gel-derived powders are reported in Chapter IV. In Chapter V, some techniques such as infrared reflection spectroscopy and X-ray diffraction technique along with several other tools have been employed to examine the in-vitro response of gel-derived powders to an aqueous

environment maintained at physiologic temperature and pH. Variables affecting bioactivity of these powders, the compositional effects and the structural effects are presented in Chapter VI. Chapter VII is a summary of the study and further discussion of the bioactivity of the materials in terms of surface chemistry and a comparison of melt-derived glass powders and the gel-derived glass powders, with the intent to identify the possible mechanisms of HA nucleation and growth on the surface of the powders. The general conclusions of this study are given in Chapter VIII.

CHAPTER II
LITERATURE REVIEW

2.1 Bioactive Glasses and Glass-Ceramics

2.1.1 Introduction

It is well documented that certain compositions of glasses and glass-ceramics bond to hard and soft tissues [2,28,34,61]. As a group, these materials are often referred to as "bioactive" [34,61]. At a Consensus Conference of the European Society for Biomaterials, England, 1986, a bioactive materials was defined as "a material which has been designed to induce specific biological activity" [62, p. 66]. Hench has proposed a definition that is more functional and capable of being measured quantitatively; "Bioactivity is the characteristic of an implant material which allows it to form a bond with living tissues" [34, p. 54]. While defining the precise magnitude of bonded implant strengths has proven to be difficult, the distinction between a bonded versus a non-bonded implant is clear cut.

The concept of a bioactive synthetic material capable of bonding with tissues originated in the work of Hench and

18

coworkers in the late 60s [63]. These pioneering efforts focused on the SiO_2-P_2O_5-CaO-Na_2O system. In-vitro studies demonstrated that in simulated physiologic solutions, specific compositions developed dual surface films consisting of a silica-rich layer and a calcium phosphate-rich layer [33,64-65]. The silica-rich layer formed at the glass interface and was coated with the calcium phosphate layer at the solution interface. Studies show that the glass composition plays a major role in the ability to form these layers as well as the kinetics of formation [65-66]. It was also demonstrated that the amorphous calcium phosphate film will crystallize to form agglomerates of hydroxyapatite crystals, and that collagen fibers if present are incorporated into the calcium phosphate layer [34]. It was postulated that the modified glass surface served as a heterogeneous nucleation site for the precipitation of hydroxyapatite [67]. These reactions were not significantly affected by partial or total crystallization treatments of the glassy phase; i.e. ceraming of the glass.

2.2.2 In Vitro and In Vivo Studies of Bioactive Glasses and Glass-Ceramics

In-vivo animal studies documented the bonding ability of these materials. Through the use of tools such as light microscopy, electron microscopy, scanning electron

microscopy, selected area diffraction, and microradiography, documentation of bone formation in direct contact with the glass surface was obtained [63,68-69]. Furthermore, by utilizing Auger spectroscopy [64], infrared reflection spectroscopy, and electron microprobe analysis [66,69], the interface between the glass and bone was shown to consist of the silica rich layer and calcium phosphate layer as was observed in the in-vitro studies.

While light and electron microscopy can be used to observe the implant-tissue interface, they can not distinguish between physical contact and chemical bonding. Mechanical testing of the interface is required to document bonding. However, developing a reliable mechanical test model for in-vivo samples is not a simple task. Ideally one should be measuring tensile strength. To accomplish this, the contribution of surface irregularities to shear strength should be eliminated. It is also very difficult to measure surface area accurately and as a result failure loads rather than strengths are sometimes reported. Other factors which can affect the results include handling conditions and elapsed time from animal sacrifice, testing jig configuration, and crosshead speed of testing device. Thus when comparing published results, one must be careful to take these factors into consideration. In any mechanical evaluation study, one or more materials with known bonding or

nonbonding behavior should be included for comparative purposes.

Miller et al. [70] employing push out tests using cylinders transversely located in the cortices of dog femurs showed that Bioglass® implants required substantially more force to dislodge them from healing bone than was the case for stainless steel, cobalt chromium alloys and alumina. Piotrowski et al. [71] measured torsional loading to failure employing rat and monkey animal models. Midshaft femoral segmental replacements of Bioglass® were tested after healing periods of 6 to 28 weeks in rats and 23 to 50 weeks in monkeys. In both models the specimens that bonded to bone, bonded very well, with the strength of the healed bone approaching the strength of the contralateral normal bone. A noted observation was that the fracture line after failure tranversed both bone and Bioglass® and did not preferentially follow the interface. To assess the chemical viability of a Bioglass® coated metallic prosthesis for orthopaedic applications, Piotrowski et al. [72] implanted femoral head replacements coated with Bioglass® in monkeys and after various time intervals measured the force required to extract the stem of the prosthesis from the femur. Stresses were not reported due to the previously discussed difficulty of determining the true contact area. Pull out forces four times greater than the weight of the animal were measured. An

additional finding of this study was the critical need for good initial fixation without which bonding did not occur.

West el al. [73] using a canine animal model and push out testing on cylinders implanted transcortically in the femur demonstrated comparable bond strengths between Bioglass® coated and hydroxyapatite coated titanium alloy up to 24 weeks. Interestingly the failure of the Bioglass® coated implants occurred at the glass-metal interface in most cases. This was attributed to a reaction between the substrate and the glass during the coating process producing bubbles at the interface.

Following in the footsteps of the Bioglass® research program at the University of Florida, several other groups have focussed on the concept of bioactive materials. A series of bioactive glass-ceramics termed Ceravital® was developed by Bromer and others in Germany [74]. Ceravital® compositions fall in the SiO_2-P_2O_5-Na_2O-K_2O-MgO-CaO system. Basically the Ceravital® system is similar to the Bioglass® system with some of the sodium replaced by potassium and some of the calcium replaced by magnesium. Bone bonding of Ceravital® implants has been confirmed by investigators including Gross, Strunz, Bromer, Blencke, and Deutscher [41-42,61,75].

In Japan, numerous investigators [38-40,43,54] have reported on the development of a glass-ceramic material based on the SiO_2-P_2O_5-Na_2O-K_2O-CaO-MgO system. Termed A-W

glass-ceramic, these materials contain hydroxyapatite and wollastonite crystals in a $MgO-CaO-P_2O_5-SiO_2$ glassy phase. Selected compositions also contain whittlockite as an additional crystalline phase [76]. In-vivo animal studies have confirmed bonding to bone with A-W glass-ceramics. A common finding with these bioactive glasses and glass-ceramics is the formation of a surface layer of hydroxyapatite. Kokubo has proposed that the essential condition for glass and glass-ceramic to bond to bone is the formation of a surface apatite layer in the body environment [77]. However, it is not essential that the parent glass or glass-ceramic contain apatite or even phosphorus. Clark et al. [65], Walker [78] and Andersson et al. [79] have observed bone bonding to silicate glass containing no phosphorous.

Nakamura et al. [38] developed an animal model to evaluate bonding to bone using rabbit tibial bones. Only tensile failure loads were reported as determination of actual bone contact area was not possible. At 8 weeks, failure loads of A-W glass-ceramic significantly higher than that of alumina ceramic implants were measured. In a subsequent study, Yoshii et al. [80] measured tensile and shear strength as a function of implantation time in rabbit tibial bones. A-W glass-ceramic was compared with alumina at 2, 4, 8 and 25 weeks. At all time periods greater than 4 weeks, the A-W glass-ceramic demonstrated significantly

greater tensile and shear strengths. The greatest increase in strength occurred between 2 and 8 weeks, after which a slight increase was noted up to 25 weeks.

Kitsugi et al. [76] measured the tensile failure load of A-W glass-ceramic and a modified material containing β-whittlockite ($3CaO-P_2O_5$) in addition to apatite and wollastonite. Using the technique of Nakamura et al. [38] no significant differences of failure loads were measured at 10 and 25 weeks. It was noted that while the presence of whittlockite in the glass-ceramic had little effect on the failure load there was a wider reaction zone as compared to the reaction zone of the A-W glass-ceramic.

In another study Yoshi et al. [81], again using the technique of Nakamura et al. [38], measured tensile failure loads of the original A-W glass-ceramic and a modified composition with B_2O_3 replacing CaF_2. Comparable strengths were measured at 10 and 25 weeks.

In Finland a team of researchers led by Andersson has examined the $SiO_2-Na_2O-CaO-P_2O_5-B_2O_3-Al_2O_3$ system. Bioactive compositions have been identified that form a calcium phosphate surface layer which serves as the bonding zone between the glass-ceramic and bone. While confirming a potential inhibitory effect of Al_2O_3 additions on bone bonding, Andersson observed bone bonding with compositions containing up to 1.5 wt% Al_2O_3 [82]. Andersson and

Kangosniemi [83] implanted conical samples in rabbit tibial bones and performed push-out testing after 8 weeks. Bonded glasses had push out strengths of 16-23 N/mm^2 while non-bonding glass compositions had interfacial strengths on the order of 2-4 N/mm^2 which were comparable with titanium implants.

Vogel and Holand [84] have developed a series of machinable bioactive glass-ceramics based on the $Na_2O-K_2O-MgO-Al_2O_3-P_2O_5-SiO_2-F$ system. These bioactive compositions containing phlogopite (mica) and apatite crystalline phases bond to bone via a thin calcium phosphate layer which forms at the surface in-vivo. To assess bonding, cubes of the material were implanted into the tibial heads of guinea pigs. At time periods of 8, 12, and 16 weeks shear strengths were on the average eight times that of dense alumina implants [85].

A common area of agreement regarding the bonding of bioactive glasses and glass-ceramics is that a calcium phosphate or hydroxyl carbonate apatite layer forms at the implant-bone interface. The ability to form this layer as well as the kinetics of formation is influenced by the composition of the implant materials. Given that bioactivity has been demonstrated in various combinations of compounds in the $Na_2O-K_2O-CaO-MgO-Al_2O_3-P_2O_5-SiO_2$ system, the compositional limitations discussed in the following section

have been only empirically defined. At present, there is no theoretical basis for understanding these compositional factors.

2.1.3 Compositional Range in Bonding of Bioactive Glasses and Glass-Ceramics

Bioactive glasses containing from 40 to 60 wt% SiO_2 have been identified. However, SiO_2 contents greater than 60% do not achieve bone bonding [34, 61]. Higher concentrations of silica result in glasses that form a silica-rich layer which elicits the formation of a nonadherent fibrous capsule rather than the calcium phosphate bonding layer. Relatively small additions or contaminations of multiple valence oxides in bioactive glass compositions can effectively eliminate bone bonding potential. Greenspan and Hench [53] demonstrated that 3 wt% additions of Al_2O_3 to a 4555 Bioglass® will destroy bone bonding. Andersson [82] on the other hand demonstrated bioactivity in glass compositions containing up to 1.5 wt% Al_2O_3. Gross and Strunz [61] have documented an inhibitory effect on mineralization with the addition of multivalent actions of Al^{+3}, Ta^{+4}, Sb^{+3} or Zr^{+4} to Ceravital® glass-ceramics. Glass compositions containing these ions exhibited bone bonding which was decreased, delayed or totally inhibited. The inhibition was characterized by the presence of a seam of unmineralized tissue or osteoid at the

implant interface. This appeared to be a local effect as normal mineralization was noted in repair areas away from the actual implant interface.

In an attempt to explain these observations, Wilson et al. have summarized [31] the established tissue-bonding mechanisms of bioactive silicate glasses as

1) Rapid exchange of Na^{+1} or K^{+1} with H^{+1} or H_3O^{+1} from solution,

2) Loss of soluble silica in form of $Si(OH)_4$ to the solution resulting from breaking of Si-O-Si bonds and formation of Si-OH and groups at the glass solution interface,

3) Condensation and repolymerization of an SiO_2-rich layer on the surface,

4) Migration of Ca^{+2} and PO_4^{-3} groups to the surface through the SiO_2-rich layer,

5) Nucleation of a $CaO-P_2O_5$-rich film on top of the SiO_2-rich layer,

6) Growth of the SiO_2-rich layer by diffusion-controlled alkali ion exchange,

7) Growth of the amorphous $CaO-P_2O_5$-rich film by incorporation of soluble calcium phosphates from solution,

8) Crystallization of the amorphous $CaO-P_2O_5$ film by incorporation of OH^{-1}, CO_3^{-2}, or F^{-1} anions from

solutions to form a mixed hydroxyl, carbonate, fluorapatite layer, and

9) Agglomeration and chemical bonding of the apatite crystallites around collagen fibrils and within absorbed mucopolysaccharides and other proteins produced by osteoblasts or fibroblasts.

Steps 1-5 occur rapidly (within minutes), whereas steps 6-9 occur over periods of 3 to 14 days depending on implant composition, animal species, surgical site, and fit of implant in surgical defect.

Holding other factors constant, the glass composition exhibits a marked effect on bonding. Step 1 in the proposed sequence of bonding occurs via the reaction:

$$2Si-O-Na^+ + H_3O^{+1} \rightarrow 2Si-O-H^{+1} + 2Na^{+1} + OH^{-1} \quad (2.1)$$
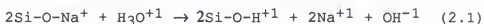
This cation exchange reaction and surface silanol formation is diffusion controlled and can be represented by the following equation:

$$R_1 = -k_1 t^{0.5} \quad (2.2)$$

where R_1 is rate constant for the reaction.

As a consequence of the hydroxyl groups produced in equation (a), the interfacial pH is raised and additional silanol groups are produced, e.g.

$$Si-O-Si + H^{+1}OH^{-1} \rightarrow Si-OH + HO-Si \quad (2.3)$$

The reaction rate for (b) is defined as

$$R_2 = -k_2 t^1 \quad (2.4)$$

where R_2 is the rate constant for this interfacial controlled reaction. With glass compositions that are bioactive, an interfacial pH <9 leads to a repolymerization of silanol groups:

(c) $Si-OH + HO-Si \rightarrow Si-O-Si + H_2O$ (2.5)

The rate for reaction (c) can be expressed as

$R_3 = +k_3 t^x$ (2.6)

Steps 4-5 occur when P_2O_5 and CaO which have been released into solution precipitate back onto the repolymerized silica films. The reaction rate for this step can be represented by

$R_4 = +k_4 t^y$ (2.7)

The time dependence for rate equations 2.3 and 2.4 has not been determined. Thus the total reaction rate for a bioactive glass surface can be represented as

$R_T = -k_1 t^{0.5} -k_2 t^1 +k_3 t^x +k_4 t^y$ (2.8)

The first two terms are negative as they represent the loss of material from the glass surface. The last two terms are positive as they represent the formation of layers on the glass surface.

The net result can be an overall increase or decrease in the volume of the material depending on the composition and its relative influence on the rate of each of the four reactions. For instance, if the glass contains enough silica, then a protective layer will form on the surface preventing

the subsequent formation of the calcium phosphate layer. Thus a net decrease of volume may occur. Bioactive glass compositions develop the double silica-rich and calcium phosphate layers which grow with time producing an increase in thickness.

Referring back to the observations that glasses containing SiO_2 in excess of 60% do not exhibit bonding, one can examine the overall rate equation (2.8) and see that the SiO_2 level will affect all four terms. As SiO_2 content increases, the network will tighten and alkali and alkaline oxide dissolution will be slowed. This will retard $[OH^-]$ production and the formation of silanols. The SiO_2 repolymerization and calcium phosphate precipitation will also be inhibited.

The compositional requirements for bioactivity influence each of the terms in the overall rate equation and have been defined by Walker and Hench and are shown in Figure 1.1. Compositions which fall within the zone labeled "bonding" exhibit a reaction rate which leads to the formation of a calcium phosphate surface layer. Compositions which fall outside of the bonding area affect one or more of the terms of the rate equation such that a calcium phosphate layer does not form.

2.2 Sol-gel processing

2.2.1 Introduction

Basically, sol-gel processing can be divided into two main categories: (a) destabilization of an inorganic salt containing one or more metal ions in aqueous solutions in which the only liquid present is water [86] and (b) controlled hydrolysis and polycondensation of alkoxide precursors in nonaqueous solutions which contain solvents other than or in addition to water. Accordingly, gels are classified into two groups: (1) "colloidal gels" [87] "particulate gels" or "aqueous gels," such as Ludox®*, made by destabilization of an aqueous silica sol and (2) "alcohol gels" or "polymeric gels," such as Gelsil®**, made by controlled hydrolysis and condensation reaction of metal alkoxides compounds.

The history of either category of sol-gel processing dates back to the mid-1800s.

As early as 1864, Thomas Graham [88] carried out an extensive investigation of inorganic gels from aqueous salts and proposed a theory that the gel consisted of a

---

®* Registered trademark, Du Pont de Nemours & Co. Wilmington, DE.

®** Registered trademark, Geltech Inc. Alachua FL.

solid network with continuous porosity. The network structure of silica gels was widely accepted in the 1930s, largely through the work of Hurd [89]. The process of supercritical drying to produce aerogels was invented by Kisler [90] in the 1930s, who was interested in demonstrating the existence of the solid skeleton of the gel, and in studying its structure. (Note, an average areagel is produces by removal of the liquid by drying above the critical point which leaves a skeleton of ~ 5% solid or less without shrinkage.)

Around the same time, mineralogists became interested in the use of sols and gels for the preparation of homogeneous powders for use in studies of phase equilibria [91-92]. This method was used for this purpose in the ceramics community by R. Roy and coworkers [55,93-95] for the preparation of colloidal gel powders with very high levels of chemical homogeneity of the oxides. They used the sol-gel method in the 1950s and 1960s to synthesize a large number of novel ceramic oxide compositions, involving Al, Si, Ti, Zr, etc., that could not be made using traditional ceramic powder methods.

During the same period Iler's pioneering work in silica chemistry [87] led to the commercial development of colloidal silica powders, Du Pont's colloidal Ludox® spheres. Stober et al. [96] extended Iler's findings to show that using ammonia as a catalyst for the TEOS hydrolysis reaction could control

both the morphology and size of the powders, yielding the so-called Stober spherical silica powder. The history of the development of colloidal silica was summarized by Iler in his famous book "The Chemistry of Silica" [87].

Much more sophisticated work, both scientifically and technologically, was going on in the nuclear-fuel industry, but it was not published until later [97-98]. The advantage of sol-gel processing of nuclear fuels was that it avoided generation of dangerous radioactive dust, as produced in conventional ceramic processing, and facilitated the formation of spheres. The small spheres (tens of μm in diameter) of radioactive oxides were obtained by dispersing the aqueous sol in a hydrophobic organic liquid, so that the sol would form into small droplets, each of which would subsequently gel.

Category (b) of sol-gel processing as defined above involves materials from hydrolysis and polycondensation of metal alkoxides in the presence of a limited amount of water. In 1864, Ebelmen [99], who synthesized the first alkoxide from silicon tetrachloride ($SiCl_4$) and isoamyl alcohol (ROH) observed that the synthesized compound, $Si(OEt)_4$ (ethylorthosilicate), slowly converted into a glassy gel due to slow hydrolysis by atmospheric moisture at room temperature [100]. However, extremely long drying times of 1 year or more were necessary to avoid the silica gels

fracturing into a fine powder, and consequently gels derived from alkoxides remained of interest only to chemists for almost a century [101]. During that period, a huge volume of descriptive literature resulted from their studies but with a relatively sparse understanding of the physical-chemical principles [102-105]. Finally, in the 1930s Geffcken et al. [106] recognized that sol-gel processing could be used in the preparation of oxide films. This process was developed by the Schott glass company in Germany and its physics is quite well understood, as explained in the excellent reviews by Schroeder [107-108], and Dislich [109].

The ceramics industry began to show interest in gels in the late sixties and early seventies. Controlled hydrolysis and condensation of alkoxides for preparation of multicomponent glasses was independently developed by Levene and Thomas [110] and Dislich [109] et al. Both glass and polycrystalline ceramic fibers have been prepared by using sol-gel processing on a commercial basis by several companies [111-113]. Compositions include TiO_2-SiO_2 and ZrO_2-SiO_2 glass fibers [114], high purity SiO_2 waveguide fibers [115-117], Al_2O_3, ZrO_2, ThO_2, MgO, TiO_2, $ZrSiO_4$ and $3Al_2O_3 \cdot 2SiO_2$ fibers [118-121]. Abrasive grains based upon sol-gel derives alumina are important commercial products [121].

A variety of coatings and films have also been developed by using sol-gel methods. Of particular importance

are the antireflection coatings of indium tin oxide (ITO) and related compositions applied to glass window panes to improve insulation characteristics [122-124]. Other work on sol-gel coatings is reviewed by Mackenzie [125-126] and Wenzel [127].

Sol-gel research has grown markedly and the fields of investigation have widened dramatically due to potentially unique applications for this new class of materials [128-134]. According to Hench and West [135], the motivation for sol-gel processing of silica is primarly by the higher purity and homogeneity and the lower processing temperatures compared with traditional glass melting methods. In addition, the dried or partially densified gels can be made in a wide range of variable surface areas and pore sizes. These advantages are summarized by Mackenzie [125], who also discussed many of the other potential applications, benefits and drawbacks offered by sol-gel technology.

As mentioned above, there are two categories of sol-gel processing, in other words, there are two significantly different methods of sol-gel technology. In fact, so called "sol-gel processing" most commonly means category (b) defined as controlled hydrolysis and polycondensation reaction of organic precursors. This is the definition used in this study.

2.2.2 One-Component Gel-Derived SiO$_2$

The various types of vitreous silicas are given in Table 2.1 [136-137]. Types I and II are based on natural quartz crystals, either chunks or sand, as raw material, so the impurity content is variable. Types III and IV are purer, but more expensive. Very pure vitreous silica usually is made from vapor-phase oxidation or hydrolysis of silicon tetrachloride (SiCl$_4$) which is Type IV, however, it still contains considerable impurities including OH groups. In recent years, two new types of pure gel-silica glasses have been produced with high reliability using sol-gel processing, Type V fully dense silica and Type VI optically transparent ultraporous silica [137]. The properties, especially optical properties of Type V gel-silica are superior than most of the commercial grades of silica [137-138]. Type VI gel-silica, first reported by Hench et al. in 1988, is a porous monolithic material exhibiting excellent optical quality [137], good thermal and chemical stability [139], and reasonably high mechanical strength [140]. Since both porosity and pore surface chemistry of Type VI gel-silica can be precisely controlled, it has many multifunctional optical applications [137-138,141].

The processing steps involving in making Types V and VI pure gel-silica are illustrated in Figure 1.3 .

Table 2.1
Different types of vitreous silica

Type	Method of manufacture	Maximum impurity concentration (ppm)								
		Al	Fe	Ca	Mg	K	Na	Li	Cl	OH
I[*]	Electrical fusion of quartz crystal	150	7	12	7	4	12	12	50	4
II[*]	Flame fusion of quartz crystal	Similar to I								400
III[*]	Flame hydrolysis of $SiCl_4$	10	6	4	3	2	2	1	60	1200
IV[*]	Vapor phase oxidation of SiCl4	Similar to III							500	low
V[**]	Dense Gel-silica	Total cation: 1-2							0-1000	<1
VI[**]	Porous Optical Gel-silica	Similar to V							>2000	0

*   [136]

**   [137]

(1) Sol preparation. A liquid precursor (starting material), either tetramethylorthosilicate (TMOS) or tetraethylorthosilicate (TEOS) is mixed with water and undergoes simultaneous hydrolysis and polycondensation reactions which lead to the formation of SiO_2. The overall reactions consist, at least formally, of two steps:

$$M(OR)_n + H_2O \rightarrow M(OH)_n + n\ R(OH) \qquad (2.9)$$

$$P\ M(OH)_n \rightarrow P\ MO_{n/2} + Pn/2\ H_2O \qquad (2.10)$$
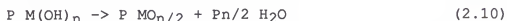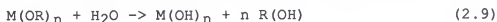
In reality, the situation is more complicated; reactions (1) and (2) are generally incomplete. When sufficient Si-O-Si bonds are formed in a region, they respond cooperatively as colloidal (submicrometer) particles or a sol. The size of the sol particle and the cross-linking within the particle depends upon the pH, the catalyst and the R ratio ($R=[H_2O]/[Si(OR)_4]$). For instance, by using HF along with HNO_3 as the catalyst, the mean pore size of the gel changes over a broad range from 1.2 to 10.0 nm [140,142].

(2) Casting. Since the sol is a low viscosity liquid, it can be cast into a mold which must be selected to avoid adhesion of the gel. The shape of the gel will be determined by the shape of the mold for casting. It has been reported [143] that it is possible to achieve as-cast tolerances for the diameter, thickness and radius of curvature of gel-silica lenses made by sol-gel processing which are within, or

surpass, tolerances achieved by precision grinding and polishing.

(3) Gelation. A gel is a form of matter intermediate between a solid and liquid [144]. It consists of an interconnected three-dimensional network of particles holding an interstitial liquid which is a mixture of alcohols and water. The gelation point of any system, including sol-gel silica, is easy to observe qualitatively and easy to define in abstract terms but extremely difficult to measure analytically. The sol becomes a gel when it can support a stress elastically. This is typically defined as the gelation time, t_{gel}, which changes significantly with the sol-gel chemistry [87,145-148].

(4) Aging. Aging is defined as the structural evolutions that occur with time after gelation prior to solvent evaporation and involves maintaining the cast object for a period of time completely immersed in liquid, either its pore liquid or an other solution. Four processes can occur, singly or simultaneously, during aging. The aging processes include: continuation of polycondensation reactions, syneresis which is spontaneous shrinkage of the gel with expulsion of solvent, coarsening (increase in pore size and reduction in surface area through depolymerization and repolymerization), and segregation (phase transformation and crystallization). The strength of the gel generally

increases with aging. A properly aged gel can develop sufficient strength to resist cracking during drying. The structure of a gel may change appreciably with aging time depending on the preparative condition, including catalyst used, pH values and the ratio of water and alkoxides of silicon (water content) [59-60]. It has been observed that under high pH and high water content, highly branched clusters are developed, while under the conditions of low pH and low water content, linear or random branches form [59]. Changes in gel structure during aging are described by Zarzycki and Scherer [149-150].

Although Iler [87] and Scherer [133,151] have made extensive efforts to describe aging theoretically, there is relatively little detailed knowledge of aging mechanisms and kinetics and even less quantitative analysis of the effects of aging on gel structure and properties. Recently, it has been found [141] that the gel-silica texture can be effectively controlled by aging treatments. This is achieved by exposing the wet gels in a solution containing ammonium hydroxide (NH_4OH) in the aging stage followed by drying up to 180°C in various media. By controlling either aging parameters or drying chamber environment, the average pore radius of the resultant gel-silica can be varied from 1.2 nm to 14.8 nm with very narrow distributions. The volume fraction of porosity can be extended from 50% to as high as

74%. The pore shape can also be changed from wide voids of differing diameters to pores with narrow necks or pores with smooth cylindrical cross sections. Combined with other unique properties, including good optical, mechanical and thermal properties, this makes it possible for a gel-silica monolith to be used as a host material for composites, such as solid state dye lasers, and other optical devices.

(5) Drying. During drying, the liquid is removed from the interconnected pore network and the wet gel experiences progressive shrinkage, hardening and stress development. The stress arises not only from differences in expansion coefficient due to variable water content, but also from the action of capillary forces which become operative when the pores start to empty and the liquid-air interface is present in the form of menisci distributed in the pores of the drying gel. The resulting gel is a visco-elastic solid which is progressively transformed into a purely elastic, porous solid during the drying process.

The drying behavior of porous solids has been extensively studied by Sherwood [152-154], Keey [155], Mujumdar [156-157], Moore [158], Whitaker [159], Cooper [160] Ford [161] and Scherer [150,162-166]. Different drying models have been proposed based on the quantitative studies conducted on large pore (> 20 nm) gels by Kawaguchi et al.

[167], Dwivedi [168] and Zarzicki [169] and on small pore (<20 nm) by Wilson [170].

The dried gel differs from a glass by its texture. The gel is essentially an agglomerate of elementary particles, the size of which may be on the order of 10 nm, aggregates of particles formed by primary particles, so-called secondary particles, and contains micro- and macro-pores [171]. Although the structural features of a gel including surface area, pore size and its distribution, may differ considerably depending on processing method, the very high surface area (>400m^2/g) remains for all gels. In addition, the constituent particles are coated with residual hydroxyl groups which are partly eliminated during the transition from a particulate texture towards a continuous solid.

Drying can be performed in two different ways. Drying by evaporation under ambient atmosphere gives rise to capillary pressure that causes shrinkage of the gel network. The resulting dried gel is called a xerogel which is often reduced in volume by a factor of 5 to 10 compared to the original wet gel. If the gel is placed in an autoclave and dried under supercritical conditions, by removing the liquid from the pores above the critical temperature (T_c) and critical pressure (P_c) of the liquid, there is no interface between liquid and vapor, so there is no capillary pressure

and relatively little shrinkage. This process is called supercritical (or hypercritical) drying, and the product is called an aerogel. These may indeed be mostly air, having volume fractions of solid as low as ~1%. Both xerogels and aerogels are very useful.

(6) Stabilization. It is a well established fact that gel-silica remains highly porous at temperatures significantly higher than those required to produce a rigid gel [139]. These pores are predominantly interconnected and open. In an alkoxide-derived silica gel, the pore diameter ranges from 1.2 nm to 10 nm, and the volume fraction of porosity can be greater than 70 percent [141,172]. Surface areas in excess of 900 m^2/g have been reported for silica gels dried at 40°C [173]. Even after heating to much higher temperatures, extensive porosity remains. It is interesting to note that subsequent heat treatments of the rigid gel do not change the average pore size much as long as the heating is below a certain temperature (<1000°C) (Figure. 2.1). However, heat treatments do change the volume fraction of porosity and the surface area (Figure 2.2) [140].

The removal of surface silanol (Si-OH) bonds from the pore network results in a chemically stable ultraporous solid. Type VI porous gel-silica made in this manner is optically transparent with interconnected porosity and has sufficient strength to be used as unique optical components
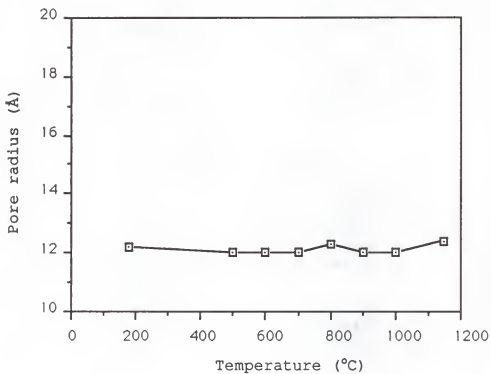
Figure 2.1   Variation of the average pore radius
             of 12Å gel-silica samples as a function
             of densification temperature [140].
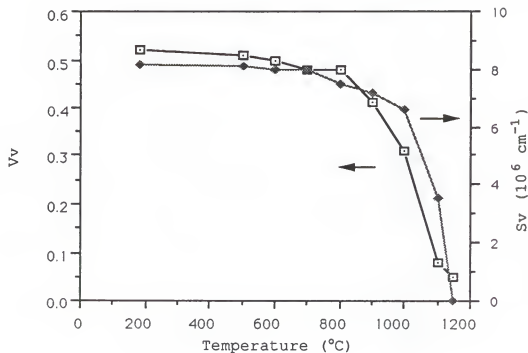
Figure 2.2 Variation of the surface area of pores
per unit volume (Sv) and the volume
fraction of pores (Vv) of 12 Å gel-silica
samples as a function of densification
temperature [140].

when impregnated with optical active polymers such as dyes, fluors, waveguide shifters or nonlinear optical polymers [137,141].

(7) Densification. Heating the porous gel at high temperatures causes densification to occur. Densification is essentially a sintering process by which the pores of a dry gel are eliminated and the density ultimately becomes equivalent to fused quartz or fused silica, e.g. 2.2 g/cm^3. The final materials convert into fully dense Type V gel-silica. The driving force for this process arises from the excess surface free energy of the gel. At least four mechanisms contribute to this process: (1) capillary contraction, (2) condensation, (3) structural relaxation, and (4) viscous sintering [174-175]. Mechanisms (1) and (2) are considered chemical processes which dominate at low and intermediate temperatures and mechanisms (3) and (4), structural relaxation and viscous sintering, are physical processes and dominate at high temperatures [176]. The temperature range in which each of these mechanisms is dominant depends on the chemical and microstructural nature of the gel as well as the heating rate. An important stage is reducing or eliminating residual hydroxyl groups, dehydration, in the pores during the densification process. Although OH can be removed through condensation reactions, viscous sintering often starts before dehydration is

complete, leading to bloating or foaming of the gel in the final stages of sintering. Even if sufficient hydroxyl content is removed so that sintering can occur without bloating, subsequent heating of the consolidated gel to its softening point, for example, during fiber drawing or sealing, may cause bloating. Thermal dehydration of silica gel has been extensively investigated [177]. Hair [177] proved that OH groups are in general gradually lost with increasing temperature, but some single hydroxyl groups are still unable to escape from the surface before commencement of viscous sintering, thus thermal dehydration is often not sufficient to avoid foaming in silica gels. Consequently, chemical dehydration procedures, primarily employing halogens have been widely investigated. Atmosphere has a strong influence on the densification process [178]. An optically clear, bubble-free, and OH-free silica glass prepared by employing a halogen treatment followed by annealing in oxygen and sintering in He was reported by Matsuyama et al. [179]. The chemical and microstructural evolution during the densification of dried gels have been described by James [180].

During densification the gel will, at the same time, tend to crystallize [86]. The successful conversion of gel into glass therefore depends on a competition between phenomena which lead to densification and those which promote

crystallization. This will be discussed later with regard to multi-component systems. The hydroxyl groups which are on the surface of gel particles tend to decrease the viscosity and promote crystallization of the silica gel [181-182] and may cause structural changes, as well.

After condensation is complete and thermal processing has occurred, the sol-gel silica monoliths should be primarily made up of silicate rings. There is roughly an equal distribution of 4-fold, 5-fold, 6-fold, and 7-fold rings of silica tetrahedra in vitreous silica and equivalent structures are believed to be present in silica gel [183].

The results of quantum mechanics calculation of water adsorption onto gel-silica [184] show that the 4-fold ring without water is uniform. However, the ring with the water adsorbed is elongated along the axis with the water. Also, the average silicon-silicon distance for neighboring atoms increases when water is present. Thus, adsorption of water into the porous gel-silica dilates the gel structure as was observed experimentally by using a dilatometer [139].

2.2.3 Binary Na_2O-SiO_2 Gel-Glass

Binary Na_2O-SiO_2 glasses via sol-gel processing have been investigated by Hench and coworkers [185-187]. Optically clear monolithic dried gels in the range of 20

mm-90 mm diameter by 3 mm to 20 mm thickness in compositions $XNa_2O-(1-X)SiO_2$ (with X from 0 mol.% to 7 mol.%) were routinely produced by acid catalyzed sol-gel processing using tetramethylorthosilicate (TMOS) and $NaNO_3$ and their ultrastructure and properties studied by Li and Hench [188].

TMOS was used as a precursor of polysilicic acid to form the soda-silicate gels. After this precursor was mixed with water at room temperature catalyzed by nitric acid, an inorganic salt, sodium nitrate ($NaNO_3$) was added. By controlling the processing schedule, complete drying and partial densification without cracking were achieved. The ultrastructure of the gels was studied by using the N_2 adsorption BET technique. The optical properties of the gels were measured including UV, IR absorption and index of refraction. The density, microhardness and dielectric relaxation from 10 Hz to 13 MHz were also measured. It was found that the ultrastructure and some properties of a 3 mol.% Na_2O-97 mol.% SiO_2 gel are similar to those of pure silica gel but the alkali-containing gels can be densified at substantially lower temperatures. In general, when Na_2O is added into the SiO_2 system, two major changes occur. The first change is the gel-glass conversion temperatures are decreased depending on the Na_2O content of the gel. The

second one is the increasing tendency towards crystallization in the system. Figure 2.3 summarizes the thermal-compositional processing diagram for the sol-gel derived system. The experimental basis for obtaining this figure is given by Hench et al. [137,185-187,189]. Gel-derived 33 mol.% Na_2O-67 mol.% SiO_2 glass was obtained at temperatures as low as 500°C which compares to 1050°C-1150°C for pure silica gel-derived glass [137].

It has been shown that alkali cations or other impurities, even in trace amounts, promote crystallization [190-191]. Densification and crystallization are complex kinetic phenomena and both depend on the structural and textural characteristics of the gel.

2.2.3 Multi-Component System

The homogeneity derived at the gel stage can be inherited to a great extent by gel-derived glasses if the glass conversion can be accomplished without considerable changes in the cation distribution achieved at the gel stage. This has stimulated further research leading to the preparation of homogeneous multicomponent gels and gel-derived glasses [192-194]. The homogeneity of gel-derived glasses in the SiO_2-B_2O_3-Na_2O system was examined using laser
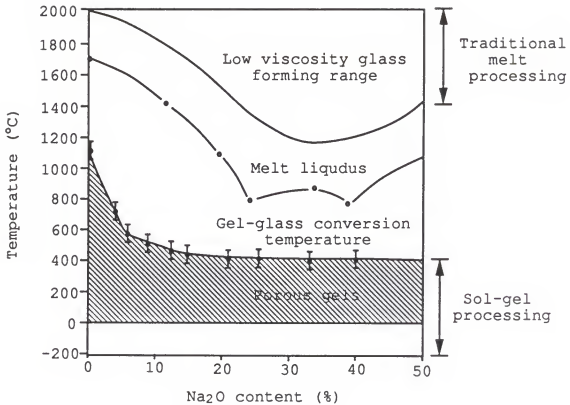
Figure 2.3 Thermal-compositional processing
            diagem for the sol-gel derived
            Na_2O-SiO_2 system [137, 185-187].

light scattering by Mukherjee and Mohr [195]. The major
experimental observation made from these scattering
measurements showed that the gel-derived glasses generally
exhibit excellent microhomogeneity. This indicates that the
intimate mixing inherent in the gel process results in this
excellent microhomogeneity. A major problem in forming
homogeneous multicomponent gels is the unequal hydrolysis and
condensation rates of the metal alkoxides used.
Tetraethylorthosilicate (TEOS), for instance, can require
more time for gelation while titanium and zirconium alkoxides
tend to precipitate almost immediately under similar
conditions [196]. So, TEOS is generally prehydrolyzed under
acid conditions prior to adding the faster hydrolyzing second
alkoxide in the processing of multicomponent gels.

It has been demonstrated that by controlling the rate
of hydrolysis and condensation, pore size distribution, pore
liquid vapor pressure, and drying stresses, a wide range of
size and shape of optically transparent dried gel monoliths
of $LiO_2-Al_2O_3-SiO_2-TiO_2$ and other ternary and quarternary
glasses can be made within a few-day processing schedule
[131].

2.2.5 Summary

The sol-gel processing of materials offers a large number of advantages. It has a great potential in producing glasses, glass-ceramics and ceramics with excellent performance in various applications. The potential of this processing is based on the fact that materials with high homogeneity and purity can be made in the forms of bulk, fiber, sheet, coating, film and powder at relatively low temperatures.

This review lays a scientific basis for making bioactive powder via sol-gel processing where the potential advantages discussed above will be extended into the field of biological applications.

CHAPTER III
EXPERIMENTAL METHODS

3.1 Preparation of Gel-Derived Powders

Table 3.1 shows the compositions of $CaO-P_2O_5-SiO_2$ gel powders investigated in this study. The gel powders were prepared from tetraethyl orthosilicate (TEOS), triethyl phosphate $[OP(OC_2H_5)_3]$ and calcium nitrate.

Previous studies used TMOS as the precursor for silicate based gels. In part, This is because the SiO_2 yield of tetramethyl orthosilicate TMOS (39.47%) is higher than that of TEOS (28.84%), Consequently, a lower amount of alkoxide will be used and less shrinkage of the gel will occur during the subsequent processing steps when TMOS is used as a precursor. However, TMOS is a flammable and corrosive liquid and may cause blindness if eye exposure occurs. Therefore, TEOS is chosen in our work to produce bioactive materials because it is less hazardous and less corrosive.

The structure of a gel is generally established at the time of gelation [135]. The type of the alkoxide precursor is one of the variables of major importance in influencing the kinetics of hydrolysis and condensation and determining the

54

Table 3.1
Compositions of gel-derived powders
(in mol.%)

Sample ID	SiO_2	P_2O_5	CaO
49S	50	4	46
54S	55	4	41
58S	60	4	36
63S	65	4	31
68S	70	4	26
72S	75	4	21
77S	80	4	16
81S	85	4	11
86S	90	4	6
90S	95	4	1

gel structure [58,145,183,197-201]. The nature of the alkoxide groups on the silicon atom also influences the rate constant. As a general rule, the longer and the bulkier the alkoxide group, the slower is the hydrolysis rate constant [202-203]. For example, in the case of the hydrolysis of $Si(OR)_4$, $k_H = 51 \times 10^{-3}$ $l \cdot mole^{-1} \cdot sec^{-1} \cdot [H^+]^{-1}$ for R = C_2H_5 and $k_H = 3 \times 10^{-3}$ $l \cdot mole^{-1} \cdot sec^{-1} \cdot [H^+]^{-1}$ for R = $(CH_3)_2CH(CH_2)_3CH(CH_3)CH_2$. From this point of view, using TEOS rather than TMOS as precursor to develop multicomponent gels usually results in a slower rate constant. Therefore, there is a longer time period to make the hydrolysis reaction rate match those of other alkoxides.

Since triethyl phosphite $[P(OC_2H_5)_3]$ is moisture sensitive and an irritant, $[OP(OC_2H_5)_3]$ was used instead.

Calcium nitrate is water soluble. It can easily dissolve into and react with a hydrous solution of the alkoxide precursors.

A schematic illustration of the sol-gel processing steps for the preparation of the $CaO-P_2O_5-SiO_2$ gels used in this work is shown in Figure 3.1. Nitric acid was used as a catalyst to adjust the hydrolysis reaction rate of TEOS. Acetic acid and hydrochloric acid were tried but rejected as they resulted in a much longer hydrolysis reaction period.

The amount of water for hydrolysis has a dramatic influence on gelation time (Figure 3.2) from Colby et al.
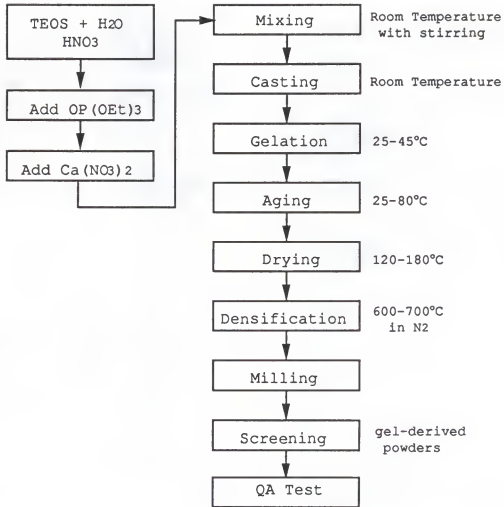
Figure 3.1   Schematic illustration of sol-gel method
              producing gel powders.
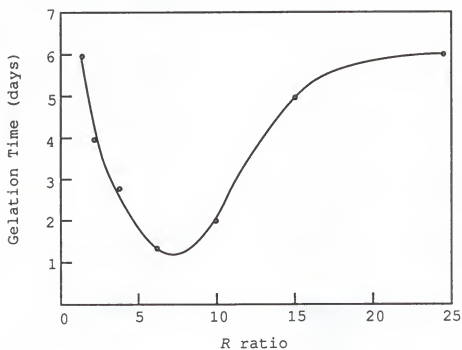
Figure 3.2   Variation of the gelation time with the
             R ratio (# mole water/# mole silicon
             alkoxide) [204].

[204]. For a R ratio (#mole water/ #mole silicon alkoxide) of 2, t_{gel} (gelation time, defined as the time when the sol becomes a gel which can support a stress elastically) is about 7 hours (gelation process at 70°C with HF as catalyst) and decreases to 10 minutes for $R = 8$ [204]. For low water contents, generally an increase of the amount of hydrolysis water decreases the gelation time, although there is a dilution effect. It can be predicted [197] that for higher water content, the gelation time increases with the quantity of water. The location of the minimum in the curve t_{gel} vs R, such as shown in Figure 3.2, depends on the chemical compositions, catalyst, and temperature of the solution.

The R ratio in this study (# of moles water/ # of moles [TEOS + OP(OC$_2$H$_5$)$_3$] was optimized carefully as both lower and higher R ratios usually result in an incomplete hydrolysis reaction depending on the types of alkoxides used. In our study, the experimental results showed that when the R ratio approached 8, the hydrolysis reaction was completed within 3-4 hours, resulting in a homogeneous sol. A reasonable aging and drying schedule then could be applied and monolithic gel samples with higher silica content could be obtained.

A major problem in forming homogeneous multicomponent gels is the unequal hydrolysis rate of various metal alkoxides. In order to achieve high homogeneity, different mixing sequences were tried. The final sequence that ensures

the homogeneity of the multicomponent gels is as follows. At first, a certain amount of TEOS, which depends on the gel composition, water and nitric acid were mixed in a covered glass beaker. A magnetic stirring bar at medium speed was used during the mixing. The solution was immiscible at the beginning, but soon became clear. No alcohol was used as the solvent since it was not effective in achieving miscibility.

After an hour, $OP(OC_2H_5)_3$ was added to the solution. The calcium nitrate was first dissolved in water and added to the solution after another one hour of mixing. The solution was stirred for an additional hour, and then maintained quiet for half an hour. The resultant clear and bubble-free sol was cast into polyethylene containers and placed inside an oven, where the sol was gelled and aged. The aged gel was then dried with a schedule shown in Figure 3.3. In principle, the heating schedule is important for drying gel monoliths, but is relatively unimportant for making gel powders. The dried gel samples were placed in a silica crucible and densified in a box furnace at a temperature range of 600°C to 700°C for several hours (schedule shown in Figure 3.4) under a slow steady flow of nitrogen. The use of a nitrogen atmosphere is to prevent gel samples from forming and crystallizing carbonate hydroxyapatite on their surface during the heat treatment. The densified samples were finally ground into powders with a particle size range of 100 to 700 microns.
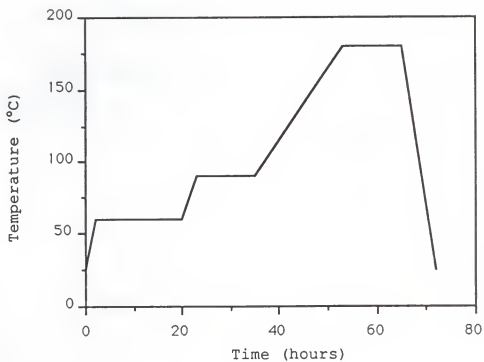
Figure 3.3   Drying schedule of gel-derived
            powders.
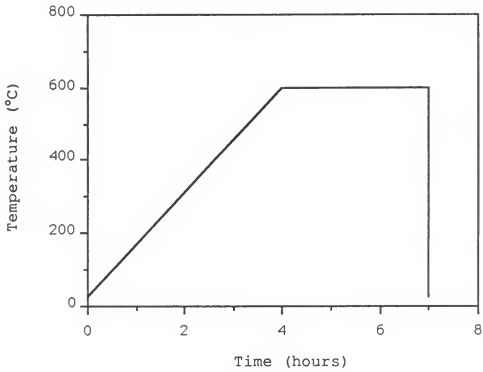
Figure 3.4   Densification schedule of gel-derived
powders.

3.2 In Vitro Testing

Previous investigations indicate that the essential condition for a material to bond with bone is the formation of a surface hydroxyapatite layer in the body environment [39]. Therefore the powders made as described above must undergo an in-vitro solution test of hydroxyapatite formation in order to evaluate the potential bioactivity of the material.

There are several quality assurance test procedures which can be used as an in-vitro test for bioactivity. For example, the bulk Bioglass quality test procedure has been established for many years [205]. This Bioglass reaction procedure includes (a) rinsing a cast Bioglass disk with reagent-grade acetone followed by air drying, (b) suspending the sample in a tris (hydroxymethyl) aminomethane buffered solution at 37°C, (c) removing the sample from the solution, dipping in reagent-grade acetone to stop the reaction, and allowing to air dry, and (d) using a Fourier Transform Infrared Spectrometer (FTIR) to record the spectrum of the reacted surface between the wave numbers 1400 cm^{-1} and 400 cm^{-1} on the sample.

The QA test procedure for powders is similar to the bulk QA test procedure described above, but it can be divided into two types: static and dynamic. In static quality

assurance test procedures, the tris-buffered solution is not moving, whereas in dynamic quality assurance procedures, the solution is in constant motion. Although the dynamic QA procedures are more complicated, they usually give more reliable and reproducible results than the static [206]. In our test, a modified dynamic quality assurance procedure was utilized. Powders were dipped directly into the tris-buffered solution in a Nalgene® polyethylene wide mouth bottle with a screw cap. The bottle was mounted in an incubator shaker (Model 3528-5, Lab-Line Instruments, Inc.). This shaker has both speed-control and temperature-control systems which is designed to deliver orbital motion in a controlled temperature environment. The operating temperature was set at 37°C ± 1°C and the speed of circular motion was kept at 220 rpm at which the powders were just suspending in the solution but not severely colliding with each other and with the wall of the bottle which might damage the surface layer. This dynamic QA test procedure allows the tris-buffered solution to surround and react with powders continuously and uniformly.

After a certain period of reaction time, the resultant reacted powders were removed from the bottle, rinsed, dried and then examined by Fourier Transform Infrared Reflection

---

® Trademark, Nalge Company, Rochester, NY.

(FTIR) Spectrometer (Nicolet 20XB) with a diffuse reflectance stage to determine whether or not the sample formed a hydroxyapatite surface layer; i.e. is bioactive. The spectrum between the wave numbers 1400 cm^{-1} and 400 cm^{-1} on the sample was recorded. Accumulation of 128 scans were used to give good resolution. If the sample is very bioactive, the sample's silicon-oxygen-silicon rocking (475 cm^{-1}) peak is diminished in the reacted sample and replaced by the hydroxylapatite (598 cm^{-1} and 566 cm^{-1}) characteristic peaks [207].

To ensure that the gel powders did not undergo any reaction prior to in-vitro testing, unreacted powders were tested by FTIR as well.

X-ray diffraction (XRD) was also used to confirm the formation of the HA crystalline phase.

3.3 Characterization Measurements

3.3.1 Thermal Analysis

Thermal analysis, Thermogravimetric Analysis (TGA) and Differential Thermal Analysis (DTA) were conducted on the dried gel powders by using a Dupont 951 thermogravimetric analyzer and 910 differential scanning calorimetry unit equipped with a 1600°C differential thermal analyzer cell.

Each unit was connected to a 1090 thermal analyzer from Dupont Instruments. The atmosphere was compressed dried air and the heating rate was 5°C/min. The gel was dried at 180°C and ground into fine powders before analysis.

3.3.2 Structural Analysis

X-ray diffraction (XRD) was used to study the partially densified powders both before and after reactions in the tris-buffered test solutions. The sample powders were ground to approximately 20 to 60 micronmeters and mounted on a glass slide using collodion-amylacetate solution. The specimens were allowed to air dry for one hour and then examined under XRD. To ensure that the solution did not react with the powders, or at least the reaction was sufficiently minimized, the samples were prepared just prior to XRD examination. The XRD range was from 5 to 85 degrees 2θ at a rate of 3 degrees per minute, using Cu-K_α radiation and operated at 40KV.

The surface area, the total pore volume and the pore sizes were measured using an automatic gas adsorption instrument, a Quantachrome Model Autosorb-6. This machine operates with nitrogen gas as adsorbate. It degasses the sample and measures the volume of nitrogen adsorbed onto (V_{ads}) or desorbed from (V_{des}) the adsorbent surface as a function of relative pressure. The samples were ground into

fine powders and outgassed in the testing cell at 150°C for 1.5 to 2 hours before the measurement. Through the Autosorb Data Acquisition mode, all the BET data, such as specific surface area, total pore volume and average pore radius etc. were automatically printed. The multi-point measurement usually takes 20 hours.

Gas (especially nitrogen) adsorption techniques and the BET theory have been extensively applied to the study of the structure of silica gels [208-212]. Results from these previous studies were compared with the bioactive gel-derived glasses and used as the basis of interpretation of the data.

3.3.3 Solution Behavior Measurement

The pH of the reacted tris-buffered solution was measured by an EA 920 Expandable ionAnalyzer (Orion Research).

The variation of concentration of Si, P, Ca and Na ions in the tris-buffered solutions during reaction were quantitatively analyzed by Inductively Coupled Plasma (IL Plasma 200) atomic emission spectrometry. Aqueous samples were nebulized by a normal method and all the data including the location and the intensity of the emission lines in the conventional UV-visible region of the spectrum were processed and printed out by the IL PDS-1 Plasma Data System.

Quantitative emission analyses demand precise control of many variables involved in sample preparation and excitation. In addition, quantitative measurements require a set of carefully prepared standards for calibration; these standards were prepared to approximate as closely as possible the composition and physical properties of the gel-derived samples to be analyzed.

CHAPTER IV
CHARACTERISTIC FEATURES OF GEL-DERIVED POWDERS

4.1 Thermal Properties

In Differential Thermal Analysis (DTA), temperature differences relative to a thermally inert material are measured during heating of a sample. The DTA curve records these differences during the heating, showing thermal effects as deviations from the zero line. The weight changes of the samples during heating can also be measured using a thermogravimetric analyzer (TGA).

Figure 4.1 shows the DTA and TGA curves of 58S gel-derived powders after drying at 180°C. The dried gel is essentially an agglomerate of particles which contains micro- and macro-pores. The sample still contains a considerable amount of liquid which is usually a mixture of water, both physically and chemically absorbed, and residual alcohol. The surface of the dried gels is generally terminated by hydroxyl groups, the silanols.

In the DTA curve, two broad endothermic peaks were observed in the temperature range between 80°C to 150°C and 450°C to 550°C. The former peak results from the evaporation of physically absorbed water, the residual alcohol entrapped
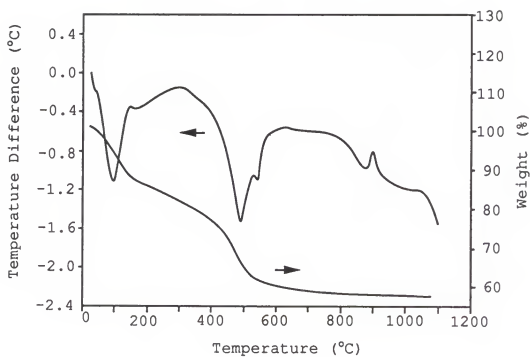
Figure 4.1   DTA and TGA of 58S gel-derived powders.

in the pores of the gel and possibly the dehydration of $Ca(NO_3)_2$ which was used as one of the starting materials.

The higher temperature peak results from the decomposition of the calcium nitrate. Duval [213] reported that when calcium nitrate, $Ca(NO_3)_2 \cdot 4H_2O$, is heated slowly, it remains unchanged up to 90°C then dehydrates smoothly up to 160°C. The anhydrous salt is stable as far as 475°C; beyond this temperature NO_2 is given off.

The exothermic peak at about 900°C is due to crystallization of the hydroxyapatite. Since DTA is a dynamic method and the sample is heated continuously, the true characteristic crystallization temperature may be delayed. The factors which influence the DTA data are heating rate, reference material and furnace atmosphere etc. The heating rate in our experiment was 5°C/min, the reference material was alumina and the furnace atmosphere was compressed air.

The TGA curve of 58S gel-derived powders (Figure 4.1) shows a substantial weight loss in the temperature region corresponding to the endothermic DTA peak, indicating a large portion of water and residual organic material were being removed. The weight loss continued until 600°C caused by decomposition of calcium nitrate and dehydration of surface silanols.

4.2 X-ray Diffraction Spectra Analysis

Figure 4.2 shows the X-ray diffraction spectra of the gel-derived powders with the various compositions listed in Table 3.1. All the samples were dried at 180°C and then further heat treated at 600°C for 3 hours. The X-ray diffraction spectrum of a standard bioactive glass (45S5 Bioglass®) is also shown in the same figure for comparison. The melt-derived Bioglass® shows no X-ray diffraction peaks, only a very broad hump characteristic of an amorphous solid.

In the X-ray diffraction pattern (through film techniques) of hydroxyapatite, three most intense diffraction lines are located at 2θ angles of $31.78°$ ($I/I_1=100\%$), $32.20°$ ($I/I_1=60\%$) and $32.91°$ ($I/I_1=60\%$) respectively. However, these lines occur at such close intervals that they do not separately resolve in the diffraction spectra. In the spectra of 49S and 54S gel-derived powders, a small peak at a 2θ of $32°$ ($\pm 0.5°$) is observed. This indicates that there was a very small amount of hydroxyapatite formed on the surface of these compositions during heat treatment. The peak intensity is not strong enough to establish the extent of crystalline order of the hydroxyapatite phase. All the other compositions of gel-derived powders show a completely amorphous X-ray spectra similar to that of the melt derived bioactive glass.
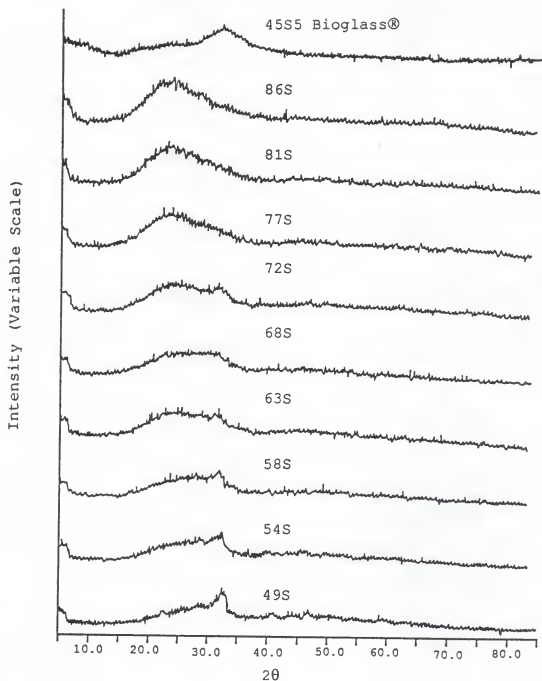
Figure 4.2 X-ray diffraction spectra of gel-derived powders after heating to 600°C and 45S5 Bioglass® made by melt method.

4.3 FTIR Reflectance Spectra

Fourier transform infrared (FTIR) reflectance spectroscopy yields structural information and also an analytical technique for surface compositional analysis because the penetration depth of the infrared beam is less than 1 μm. This technique is rapid, non-destructive, no vacuum is required, and samples of any dimension and even powders can be analyzed. The technique gives information about the change in composition as well as the structural modifications that occur on the surface accompanying compositional changes.

The powders derived by sol-gel processing were analyzed using FTIR before and after in-vitro testing.

Figure 4.3 shows the reflectance spectra of a series of gel-derived powders after being heated at 600°C for 3 hours but before the in-vitro test.

The FTIR reflectance spectra of gel-derived powders have been characterized basically by the peaks of silica oxides at the wavenumbers of 1202 cm^{-1}, 1090 cm^{-1}, 800 cm^{-1} and 482 cm^{-1}. The most intense 1090 cm^{-1} and 1202 cm^{-1} bands correspond to the TO (transverse optical) and LO (longitudinal optical) modes of the asymmetric Si-O-Si stretching vibrations respectively, the 800 cm^{-1} band is
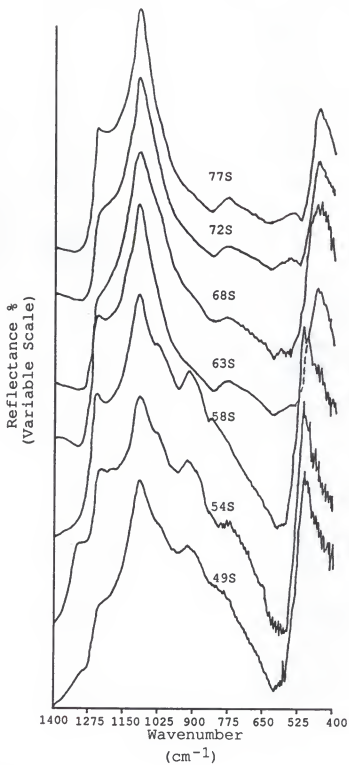
Figure 4.3 FTIR spectra of gel-derived
powders after heating to 600°C.

assigned to symmetric Si-O stretching vibration and the strong 482 cm^{-1} band is assigned to a Si-O-Si bending vibration mode [214-216].

Under certain circumstances, some other peaks can also be seen in the spectra. The peak at 1025 cm^{-1} is assigned as a Si-O stretching vibration with one non-bridging oxygen in the [SiO_4] unit and the peak at 938 cm^{-1} is attributed to a Si-O stretching vibration in a [SiO_4] unit with two non-bridging oxygens [217]. Si-OH stretching of terminal silanol groups occurs at 950 cm^{-1} [216].

In the spectra of gel-derived 77S, 72S, 68S and 63S samples, which contain more silica, only four basic peaks of silicon oxides can be observed at 1202 cm^{-1}, 1090 cm^{-1}, 800 cm^{-1} and 482 cm^{-1}.

It is proposed that the basic structure of gel-derived powders is composed of symmetrical SiO_4 tetrahedra. Adjacent tetrahedra are connected together at common, or bridging, oxygen atoms. The relative position of two such adjacent units may vary considerably because of two disordering mechanisms: first the Si-O-Si angle can take any value from about 120° to 180°; secondly, each tetrahedral unit may take on a range of possible positions formed by a rotation about the appropriate Si-O bond.

When CaO is added and its content is increased, the structural network becomes more complicated. Calcium ion is a

network modifier. When added to the composition, CaO breaks the silicate glass network and creates more non-bridging oxygens. As a result, when CaO content reaches certain values such as 36 mol.% CaO in 58S, two peaks around 1025 cm^{-1} and 938 cm^{-1} resulting from the Si-O stretching vibration with one non-bridging oxygen and Si-O with two non-bridging oxygens respectively, start to appear. Their intensities increase with the increasing CaO content as shown in Figure 4.3 indicating that the increased calcium ion content decrease the network connectivity and gradually "loosens" the gel structure.

In glasses containing calcium, one may expect a slight increase of Si-O bond length which minimizes the force constant of the stretching vibration, and therefore, its wavenumber [218]. In gel-derived gel powders (Figure 4.3), however, those changes can hardly be seen with the increasing calcium content (i.e. the decreasing of the silica content).

4.4 Characterization of Texture

The surface area, the total pore volume and the average pore radii of the gel-derived powders were measured using the automatic Quanta Chrome Autosorb-6 instrument. Table 4.1 shows the BET data of a series gel-derived powders after heating at 600°C for 3 hours.

Table 4.1
BET data of gel-derived powders
after heating to 600°C

Sample ID	Surface Area (m^2/g)	Total Pore Volume (cm^3/g)	Average Pore Radius (Å)
49S	203	0.57	57
54S	213	0.53	50
58S	289	0.49	34
63S	324	0.44	27
68S	326	0.41	25
72S	380	0.38	20
77S	431	0.32	15
81S	547	0.37	14
86S	627	0.45	14

Surface area plays an important role in bioactivity of biomaterials. The previous investigations [78] of melt-derived glasses show that if the surface area that developed on glasses in simulated test solutions is in the range of 200-500 m^2/g, they bond with bone in-vivo within 10 to 30 days. In contrast, if the surface area develops less than 0.1 m^2/g when exposed to simulated test solutions, the compositions of glass do not bond to bone and are not bioactive.

Compared with conventional Bioglass®, all the sol-gel derived powders initially have considerably larger surface areas, ranging from 200 m^2/g to 650 m^2/g, which increase even more after reactions in tris-buffered solutions (See Chapter VI). Therefore, the gel-derived powders are predicted to be good candidates for bioactive materials based upon earlier work [78].

The total pore volume of the powders ranges between 0.3 and 0.6 cm^3/g and basically decreases with increasing SiO_2 content. The average pore radii varies from 1.4 nm to 6.0 nm for the various compositions and also decreases with increasing SiO_2 content as shown in Figure 4.4.

The general trend of the surface area of gel-derived powders increaseing with the SiO_2 content demonstrated in Figure 4.5, was also found in the Na_2O-SiO_2 binary system [188], though the latter was made from TMOS with a different
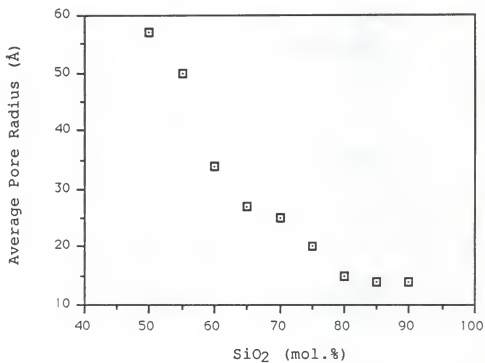
Figure 4.4   Variation of pore size with
SiO_2 content.
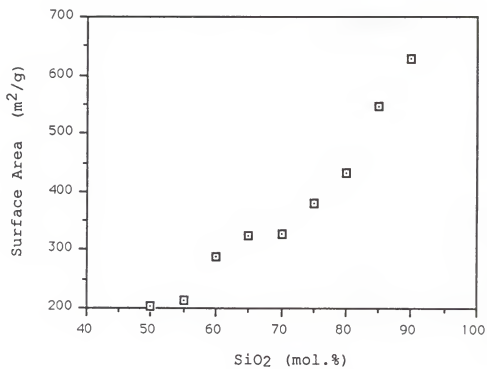
Figure 4.5   Variation of surface area with SiO_2 content.

R ratio and the preparative conditions are not comparable. The surface area of dried Na_2O-SiO_2 gels varied as a function of SiO_2 content is shown in Figure 4.6. The surface area increased with SiO_2 content drastically. In contrast, in the TiO_2-SiO_2 system [219], there was no significant changes in surface area with increasing SiO_2 content for the dried TiO_2-SiO_2 gels. This demonstrates that structures of silicate based gels change differently when second components are introduced into the pure silica gel system.

Silica gels are essentially agglomerates of elementary particles of SiO_2, the size of which may be about 10 nm depending on the composition. The aggregates of particles formed by primary particles are so-called secondary particles [171]. It is well known that CaO is a glass modifier as well as Na_2O. When added to a pure silica system, both break the SiO_2 network and loosen the structure which may cause an increase in particle size resulting in an increase in pore size and increase in total pore volume of the gel network. In BET theory, the surface area is proportional to the total pore volume and inversely proportional to the pore size. The decrease in surface area of the gel-derived powders with an increasing CaO content suggests that the effect of CaO content on the average pore size outweighs that of the total pore volume. In contrast, TiO_2 is a glass network former which does not break up the silica network and loosen the
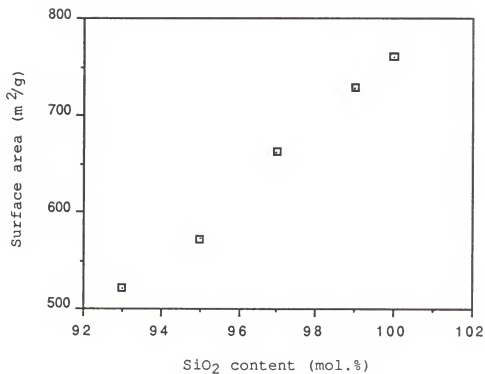
Figure 4.6   Variation of surface area with SiO_2 content of dried gels in Na_2O-SiO_2 system [188].

structure so it is reasonable that the effect of TiO_2 as a second component differs from Na_2O or CaO. Binary SiO_2-P_2O_5 sol-gel systems have not been studied. Therefore, there is little information from which to generalize the findings of this study to other systems.

Pure silica dried gels have surface areas between 300 m^2/g to 760 m^2/g depending on the preparative conditions, the catalyst used, the R ratio and the schedules of aging, drying and densification [140,142,220].

CHAPTER V
BIOACTIVITY OF GEL-DERIVED POWDERS

5.1 INTRODUCTION

Bioactivity is the characteristic of an implant material which allows it to form a bond with living tissues [30,34]. Materials that are not bioactive form a nonadherent layer of fibrous tissue at the implant interface. In contrast, bioactive materials develop an adherent interface with tissues even when the material has a smooth surface. This type of material with a controlled surface reactivity will induce a direct chemical bond between the implant and surrounding tissues.

It was found that a bioactive glasses or glass-ceramics form a calcium and phosphorus-rich layer which consists of small crystallites of hydroxyapatite [39] on its surface in a simulated body fluid (i.e. in the so-called QA test or in-vitro test, see Chapter III) but non-bioactive glasses or glass-ceramics do not have this character. Therefore, the formation of a surface hydroxyapatite layer in a simulated body environment [39] can be considered as the essential condition for materials such as glasses or glass-ceramics to bond to bone. Bioactivity can thus also be defined as the

ability of a material to form a surface hydroxyapatite layer in a controlled simulated body fluid.

Accordingly, bioactivity or hydroxyapatite formation of the gel-derived powders in this work was determined after exposure in the tris-buffered solution for various periods by using FTIR spectroscopy, X-ray diffraction analysis and other techniques. The relationship between the formation of surface hydroxyapatite layer and the composition of gel-derived powders and the exposure time were investigated.

5.2 FTIR Reflection Spectra

Figures 5.1-5.4 show the FTIR diffuse reflectance spectra of the gel-derived powders of various compositions after exposure to tris-buffered solutions for 1, 2, 4 and 8 hours respectively. Figures 5.5 and 5.6 are FTIR spectra of the 77S gel-derived powders after reaction in the tris-buffered solutions for 1 and 6 days respectively. The FTIR spectrum for the 86S gel-derived powders, which contain 90 mol.% SiO_2, 4 mol.% P_2O_5 and 6 mol.% CaO, after an exposure time of 7 days in the in-vitro test solution is shown in Figure 5.7.

As a comparison, the FTIR spectrum for 45S5 Bioglass® powder derived by the conventional melt method before reaction in the tris-buffered solutions is illustrated in
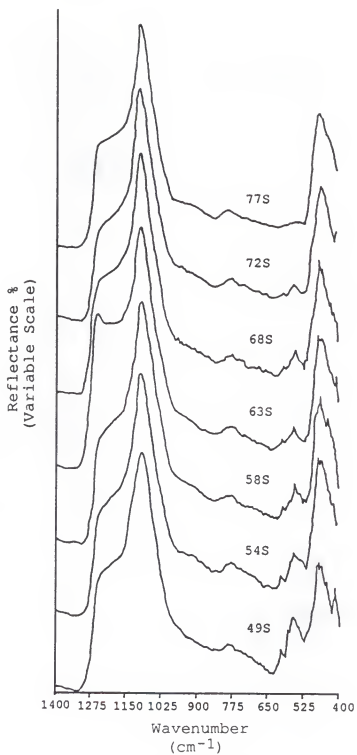
Figure 5.1 FTIR spectra of gel-derived powders with various compositions after 1-hour reaction.
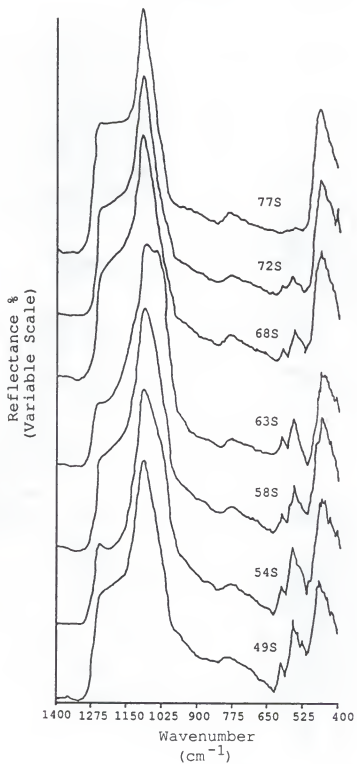
Figure 5.2 FTIR spectra of gel-derived powders
with various compositions after
2-hour reaction.
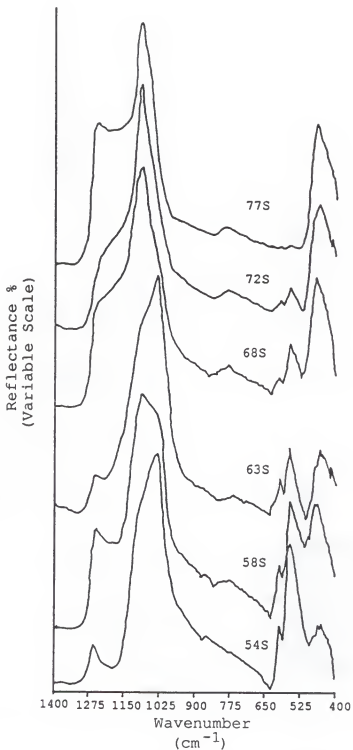
Figure 5.3   FTIR spectra of gel-derived powders
             with various compositions after
             4-hour reaction.
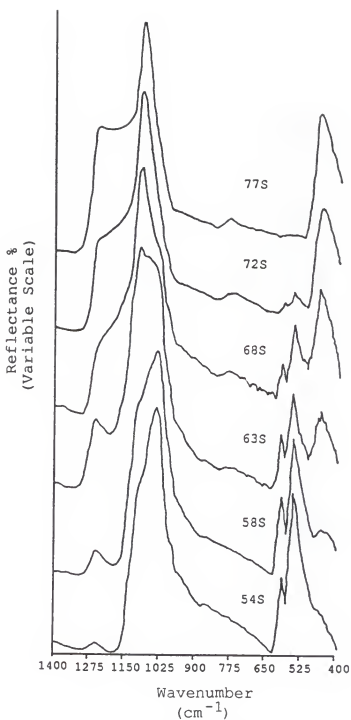
Figure 5.4   FTIR spectra of gel-derived powders
with various compositions after
8-hour reaction.
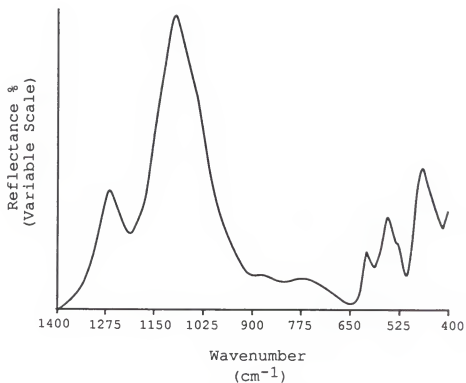
Figure 5.5   FTIR spectrum of 77S gel-derived
            powders after 1-day reaction.
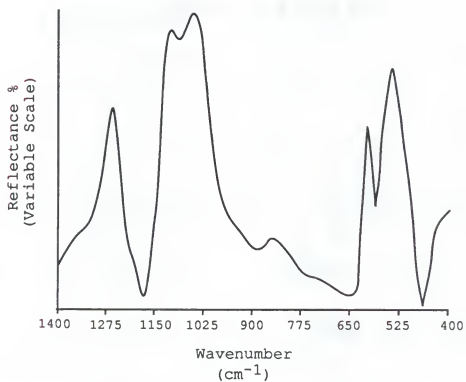
Figure 5.6 FTIR spectrum for 77S gel-derived
powders after 6-day reaction.
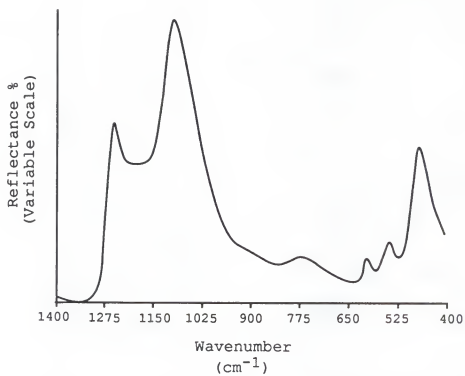
Figure 5.7 FTIR spectrum of 86S gel-derived
            powders after 7-day reaction.

Figure 5.8 with the appropriate peak assignments. Figure 5.9 depicts two FTIR spectra of melt-derived glass powders, 45S5 Bioglass® and 60S which contains 60 mol.% SiO_2, after 20 hours in tris-buffered solutions.

In principle, conventional Bioglasses® contain less than 60 mol.% SiO_2, have a high Na_2O and CaO content and a high calcium/phosphorus (Ca/P) ratio. For instance, 45S5 Bioglass® contains 24.5 wt % Na_2O, 24.5 wt % CaO and a Ca/P ratio of 5.2. When those materials in the form of either bulk or powder are exposed to water or body fluids, several key reactions occur in the system. There is a cation exchange of Na^{+1} and Ca^{+2} cations from the glass for protons in the solution producing silanol groups by hydrolysis of the surface silica [87].

The cation exchange also increases the hydroxyl concentration of the solution which leads to attack of the silica glass network producing additional silanol formation and controlled interfacial dissolution [63]. As the interfacial pH becomes more alkaline, the hydrolyzed surface silanol groups repolymerize producing a silica rich surface layer [63]. Another consequence of the alkaline pH at the glass solution interface is that CaO and P_2O_5, which have been released into solution during network dissolution, crystallize into a mixed hydroxycarbonate apatite (HA) on the surface [63]. The crystallites of the hydroxyapatite
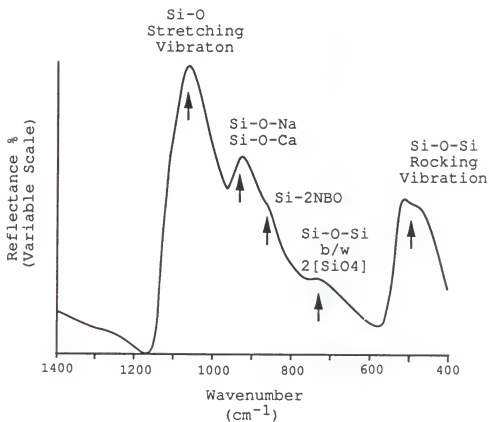
Figure 5.8 FTIR spectrum of 45S5 Bioglass®
before reaction [66].
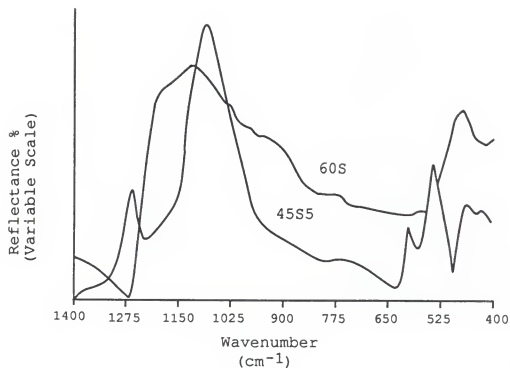
Figure 5.9 FTIR spectra of 45S5 Bioglass® and
60S after 20-hour reaction [66].

phase are proposed to bond to interfacial metabolites such as mucopolysaccharides and collagen [63]. It is hypothesized that this incorporation of organic biological constituents within the growing HA and SiO_2-rich layers appears to be the initial step in establishing bioactivity and bonding to tissues [34].

Studies have shown that there is a minimum rate of hydroxyapatite formation which is necessary to achieve bonding with hard tissues [35]. Both the glass composition and the microstructure exert influences on the development and growth of the HA phase.

The peak assignments for the spectrum of 45S5 Bioglass® before the reaction are in Figure 5.8 (also see Chapter IV). Figure 5.9 shows that after reaction, a pair of peaks from hydroxyapatite are present in the FTIR spectrum from the 45S5 Bioglass® surface. These peaks grow as the broad Si-O-Na and Si-O-Ca peaks, shown in Figure 5.8 for 45S5 Bioglass® before reaction, disappear. In contrast, the melt-derived 60S composition does not develop any apatite layer, even after several weeks in the solution [35]. In fact, the 45S5 Bioglass® is very bioactive and bonds to both hard and soft tissues while 60S is not bioactive and does not bond to bone or soft tissues [35]. This result indicates that the maximum SiO_2 content that can be present in melt-derived glasses and still exhibit bioactivity is around 60 mole percent. As the

SiO_2 content of the standard melt-derived bioactive glasses approaches and exceeds 60 mole percent, the rates of network dissolution and hydroxyapatite crystallization are retarded and the bioactivity is reduced and eventually eliminated.

The only difference between the spectra for melt-derived and the gel-derived samples is a slight shift of the 1095 cm^{-1} Si-O-Si stretching vibrational mode towards lower frequencies for the gel-derived powders (see Figure 5.5, 5.6, 5.7, 5.8 and Figure 5.9) which could in part be due to a certain degree of strain in the Si-O-Si bridging bonds at the surface of the gel pores. This phenomenon was investigated by Alneida et al. using Kramers-Kronig analysis [221]. It has been found that in dried or partially densified gels the Si-O-Si bridging sequences usually were strained at the surface of the gel pores, with larger bridging angles and longer Si-O-Si bonds, the latter effect being dominant. The same explanation could also be applied to the shift to lower frequencies of the peak at 800 cm^{-1} assigned to the symmetric Si-O-Si vibration.

The gel-derived powders contain no Na_2O. Comparing Figure 5.1 with Figure 4.3, which shows the FTIR reflectance spectrum of the gel-derived powders before exposure to the test solution, the peak at 950 cm^{-1}, which is associated with the presence of Si-OH bonds in the tetrahedra at the surface, disappeared during reaction of those powders with a lower

silica content, such as 49S, 54S and 58S. The loss of the Si-OH bonds indicates that a reaction layer was formed. The comparison also shows that after only one hour reaction in the tris-buffered solution, the peaks at 1025 cm^{-1}, assigned to Si-O with 1 NBO (non bridging oxygen), and 938 cm^{-1} assigned to Si-O-Si with 2 NBO, disappear. The symmetric Si-O-Si stretching vibration at about 800 cm^{-1} is related to the Si-rich surface layer newly formed through the condensation reaction stated earlier [217]. This peak intensity increases and shifts to lower wavenumbers with longer reaction times. The following surface reaction would account for this observation:

$$Si-O-Ca-O-Si \xrightarrow[\text{of Ca ions}]{\text{release}} Si-O^- + {}^-O-Si \longrightarrow Si-O-Si \quad (5.1)$$
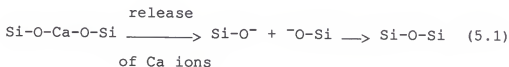
Two new peaks appear at 598 cm^{-1} and 566 cm^{-1} (Figure 5.1-5.4), which are very similar to the spectrum of 45S5 Bioglass® in Figure 5.9. These two peaks are assigned as P-O bonding vibrations in the [PO$_4$] tetrahedra [207] and are characteristic of a hydroxyapatite crystalline phase. The appearance of these vibrational modes indicates that a surface hydroxyapatite layer has formed. The P-O stretching vibration mode of a [PO$_4$] unit occurs in the range of 1030 cm^{-1} to 1120 cm^{-1}. Since there is a strong vibration mode of

the Si-O-Si bond in the [SiO$_4$] tetrahedra located at the same region, they are superimposed and it is hard to distinguish the P-O vibration from the Si-O-Si vibration.

When gel-derived powders with lower SiO$_2$ content, such as 54S and 58S, were reacted for 4 hours, a small peak appears around 918 cm^{-1}. This peak can be assigned as a C-O vibration mode in CO$_3^{-2}$, which results from the CO$_3^{-2}$ anion being taken from solution and incorporated within the apatite crystal lattice. Carbonate solid solution is a well-known phenomenon for apatite crystals [222].

With a reaction time of only one hour, the characteristic hydroxyapatite peaks at 598 cm^{-1} and 566 cm^{-1} increase their intensities for most compositions, including 49S, 54S, 58S, 63S and 72S gel-derived powders. However, no such peaks were found for 77S gel-derived powders within a one-hour reaction time. The intensities of those characteristic hydroxyapatite peaks decrease with increasing SiO$_2$ content in the gel-derived powder composition. The same trend can be observed after 2, 4 and 8 hours reaction (Figure 5.1-5.4).

The peaks at 598 cm^{-1} and 566 cm^{-1} increase their intensities rapidly with reaction time for all compositions except 77S, which is indicative of extremely fast formation of the hydroxyapatite phase on the surface (Figure 5.2-5.4).

The Si-O-Si rocking vibration peak at 482 cm^{-1} is diminished for the 54S and 58S gel-derived powder samples and replaced by the P-O bending vibration in the [PO$_4$] groups of hydroxyapatite after eight hours reaction in the tris-buffered solutions (Figure 5.4). This indicates that for both 54S and 58S gel-derived powders the formation of surface hydroxyapatite layer is completed within that period of time.

The hydroxyapatite layer does not develop on the surface of the 77S gel-derived powders until the reaction time reaches 1 day (Figure 5.5). After reacting with the tris-buffered solution for 6 days, the surface of the 77S gel-derived powders is totally covered by the hydroxyapatite crystalline layer, as shown in Figure 5.6. The characteristic peaks at 566 cm^{-1} and 598 cm^{-1} for hydroxyapatite replace the Si-O-Si rocking vibration peak at 462 cm^{-1}.

Even 86S gel-derived powders, which contain 90 mol.% SiO$_2$, only 4 mol.% P$_2$O$_5$ and 6 mol.% CaO, develop a surface hydroxyapatite layer after exposed to a tris-buffered solution for 7 days. It is surprising that the gel-derived powders with such high SiO$_2$ content can form a hydroxyapatite surface layer after exposure in the test solution within 7 days, whereas the 60S melt-derived glass powders do not develop any hydroxyapatite surface layer even after several weeks reaction [35].

Thus, for conventional melt-derived bioactive glasses or glass-ceramics, the SiO_2 compositional boundary is only 60 mol.%, but for gel-derived powders it is extended considerably up to 90 mol.% silica.

Since the source of calcium and phosphorus for the hydroxyapatite surface layer is the parent gel powders, it should be noted that as the silica compositional limit for hydroxyapatite formation is extended, the kinetics or rate of hydroxyapatite formation is retarded to some extent as the CaO content of the gel-derived powders decreases. This is probably because the increase in SiO_2 content in the composition is at the expense of CaO content. For example, the composition which has 90 mol.% SiO_2 (86S) contains only 6 mol.% CaO. This is a small fraction (<1/4) of the CaO content in the standard 45S5 formula. Consequently, the interpretation of the influence of SiO_2 content on hydroxyapatite formation is complicated.

5.3 X-Ray Diffraction Analysis

The formation of a surface hydroxyapatite layer on the gel-derived powders is confirmed by X-ray diffraction analysis.

Figure 5.10 shows the X-ray diffraction spectra for the 58S bioactive gel-derived powders before and after 8-hour
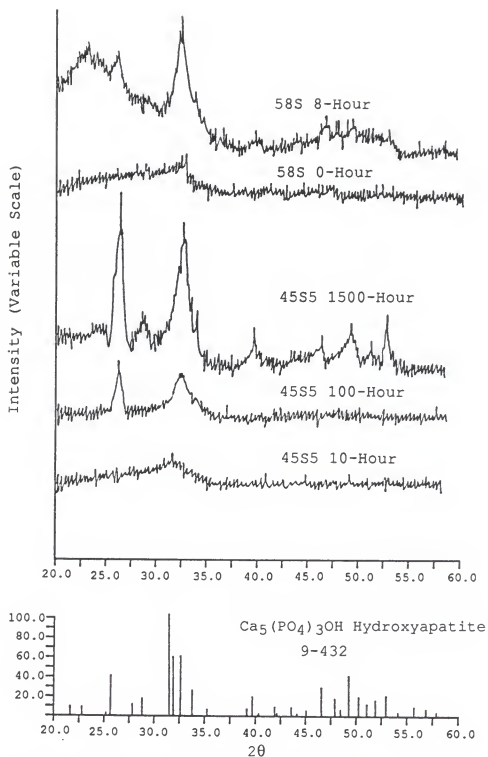
Figure 5.10   X-ray diffraction spectra of 45S5
Bioglass® and 58S gel-derived powdrs
after various reaction times in
tris-buffered solution.

reaction in the tris-buffered solutions. The X-ray diffraction spectra of 45S5 Bioglass® after reaction in tris-buffered solutions for 10 hours, 100 hours and 1500 hours are also illustrated in the figure as comparisons.

As mentioned before, the three most intense X-ray diffraction lines from hydroxyapatite are located at 2θ angles of 31.76° (I/I_1=100%), 32.20° (I/I_1=60%) and 32.91 (I/I_1=60%). However, the peaks representing those lines can not be separately resolveed on the spectrum as they occur at very close intervals. Instead, a superimposed single strong peak appears at a 2θ angle of 32° (± 0.5 degrees). The spectrum of the unreacted 58S gel-derived powders (58S-0HR) exhibits a slight peak at 32°, which is possibly due to the effect of sintering temperature (600°C for 3 hours) combined with the increased reactivity of the glass. It has been noticed that even though the crystallization temperature for 58S is about 900°C, as confirmed by its DTA curve (Figure 4.1), the increased reactivity of the gel-derived powders may have resulted in so-called "hydroxyapatite-precursors" nucleating at lower temperatures. Since the intensity is so weak, the observed peak is probably due to a small percentage of partially ordered crystallites on the surface.

In contrast, after reaction the 58S gel-derived powders develop strong X-ray diffraction peaks, which index as hydroxyapatite (JCPDS card #9-432). It requires only 8 hours

reaction in the in-vitro testing environment for the hydroxyapatite layer to form. As for 45S5 Bioglass®, the spectrum does not show any crystalline pattern after reaction for 10 hours (Figure 5.10). It requires more than 100 hours to demonstrate sharp hydroxyapatite peaks for the melt-derived 45S5 Bioglass® (Figure 5.10).

The X-ray diffraction spectra along with the FTIR reflection spectra suggest that the 58S gel-derived powders have a very rapid rate of hydroxyapatite formation on the surface. The explanation for the rapid rate of HA formation is the presence of very small pores and large surface area in the gel-derived powders (Table 4.1) which will be discussed in more detail in the following chapters.

5.4 Solution Behavior

5.4.1 pH Variation

The development of hydroxyapatite on the surface of the material is a time dependent phenomenon. The rates of formation of hydroxyapatite vary greatly for different bioactive glass or glass-ceramics depending on composition and structure. Both the interfacial solution pH and the ratio of surface area to solution volume will affect the rate of the formation of hydroxyapatite.

Figure 5.11 depicts the variation of pH of the tris-buffered solution as a function of reaction time for the 58S gel-derived powders. It is observed that there is a sharp increase in pH at the beginning, i.e. within 30 minutes. The pH curve of the solution then flattens and gradually approaches the value of pH=8.1 by 250 minutes.

The 58S gel-derived powders contain no Na_2O which is typically ascribed to be the reason for the pH change of bioactive glass solutions [63]. However, CaO is present in the gel-derived powders. Figure 5.11 indicates that there is a cation exchange of Ca^{+2} cations from the powders for protons or hydroniums in the solution producing silanols on the surface of the powders, i.e.,

$$Si-O-Ca-O-Si + 2H_2O \rightarrow 2Si-OH + Ca^{+2} + 2OH^{-1} \quad (5.2)$$
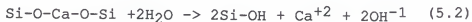
It is this cation exchange reaction that causes the increase of the hydroxyl group concentration in the solution. Since the gel-derived powders are porous with a huge surface area (Table 4.1), consequently, they are very reactive and the rate of equation 5.2 is very rapid. This may explain the sharp increase in pH at the early stages of the exposure. As the interfacial pH becomes more alkaline, the following repolymerization reaction occurs:
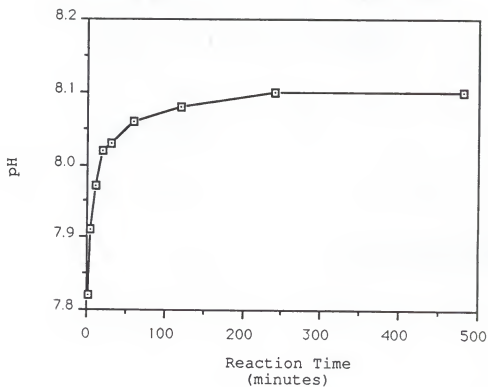
Figure 5.11   Variation of pH as a function of
reaction time of 58S gel-derived
powders.

$$2SiOH \rightarrow Si-O-Si + H_2O \qquad (5.3)$$
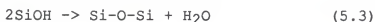
The variation of pH of the testing solution as a function of reaction time for 45S5 Bioglass® powders prepared by melting and crushing is demonstrated in Figure 5.12. These are non porous powders. The increase in pH does not appear as sharp as that for the 58S gel-derived powders, but continuously changes its value with the reaction time (Figure 5.12). The pH continually increases its value and reaches 7.95 after a reaction time of 500 minutes. The increase in pH is due to cation exchange of both Na^{+1} and Ca^{+2} from the glass for protons or hydronium ions in the solution as mentioned earlier.

McGrail [69] found the ion exchange of cation ions from glass for protons or hydronium ions to be independent of pH in the interval from pH=6 to pH=9. Silica dissolution occurs at pH of 9 and increases rapidly above this pH [61]. The pH of the reacted solution remains at 8.1 after 8 hours reaction for the 58S gel-derived powders. This suggests that the ion exchange reaction proceeds very rapidly at the early stage for the gel-derived 58S powders after exposure to the tris-buffered solution.
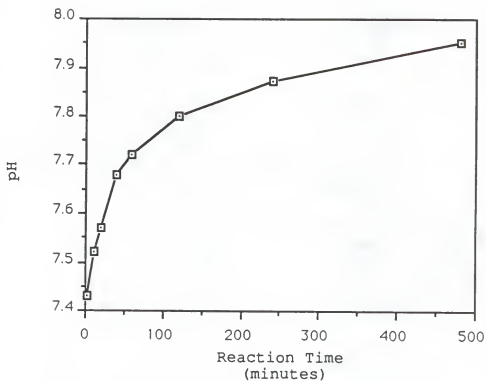
Figure 5.12 Variation of pH as a function of
reaction time of 45S5 Bioglass®
powders.

5.4.2 ICP Analysis

The calcium (Ca), phosphorus (P), sodium (Na) and silicon (Si) ion concentrations in the reacted solutions were measured by Inductively Coupled Plasma (ICP) analysis. According to the estimated concentrations of various ions of unknown samples, wavelengths of emission lines were chosen at 317.83 nm, 213.62 nm, 589.59 nm and 288.16 nm for Ca, P, Na and Si ions respectively. The emission types were atomic for all ions except for the Ca^{+2} ion, which is ionic.

The variation in solution concentration of these ions as a function of reaction time for 58S gel-derived powders are in Figures 5.13, 5.14, 5.15 and 5.16. Figures 5.17, 5.18, 5.19 and 5.20 are the variations of Na, Ca, P and Si ions in the tris-buffered solutions as functions of reaction time for melt-derived 45S5 Bioglass® powder samples. The ICP data for 45S5 Bioglass® bulk samples were reported by Kim [66] and are also plotted in Figure 5.17 to 5.20 for comparison. The ratio of surface area of the sample to solution volume (SA/V) is high for a finely ground 45S5 Bioglass® powders, 1 to 10 cm^{-1}. In contrast, SA/V ratio for 45S5 Bioglass® bulk sample is only less than 0.1 cm^{-1}. The data show that both 58S gel-derived powders and the surface reactive 45S5 Bioglass® samples produce changes in the local pH as Ca, P and Na ions
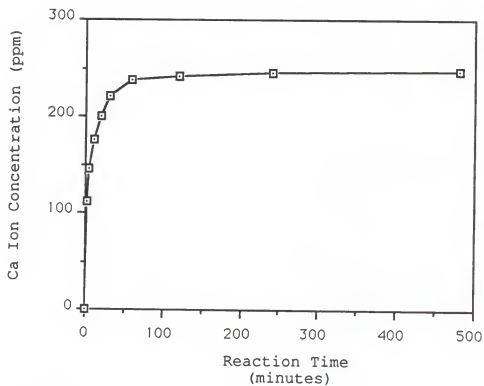
Figure 5.13 Calcium ion oncentration in reacted
solution versus reaction time for 58S
gel-derived powders.
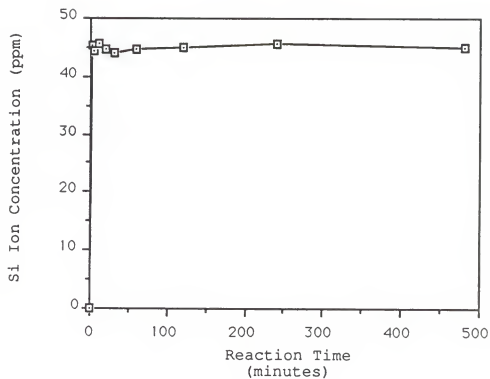
Figure 5.14   Silicon ion concentration in reacted
               solution versus reaction time for 58S
               gel-derived powders.
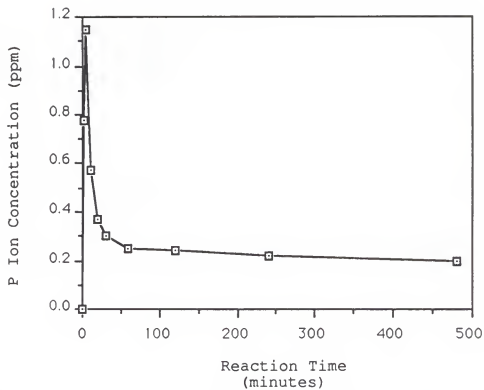
Figure 5.15   Phosphorus ion concentration in reacted
solution versus reaction time for 58S
gel-derived powders (I).
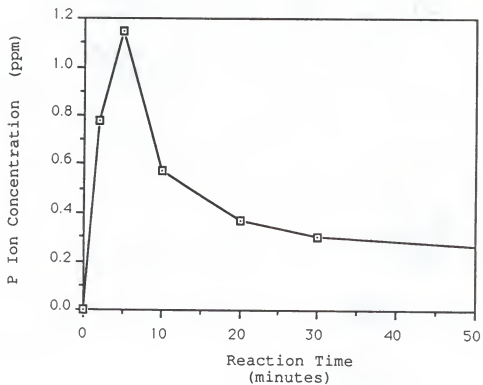
Figure 5.16 Phosphorus ion concentration in reacted
solution versus reaction time for 58S
gel-derived powders (II).
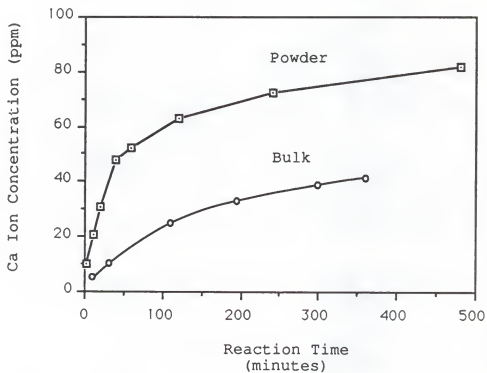
Figure 5.17   Calcium ion concentration in reacted solution versus reaction time for 45S5 Bioglas® powders and bulk samples.
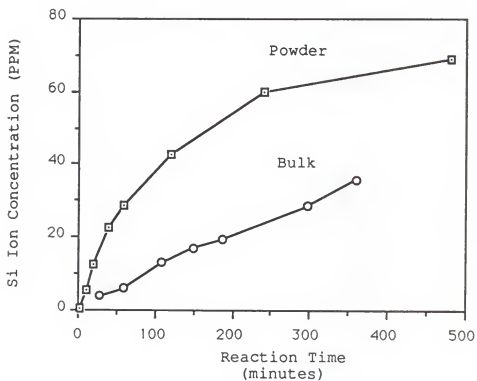
Figure 5.18   Silicon ion concentration in reacted
solution versus reaction time for 45S5
Bioglass® powders and bulk samples.
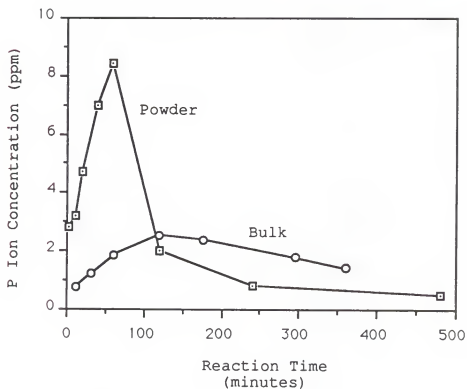
Figure 5.19   Phosphorus ion concentration in reacted
solution versus reaction time for 45S5
Bioglass® powders and bulk samples.
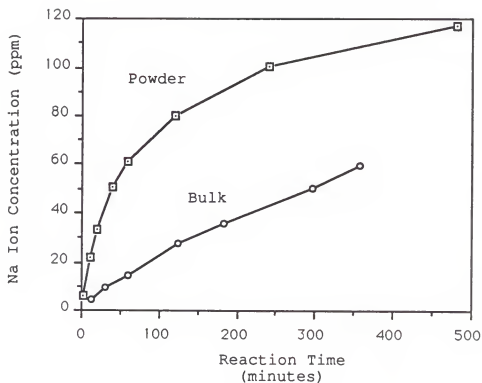
Figure 5.20   Sodium ion concentration in reacted
solution versus reaction time for 45S5
Bioglass® powders and bulk samples.

are exchanged for protons or hydronium ions from the solution.

The same trend is observed for the increasing rate of Ca ion concentration in the solution reacted with 58S gel-derived powders (Figure 5.13) as with 45S5 Bioglass® powders (Figure 5.17). However, Ca ions in 58S gel-derived powders release into the reacting solution more quickly and approach a higher concentration of approximately 250 ppm after only 30 minutes reaction. In contrast, for 45S5 Bioglass® powders, Ca ions release relatively slowly but continually increase in concentration. The Ca ion concentration reaches 85 ppm after a reaction time of 500 minutes.

Si ion concentration jumps to about 45 ppm after less than 2 minutes reaction and remains at almost the same value with reaction time in the solutions reacted with 58S gel-derived powders (Figure 5.14). However, Si content increases gradually with reaction time in the solution reacted with 45S5 Bioglass® powders (Figure 5.18). This observation shows that Si ion release in the solution with 58S gel-derived powders is very rapid at the beginning and quickly reaches a dynamic equilibrium. The results suggest that the surface is stabilized and the leaching process of Si ions is retarded even before hydroxyapatite crystals are observed by FTIR or X-ray diffraction techniques.

Na ion concentrations in solution increase their values continuously from melt-derived powders and bulk 45S5 Bioglass® samples. This indicates that Na ions keep releasing from the Bioglass® powders and bulk samples into the solution during the entire reaction (Figure 5.20).

It is important to notice that the phosphorus ion concentrations drop in the solutions after a certain reaction time for all 58S gel-derived powders and 45S5 Bioglass® bulk and powder samples (Figure 5.15 - 5.16 and Figure 5.19). The P ion concentrations in the solution drop after only 5 minutes for 58S gel-derived powders. However, for 45S5 Bioglass® powders, the time for phosphorus ion concentrations to drop takes more than 60 minutes. For bulk Bioglass® samples, the time for the phosphorus concentrations to decrease increases to 120 minutes.

This phenomenon can be explained by the uptake of P ions from solution as the hydroxyapatite layer develops on the sample surface [66]. Because of the more rapid rate of P ion release, the formation of the hydroxyapatite layer occurs at shorter reaction times for 58S gel-derived powders than that for 45S5 Bioglass® powders and much shorter than that for 45S5 Bioglass® Bulk samples.

After 45S5 Bioglass® powders and 58S powders are reacted with the solution for more than 500 minutes, a very small amount of P ions is found in the solution (Figure 5.16

and Figure 5.19). The decrease of phosphorus in the solutions after a certain reaction time is due to precipitation onto the gel or the glass surface which is related to the formation of hydroxyapatite. The shorter phosphorus uptake time of 58S gel-derived powders indicates again that 58S develops surface hydroxyapatite more quickly than 45S5 Bioglass® powders. This comparison of the time-dependent ion release for gel samples versus melt-derived samples is supported by FTIR and X-ray diffraction analysis results.

The surface area plays an important role in the rate of development of hydroxyapatite crystals. The surface area to volume ratio, SA/V, is more than 5000 cm^{-1} for 58S gel-derived powders, whereas it is only 1 to 10 cm^{-1} for very fine powders of 45S5 Bioglass®. This gives an explanation for the fast leaching rate of cation ions and rapid formation of surface hydroxyapatite crystals for gel-derived 58S powders.

Comparing the powder samples with the bulk samples of melt-derived 45S5 Bioglass®, (Figure 5.17 to Figure 5.20), it has been found that the Ca, Si and Na ion concentrations increase more rapidly and reaches higher values for the powders than for the bulk samples. Also, the peak of the phosphorus concentration curve appears at a longer reaction time of about 2 hours for bulk 45S5 Bioglass® samples with a surface area to volume ratio (SA/V) of only 0.1 cm^{-1} [66,223]. Figure 5.21 shows the SA/V dependence of 45S5
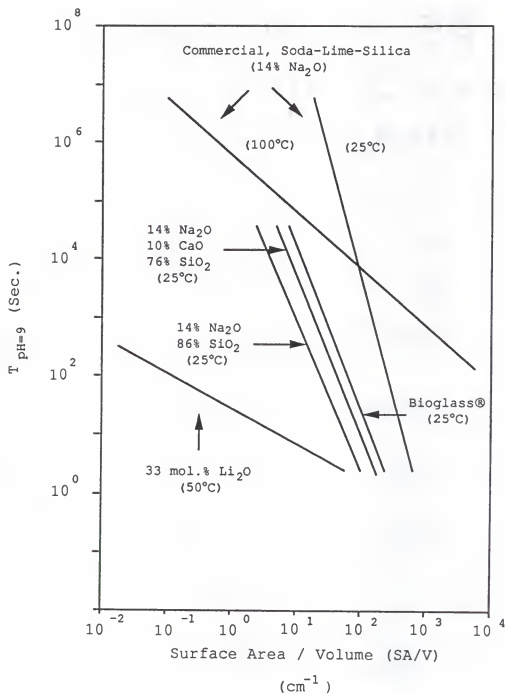
Figure 5.21 The time required for a static buffered
solution to reach pH=9 versus SA/V ratio
[224].

Bioglass® with reaction time [224]. The time required for a static buffered solution to reach pH=9 is plotted versus SA/V. Consequently, 45S5 Bioglass® bulk samples with very small surface area show a much slower rate of formation of surface hydroxyapatite crystals.

5.5 Changes In Texture

It was mentioned in Chapter IV that the surface areas of all the sol-gel derived compositions are extremely high ranging from 200 m^2/g to 650 m^2/g (Table 4.1). The exposure to the tris-buffered solutions increases these surface areas even further. The variation of surface area as a function of reaction time for 58S gel-derived powders is shown in Figure 5.22. The initial surface area of 58S gel-derived powders is 289 m^2/g. The surface area continues to increase at the early stage of the reaction and approaches 400 m^2/g after only 4-hour reaction. This observation confirms the very bioactive nature of 58S gel-derived powders.

In summary, besides the difference of the surface nature between the gel-derived powders and the melt-derived Bioglasses®, the surface area or the surface area to volume ratio, SA/V, is very important for the formation rate of the hydroxyapatite surface layer. The gel-derived powder with a larger surface area has a more rapid rate of formation of
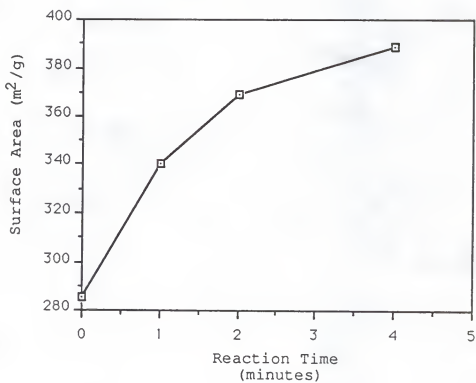
Figure 5.22   Variation of surface versus reaction
             time for 58S gel-derived powders.

hydroxyapatite than the conventional melt-derived Bioglass®. It suggests that the larger surface area or SA/V ratio provides a higher density of nucleation sites for crystallization of hydroxyapatite.

CHAPTER VI
VARIABLES AFFECTING BIOACTIVITY OF GEL-DERIVED POWDERS

6.1 Compositional Effect

6.1.1 SiO$_2$ Effect

The bioactivity of biomaterials are affected by many factors including composition, texture, porosity, interfacial pH , age and type of tissues, type of animals, etc. Only the compositional and the textural effects on the bioactivity of gel-derived powders developed in this study will be discussed in this chapter.

In the previous literature review, it was described that for melt-derived bioactive glasses their bioactivity depended greatly upon composition, especially silica (a glass network former) content. Bioglasses with a composition containing 45 wt.% SiO$_2$, 24.5 wt.% Cao, 24.5 wt.% Na$_2$O and 6.0 wt.% P$_2$O$_5$, i.e. 45S5 Bioglass®, has the highest level of bioactivity. As SiO$_2$ content increases, the bioactivity decreases due to the change of glass from an amorphous structure comprised primarily of ionically bonded 2-dimensional sheets or chains to a 3-dimensional structure.

In our work, a series of compositions was designed and successfully synthesized as listed in Table 3.1. At a constant P_2O_5 content, the SiO_2 content was varied from 50 mol.% to 95 mol.% at the expense of CaO content. Figures 5.1 to Figure 5.4 depict Fourier transform infrared reflection (FTIR) spectra of gel-derived powders with those compositions after reaction in tris-buffered solutions for 1, 2, 4 and 8 hours. As a general rule, the intensities of the hydroxyapatite characteristic peaks at 566 cm^{-1} and 598 cm^{-1} decrease with the increase of SiO_2 content in all figures. An attempt to describe and explain the different rates of formation of the hydroxyapatite surface layer and the compositional dependence is made as follows.

In Figure 6.1, the rate of formation of the hydroxyapatite surface layer for different compositions of the gel-derived powders is compared by the ratio of peak intensities, A_1/A_2, obtained from the FTIR spectra, where A_1 refers to the intensity of P-O bending vibration at about 566 cm^{-1} and A_2 refers to Si-O-Si bending vibration at about 482 cm^{-1}. The ratio was calculated and plotted as a function of reaction time. The increasing value of the ratio shows that the rate of hydroxyapatite formation is increasing with decreasing SiO_2 content of the gel-derived powders. It also shows there is a delay in HA formation with an increase of SiO_2 content at early stages for the gel-derived powders.
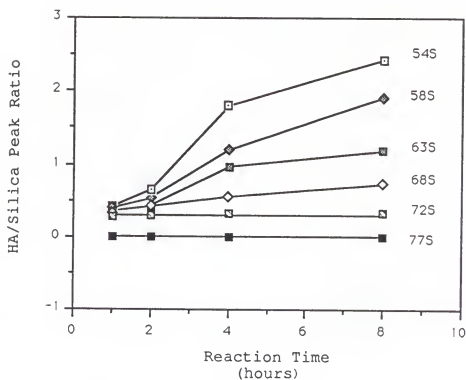
Figure 6.1   Ratio of hydroxyapatite peak intensity
to silica peak intensity as function of
reaction times for gel-derived powders.

This ratio of hydroxyapatite peak intensity to silica peak intensity, A_1/A_2, increases very rapidly for gel-derived 54S and 58S at the early stages compared to that of the melt-derived 45S5 Bioglass®, which does not show any characteristic crystalline hydroxyapatite peak until 2 hours reaction in the tris-buffered solutions.

The FTIR spectra in Chapter V show that if the exposure time is increased to seven days, HA formation is also demonstrated for the gel-derived powders containing up to 90 mol.% SiO_2, i.e. 86S gel-derived powders (Figure 5.7), while a calcium phosphate-rich layer does not form at the surface of the 60S melt-derived bioactive glasses even after exposure time is increased to weeks or months (Figure 5.9). These results indicate that the sol-gel processing of the $CaO-P_2O_5-SiO_2$ gel-derived powders increases the compositional range of bioactivity by a significant amount. It is thus possible to extend the SiO_2 compositional boundary for the formation of hydroxyapatite, i.e. the bioactivity of the materials, up to 90 mol.% SiO_2 by using sol-gel processing (Figure 6.2). This new compositional field of bioactivity is schematically illustrated in Figure. 7.7 on a four component $Na_2O-CaO-P_2O_5-SiO_2$ diagram in Chapter VII.

Thus, an important advantage of the low temperature solution processing of bioactive gel-glasses is the

130
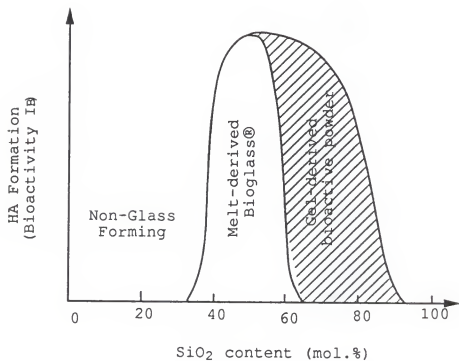
Figure 6.2   The difference in compositional range
             of bioactivity for the gel-derived
             powders and melt-derived bioactive
             glasses.

development of new bioactive compositions. The potential of the sol-gel method has been realized.

6.1.2 P_2O_5 Effect

A previous investigation [33] examined the P_2O_5 dependence of bioactivity in the melt-derived bioactive glasses and found that bone bonding or the formation of surface hydroxyapatite was more favorable within the range of 3-6 wt.% P_2O_5. However, a study carried out in Japan about the bone-bonding ability of P_2O_5-free $CaO \cdot SiO_2$ glasses reported that even P_2O_5-free $CaO.SiO_2$ glass formed a Ca,P-rich layer on its surface and bonded tightly with living bone via these layers [225]. However, the study by Ohura et al. was in a test solution that contained phosphate ions.

It has been concluded that if glasses and glass-ceramics release at least Ca^{+2} and $HSiO_3^{-1}$ ions, this would be sufficient for them to form the Ca,P-rich layer on their surfaces in-vivo, enabling them to bond directly with bone. This is because the in-vivo environment contains a saturated concentration of phosphates. It should be noted that the later conclusion was only based on in-vivo experiments.

In our work, the effect of P_2O_5 on the formation of hydroxyapatite at the surface of gel-derived powders in the $CaO-P_2O_5-SiO_2$ system is examined under in-vitro conditions.

Table 6.1 gives two series of compositions of gel-derived powders with a variation of P_2O_5 content, 58S-nP and 68S-nP (n = 2, 4 and 8). In fact, those compositions were designed based on 58S and 68S gel-derived powders (actually, 58S-4P is 58S and 68S-4P is 68S) by keeping the remaining SiO_2 content constant (60% and 70% for the two series respectively) and changing the P_2O_5 and CaO content. All powders were made by sol-gel processing using the same procedure described in Chapter III. After the powders were dried and heated at 600°C for 3 hours, the BET measurement and X-ray diffraction analyses were applied. After exposure to 37°C tris-buffered solutions for various times, a FTIR spectrospopy analysis of the surface layers was conducted.

The surface areas, total pore volumes and average pore radii of both 58S-np and 68S-np gel-derived series are listed in Table 6.2. Figure 6.3 to Figure 6,6 describe the variation of surface areas and average pore radii with P_2O_5 content for both series. Since P_2O_5 is a glass network former just as SiO_2, the same trend as shown in Table 4.1 is observed for these powders. The surface area increases and the average pore radii decreases with the increase of P_2O_5 content for all the compositions.

Figure 6.7 shows the X-ray diffraction spectra for these compositions. The X-ray diffraction spectra depict a completely amorphous structure for all the compositions

Table 6.1
Compositions of gel-derived powders
with different P_2O_5 content
(in mol.%)

Sample ID	SiO_2	P_2O_5	CaO
58S-2P	60	2	38
58S-4P(58S)	60	4	36
58S-8P	60	8	32
68S-2P	70	2	28
68S-4P(68S)	70	4	26
68S-8P	70	8	22

Table 6.2
BET data of gel-derived powders
with different P_2O_5 content

Sample ID	Surface area (m^2/g)	Total pore volume (cm^3/g)	Average pore radius (Å)
58S-2P	142	0.49	70
58S-4P(58S)	289	0.49	34
58S-8P	343	0.41	24
68S-2P	231	0.44	38
68S-4P(68S)	326	0.41	25
68S-8P	415	0.37	18
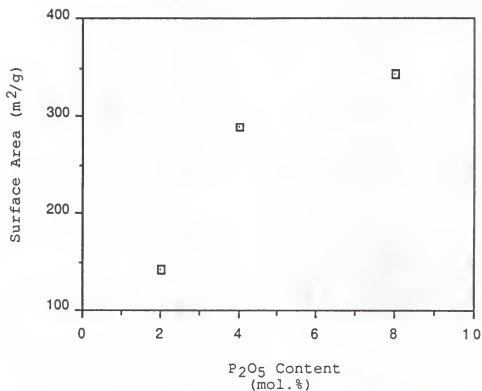
Figure 6.3   Variation of surface area with
             different P_2O_5 contents of 58S
             gel-derived powders.
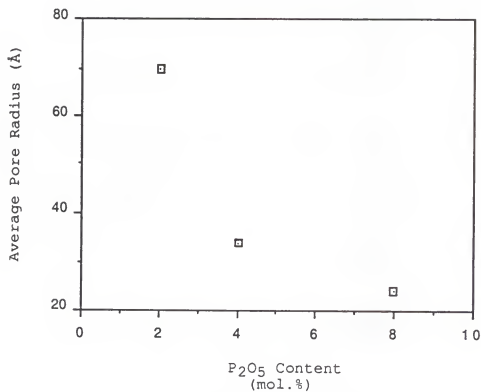
Figure 6.4   Variation of pore size with
             different P_2O_5 contents of 58S
             gel-derived powders.
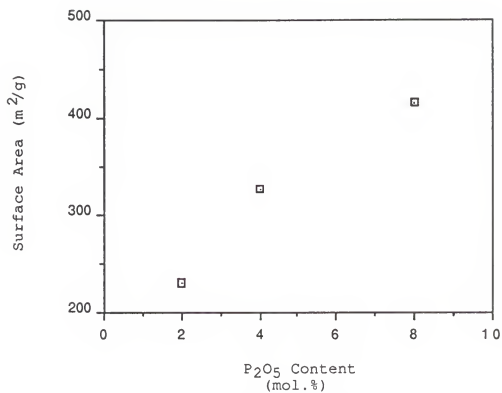
Figure 6.5   Variation of surface area with
different P_2O_5 contents of 68S
gel-derived powders.
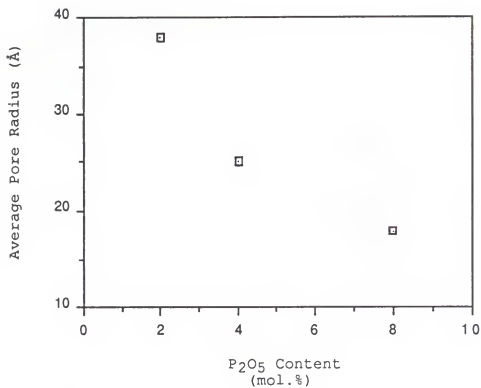
Figure 6.6   Variation of pore size with
              different P_2O_5 contents of 68S
              gel-derived powders.
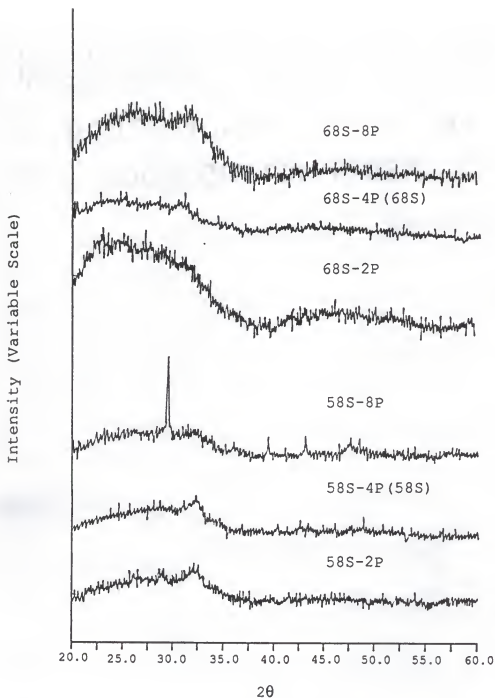
Figure 6.7   X-ray diffraction spectra of gel-derived powders with different P_2O_5 contents.

except 58S-8P, which shows a crystalline peak at 2θ of $29.2°$. This peak is assigned to crystalline calcium carbonate (JCPDS card # 5-586), see Figure 6.8. In this case, calcium must pick up some carbon dioxide from the air and form calcium carbonate during the heat treatment. This process may be promoted by the presence of the higher P content in this composition.

FTIR spectra for the gel-derived powders with variable P_2O_5 content after 8-hour reaction in tris-buffered solutions are shown in Figure 6.9(a) and 6.9(b). It can be seen that the crystalline hydroxyapatite surface layers were formed on all the samples except on the 68S-8P powder in Figure 6.9(b). The general rule of the effect of SiO_2 content on bioactivity of the gel-derived powders still remains. In principle, the 58S-nP series has a higher A_1/A_2 intensity ratio of hydroxyapatite peak at 566 cm^{-1} to silica rocking vibration peak at 482 cm^{-1} in Figure 6.9(a) than does the 68S-nP series in Figure 6.9(b). However, in each series the sample with moderate P_2O_5 content (4 mol.%) has the highest A_1/A_2 ratio. The 68S-8P composition does not develop characteristic hydroxyapatite peaks after exposure to the tris-buffered solutions for 8 hours, but it does form high intensity hydroxyapatite peaks when the exposure time was increased to 48 hours (Figure 6.10).
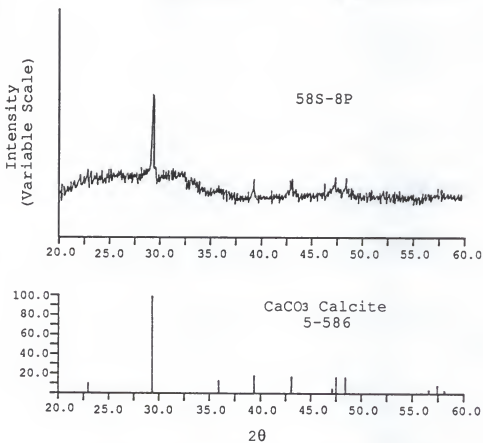
Figure 6.8   X-ray diffraction spectrum of 58S-8P
             gel-derived powders.
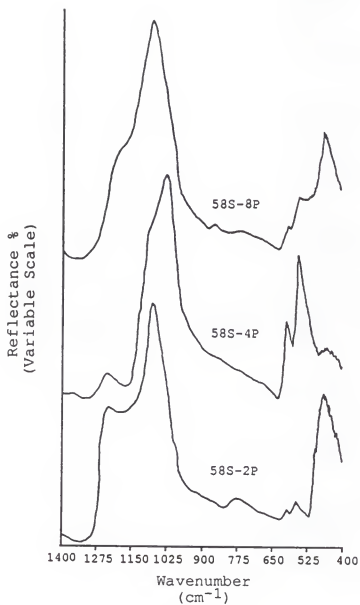
Figure 6.9(a) FTIR spectra of 58S gel-derived
powders with different P_2O_5
contents after 8-hour reaction.
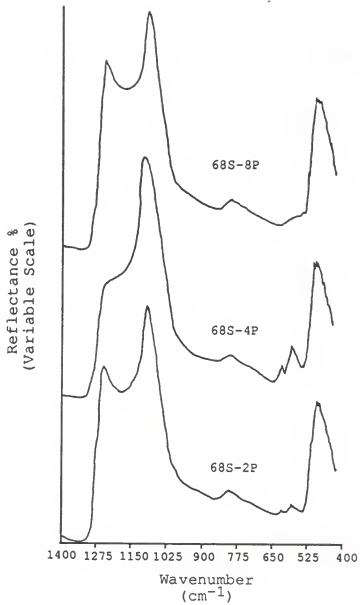
Figure 6.9(b)   FTIR spectra of 68S gel-derived
powders with different P_2O_5
contents after 8-hour reaction.
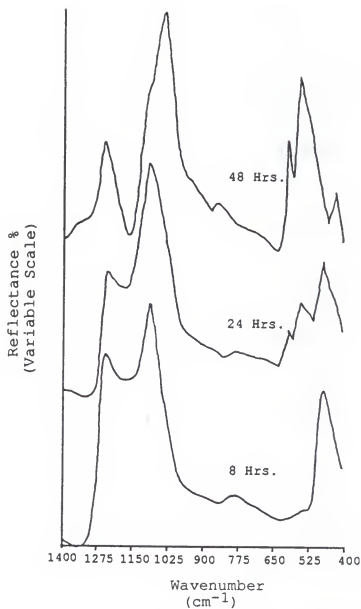
Figure 6.10   FTIR spectra of 68S-8P gel-derived
powders after various reaction times.

In order to understand these results, it is necessary to consider the effects of adding P_2O_5 to a silicate-based structure. Figure 6.11 is a SiO_2-P_2O_5-CaO ternary phase diagram [226]. There is a liquid-liquid separation region in this phase diagram. The reasons for the separation of a liquid into two phases may be found by considering the thermodynamics of a nonideal solution. In such solutions, the attractions between like and unlike atoms are not equal; consequently, there will be an enthalpy change as well as increase in entropy due to mixing of unlike atoms. The presence of the liquid-liquid separation can also be explained through the following mechanism. Phosphorus is a network former which exists in four-fold coordination. Due to the charge of +5 of the phosphorus atom, one of the phosphorus oxygen bonds must exist as a double bond. McMillan [227] has stated that the existence of the double bonds in the phosphorus tetrahedra leads to conditions which promote separation of the phosphate groups from the silica network. Furthermore, he stated that it would be probable for the P_2O_5 to be associated with alkali or alkali earth oxides present in the composition in order to preserve charge balance on the phosphate tetrahedra.

The six different compositions of both 58S-nP and 68S-nP series are indicated down in the diagram and it should be noted that the 58S-8P and 68S-8P compositions fall into
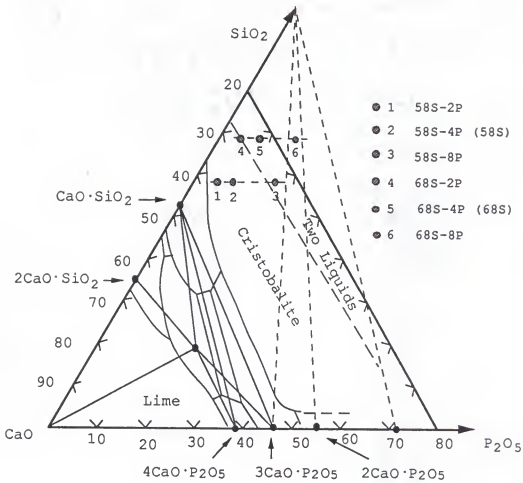
Figure 6.11 Phase diagam of CaO-P_2O_5-SiO_2 [226].

the phase separated region. The liquid-liquid separation may occur in both 58S-8P and 68S-8P compositions either in the sol mixing stage or in the later heating stage. If this is so, the P_2O_5-rich droplets with a concentrated CaO content will be formed and surrounded by the SiO_2-rich matrix. The presence of a liquid-liquid phase separation would explain why it took time for P and Ca ions to leach from the 58S-8P and 68S-8P powders to the solution and then deposit back on the surface of the samples finally converting into hydroxyapatite crystalline phase.

Both 58S-2P and 68S-2P gel powders contain a low P_2O_5 content of only 2 mol.% which is probably not sufficient to form a considerable amount of hydroxyapatite on the surface.

It therefore can be concluded that P_2O_5 content affects the bioactivity of the gel-derived powders. Based on these studies, a P_2O_5 content of 4 mol.% is more favorable for the formation of surface hydroxyapatite.

6.2 Texture Effect

6.2.1 Introduction

One of the advantages of sol-gel processing over conventional melt processing is the ability to control the texture of materials, including the surface area, the total

pore volume and the average pore radius. Textural changes are achieved by varying processing conditions, such as pH, the *R* ratio of the moles of alkoxides to the moles of water and the solvent in the mixing stage and the heat treatment temperatures, time and even the furnace atmosphere in the subsequent stages. This work chose heat treatment temperature as the parameter to control the gel texture, especially the surface area. In order to reveal the relationship between bioactivity and the texture of the gel-derived powders, the following experimental procedures were designed.

6.2.2 Experimental

58S, containing 60 mole % SiO_2, 4 mole % P_2O_5 and 36 mole % CaO, was chosen as the composition in the study, since it shows no crystallization tendency during the heat treatment and high bioactivity in the in-vitro test.

Samples were prepared from tetraethyoxysilane (TEOS), triethyl phosphate [$OP(OEt)_3$] and calcium nitrate. Nitric acid was added to accelerate the hydrolysis reaction of TEOS. After mixing the components, the sol was cast into polyethylene containers and placed inside an oven for gelation and aging. After aging, the gels were transferred into drying chambers and dried at 180°C. The dried gels were heated in silica crucibles at 600°C for 3 hours and then

ground into powders with a particle size range of 100 to 700 microns which yields the 58S (in this Chapter also called 58S-600) gel-derived powders.

To change the texture, the 58S gel-derived powders were further heat treated in a furnace at different temperatures, i.e. 700°C, 800°C, 825°C, 850°C and 900°C, for twenty-five minutes. A series of samples named 58S-700, 58S-800, 58S-825, 58S-850 and 58S-900 respectively were obtained. A Quanta Chrome Autosorb-6 was employed to measure the textural change, especially the surface area change of all the samples using N_2 as an absorbent.

X-ray diffraction (XRD) was used to study the powders after heating at all temperatures.

As stated earlier, the essential condition for a material to bond with living bone is the formation of a hydroxyapatite layer on its surface in a real (in vivo) or simulated (in vitro) body environment. Using the same modified dynamic quality assurance procedure mentioned in Chapter III, heat treated powders were dipped directly into tris-buffered solutions at 37°C in a Nalgene® bottle and stirred in an incubator shaker. The reacted powders were later examined by Fourier Transform Infrared Reflection (FTIR) Spectroscopy and X-ray diffraction for phase changes indicative of their potential bioactivities.

6.2.3 Results and Discussions

Table 6.3 lists the BET data of 58S-600, 58S-700, 58S-800, 58S-825, 58S-850 and 58S-900 gel-derived powders. The surface area varies from 90 m^2/g to 300 m^2/g, depending on the heating temperatures. 58S-600 has a surface area of 289 m^2/g. During the subsequent sintering, its structure evolves as the polycondensation reaction continues. A reduction in surface area, which is actually the driving force for sintering, is found when the sintering temperature increases (Figure 6.12). A similar trend has also been observed for the gel-derived pure SiO_2 and binary Na_2O-SiO_2 systems [140,188]. In addition, both the total pore volume and the average pore radii decrease with temperature as a result of the sintering process (Figure 6.13 and Figure 6.14).

Figure 6.15 is the X-ray diffraction spectra of 58S-600, 58S-700, 58S-800, 58S-825, 58S-850 and 58S-900 gel-derived powders which show no X-ray diffraction peaks. Only a broad peak characteristic of an amorphous solid is observed for 58S-600, 58S-700, 58S-800, 58S-825 samples. The spectrum of 58S-850 shows a very small amount of crystallinity. 58S-900 gel-derived powders heat treated at 900°C for 25 minutes, show strong X-ray diffraction peaks which index as a mixture of wollastonite and nagelschmidtite

Table 6.3
BET data of 58S gel-derived powders
after heating to different temperatures

Sample ID	Treatment Temperature (°C)	Surface Area (m^2/g)	Total Pore Volume (cm^3/g)	Average Pore Radius (Å)
58S-600	600	289	0.49	34
58S-700	700	269	0.46	33
58S-800	800	223	0.34	30
58S-825	825	154	0.20	27
58S-850	850	128	0.18	26
58S-900	900	92	0.15	–
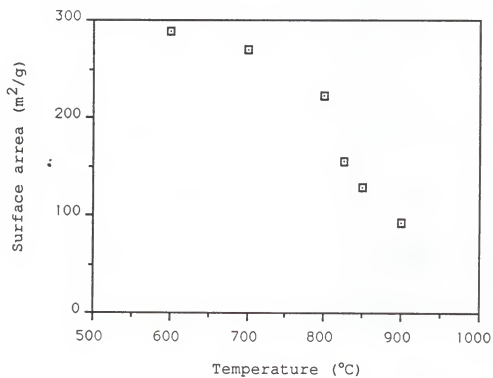
Figure 6.12 Vatiation of surface area with temperature for 58S gel-derived powders.
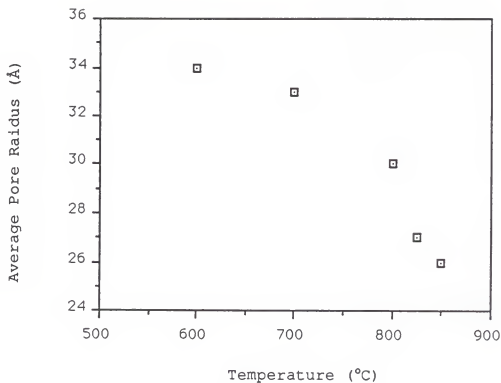
Figure 6.13   Variation of pore size with temperature
for 58S gel-derived powders.
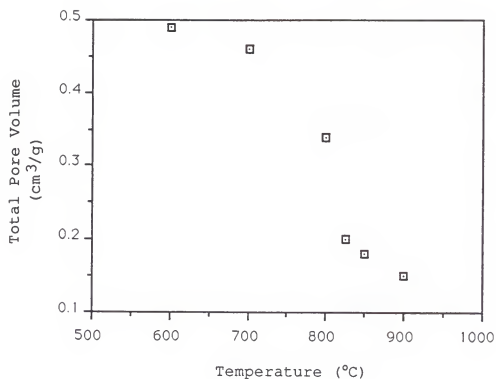
Figure 6.14 Variation of total pore volume with temperature for 58S gel-derived powders.
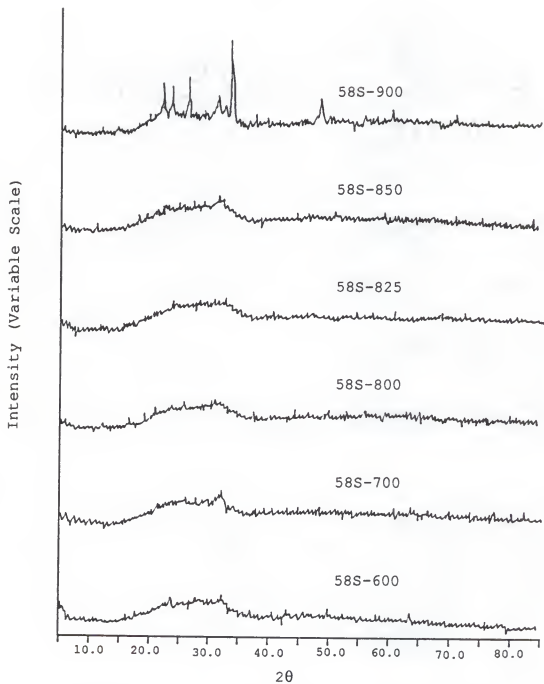
Figure 6.15 X-ray diffraction spectra of 58S
            gel-derived powders after heating
            at various temperatures.

crystals (JCPDS card #: 27-1064 and 5-646), see Figure 6.16. This is consistent with the DTA spectrum of 58S (Figure 4.1), which shows an exothermic reaction at 900°C and further confirms that the amorphous gel powder of 58S begins to crystallize at about 900°C producing a material composed of a CaO-SiO_2-rich glass and a mixture of wollastonite and nagelschmidtite crystallites.

Figure 6.17 shows the FTIR diffuse reflectance spectra of 58S (58S-600) gel-derived powder, which has the largest surface area among the series, after in-vitro reaction with tris-buffered solutions for 1, 2, 4 and 8 hours respectively at 37 °C. The peak assignments are detailed in the previous Chapters. The figure shows that the peaks at 598 cm^{-1} and 566 cm^{-1}, indicative of the formation of a hydroxyapatite crystalline phase, appear after a reaction time of only one hour. These two peaks keep increasing in intensity with the increasing exposure time. At the same time, the Si-O-Si rocking vibration peak at 482 cm^{-1} decreases and finally diminishes after eight hours reaction in the solution. Because of the very small penetration depth of the IR beam (<1μm), the hydroxyapatite crystalline phase must be formed on the surface of the gel-derived powders.

Figure 6.18 shows the FTIR spectra of the 58S gel-derived powders with different surface areas (i.e. produced by heating at different temperatures) obtained after
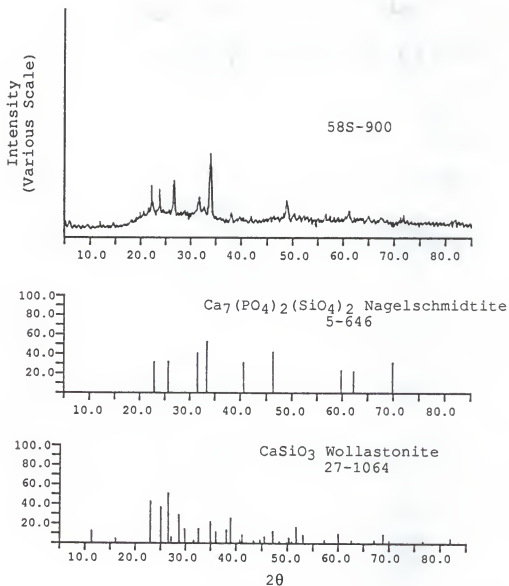
Figure 6.16   X-ray diffraction spectra of 58S-900
gel-derived powders.
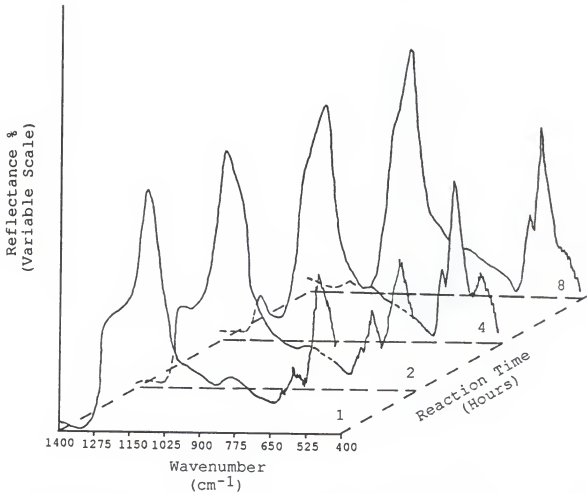
Figure 6.17   FTIR spectra of 58S gel-derived
              powders with various reaction times.
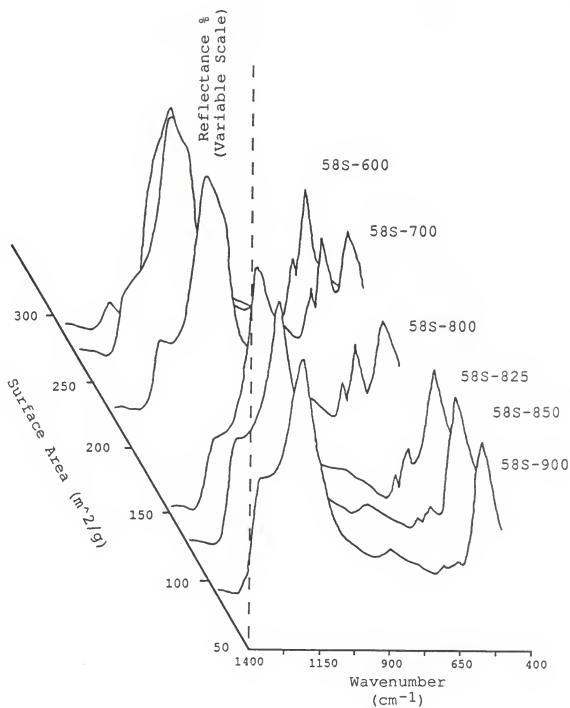
Figure 6.18 FTIR spectra of 58S gel-derived
powders with various surface areas
after 8-hour reaction.

the samples were exposed to the tris-buffered solutions for 8 hours. Figure 6.19 plots the ratio of hydroxyapatite peak intensity of the P-O bending vibration at 566 cm^{-1} divided by silica peak intensity of the Si-O-Si bending vibration at 482 cm^{-1} as a function of the surface area of 58S gel-derived powder after 8 hours reaction in the tris-buffered solutions.

In Figure 6.18, the intensities of the characteristic peaks of crystallized hydroxyapatite at the 598 cm^{-1} and 566 cm^{-1} decrease with the decreasing surface area of the gels. The spectrum of 58S-900 gel-derived powders shows that there is only a small amount of hydroxyapatite formed on its surface after the exposure. This indicates that after the 58S gel-derived powders are heat treated at 900°C for 25 minutes, they have almost lost their bioactivity.

The surface silanol concentration is closely related to the surface area of the gel-derived powders. The gel-derived powder is essentially an agglomerate of particles and pores. The surface of the gel powders is terminated by hydroxyl groups, silanols [87]. Although thermally induced desorption may occur (at temperatures > 500 °C) [220] and a condensation reaction may remove a considerable fraction of the silanols [220], a certain amount of silanols still remain on the surface after the 600°C heat treatment. Furthermore, when exposed to the tris-buffered solution, a cation exchange of Ca^{+2} from the gel-derived powders for protons in the solution
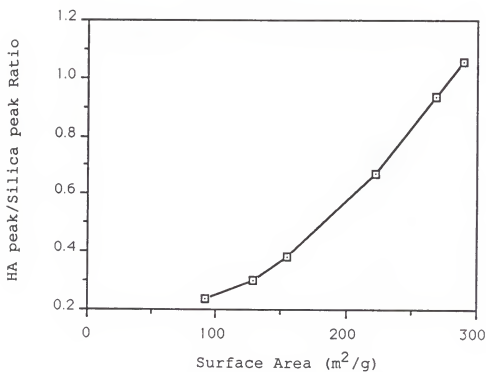
Figure 6.19   Ratio of hydroxyapatite peak intensity
to silica peak intensity as a function
of surface area for 58S gel-derived
powders after 8-hour reaction.

produces additional silanols. It is proposed that after the calcium and phosphorus ions reprecipitate back to the surface, the silanols may act as nucleation sites and also the exothermal condensation reaction of the surface silanols may promote nucleation and crystallization of the hydroxyapatite at the surface. However, it is very difficult to separate the possible mechanisms for heterogeneous nucleation of hydroxyapatite on the gel powders.

The textural features of the gel-derived powders give rise to a large surface area of potential nucleation sites that result in a rapid formation of the hydroxyapatite at the surface. The evidence for this is the rapid decrease in hydroxyapatite formation as the sintering temperature increases which results in a large decrease in surface area and surface silanol concentration. It was described earlier that the melt-derived bioactive glasses which exhibit bonding with bone in-vivo within 10 to 30 days develop a surface area ranging from 200 to 500 m^2/g in a tris-buffered in-vitro test solution. In contrast, compositions of glass that do not bond to bone, i.e. are not bioactive, develop less than 0.1 m^2/g surface area when exposed to equivalent simulated test solutions. In our studies, the surface area of the gel-derived powders ranged from 128 m^2/g and up prior to in-vitro exposure. Therefore, the effective surface area available for development of HA is initially very much larger

than the melt-derived Bioglasses®. This is one of the possible reasons why the gel-derived powders show much higher hydroxyapatite formation rate than the conventional melt-derived Bioglasses®.

Thus, these results suggest that it is possible to influence the rate of hydroxyapatite formation and therefore the level of bioactivity of a material by using sol-gel processing to control texture as well as composition of the material. This is the first time this important finding has been observed. However, additional work is required to identify the ultrastructural features responsible for the accelerated formation of HA.

The conclusions for this section are as follows:

1. The surface area of 58S decreases with increasing sintering temperatures over the range of 600°C to 900°C which makes it possible to change the texture of bioactive gel-derived powders.

2. The rate of hydroxyapatite formation decreases with the decrease of surface area for 58S bioactive gel-derived powders.

3. The surface silanol concentration may play an important role in the formation of hydroxyapatite crystalline phase as well as the surface area.

4. Texture as well as composition can be used to control the bioactivity of a material.

6.3 Relative Importance of Surface Area vs Composition on Bioactivity

The earlier discussion in this Chapter indicates that the rate of formation of hydroxyapatite on the surface depends on both composition and texture. However, Figure 6.20 indicates that the SiO_2 content in the composition plays the more important role in developing hydroxyapatite crystalline phase than the texture.

Figure 6.20 shows the A_1/A_2 ratio (the ratio of hydroxyapatite peak intensity to silica peak intensity as defined before) as a function of surface area of 58S, 68S and 77S gel-derived powders after 8-hour reaction in tris-buffered solutions. There seems to be a nearly linear relationship between the A_1/A_2 ratio and the surface area. It is noticed that the straight line correlation for 58S gel-derived powders, which contain the least SiO_2 content, has the steepest slope. The A_1/A_2 ratio of 58S gel-derived powders increases with increase of surface area more quickly than that of 68S. The ratio for 77S gel-derived powders remains zero and unchanged with the surface area. This means that when the SiO_2 content becomes high enough, the effect of the texture can no longer be observed.

The figure also shows that 58S, 68S and 77S gel-derived powders have different A_1/A_2 ratios even when they have the same surface area. By holding the surface area constant, 58S
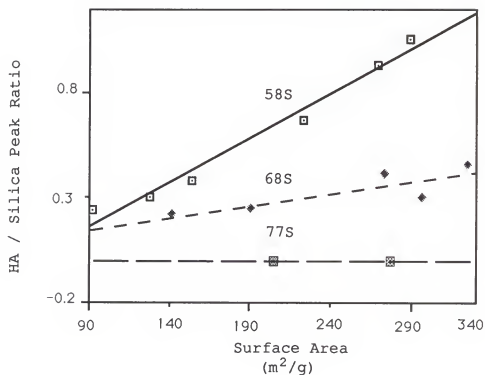
Figure 6.20 Variation of ratio of hydroxyapatite peak
intensity to silica peak intensity as a
function of surface area for 58S, 68S and
77S gel-derived powders after 8-hour
reaction.

gel-derived powders, which contain the least SiO_2, give the highest rate of formation of the hydroxyapatite crystalline phase. The A_1/A_2 ratio of 58S gel powders with a surface area 140 m^2/g is almost as same as that of 68S gel-derived powders with 290 m^2/g surface area. However, the difference in the SiO_2 content between those two compositions is only 10 mol.%. It is, therefore, concluded that the SiO_2 content plays the most important role in developing hydroxyapatite for the bioactive gel-derived powders. The formation of a surface hydroxyapatite crystalline phase is favored for the bioactive gel-derived powders with a lower SiO_2 content.

CHAPTER VII
SUMMARY

7.1 Surface Chemistry

Surface chemistry is important in the field of bioactive materials, especially in gel-derived bioactive materials. The preceding Chapters show that the bioactive powders derived by sol-gel processing are characterized by a high surface area over a broad range of heating temperatures. It is this high surface area and its chemistry that dominate the unique properties of the powders [87].

It has been recognized [228-229] that the silicate surface can be hydrolyzed by water to create silanols, Si-OH, and the surface of active gel is covered by hydroxyl groups (OH). Zhuravlev [230] determined that values of the hydroxyl coverage of different samples of silicate particles and gels fall between 4 and 7 OH/nm^2. Since surface hydroxyl groups serve as adsorption sites for molecular water or other polar molecules, the surface coverage of OH groups determines the adsorption behavior and consequently the surface activity of the material.

The types of hydroxyl species that may exist on the silicate gel surface are shown schematically in Figure 7.1
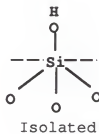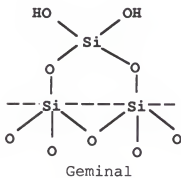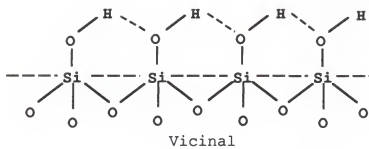
Figure 7.1 Schematic illustration of silanol
            types on the surface of gels [58].

[58]. The three types of hydroxyl species are postulated to be isolated, vicinal and geminal [58].

An isolated hydroxyl is an OH group located on a Q^{3*} silicon site that is not hydrogen-bonded. Vicinal hydroxyls are OH groups located on neighboring Q^3 sites in which hydrogen bonding may occur. Geminal hydroxyls are defined as two hydroxyl groups located on a Q^2 silicon site.

These various configurations of surface hydroxyl groups or silanol groups has been identified by high-resolution IR spectroscopy [231]. However, Iler [87] suggested that the types of silanols on various forms of silicates and gels do not behave the same. Thus, understanding the SiO_2–CaO–P_2O_5 gel-glass system is important from a basis chemistry stand point as it is for the practical application in biomaterials technology.

The gel surface can be visualized as the truncation of a random network composed of siloxane rings containing on average six silicons per ring. The open rings created by the surface are terminated with hydroxyl groups on the basis of the ring size and number of hydroxyl groups. In addition to the ring size and the degree of ring opening, the extent of hydrogen bonding of surface OH groups is greatly influenced by the surface curvature which is depicted in Figure 7.2

---

* In Q^n terminology, n equals the number of bridging oxygens (-OSi) bonded to the central silicon (n = 0-4).
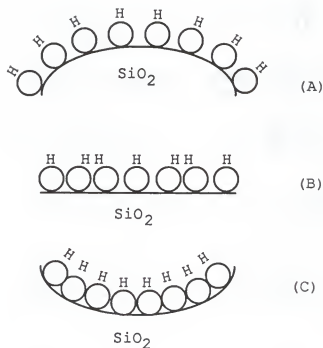
Figure 7.2 Effect of surface curvature on hydrogan
bonding [58].
(A) Small positive radius of curvature
(small paticles) has fewer hydrogen
bonds facilitating dehydroxylation.
(B) Large radius of cuvature (large
particles flat surface) allow more
hydrogen bonds, inhibiting dehydroxylation.
(C) Small negative radius of curvature
(small cylindrical pores or necks) has
the most hydrogen bonding and is the
most difficult to dehydroxylate.

[58]. A small positive radius of curvature increases the O-H--O distance of neighboring hydroxyl sites, decreasing the extent of hydrogen bonding on a particle compared to a flat surface with the same coverage of OH groups, facilitating dehydroxylation and consequently reducing the activity of the surface. In contrast, a small negative radius of curvature reduces O-H--O separation between neighboring hydroxyl groups, increasing the extent of hydrogen bonding over that of a flat surface, inhibiting dehydroxylation and finally promoting the activity of the surface. From this point of view, gel-derived powders which are characterized as microporous with a very small negative curvature containing a large amount of hydrogen bonded silanol groups on the surface should be remarkably active.

It is recognized that water is present in the gel in two forms: free water within the ultraporous gel structure, i.e., physically absorbed water, and hydroxyl groups associated with the gel structure, i.e., chemically absorbed water. The sequence of surface dehydration is the initial removal of physically adsorbed water at low temperatures followed by the progressive removal of weakly hydrogen bonded hydroxyls, strongly bonded hydroxyls and finally isolated hydroxyls [220,232]. During thermal dehydration, condensation reactions occur on the gel surface. It is postulated that the removal of isolated silanols occurs in part by diffusion of

protons along strained siloxane bridges followed by a condensation reaction after an adjacent pair of hydroxyls is formed.

Dehydration is a nonequilibrium process, the rate at which hydroxyl groups are lost at any stage is a function of temperature and the concentration of remaining silanol groups. During dehydration, hydroxyl groups are gradually lost with increasing temperature (Figure 7.3) [58]. However, the surface curvature also affects the extent of dehydration as mentioned before. For pure silica gel with extremely small negative curvature, even when the temperature reached 800°C where the extent of viscous sintering may be substantial, the hydroxyl groups are still high, about 1 OH/nm^2 [233-234]. Thus the silanol concentrations are often not completely eliminated by the thermal dehydroxylation.

In our study, the $SiO_2-CaO-P_2O_5$ bioactive powders were produced by sol-gel processing. Although a proper way to measure quantitatively the silanol concentrations on the surface for these bioactive gel-derived powders has not yet been found, it is proposed that their large surface areas ranging from 200 m^2/g to 650 m^2/g must be covered by a large number of hydroxyl groups and therefore a substantial amount of silanol groups must still exist even after the dried gel-derived powders were heated to 600°C and higher temperatures.
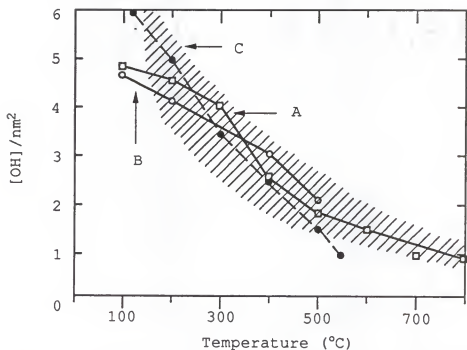
A: Dehydration of annealed (700°C) and rehydratied
   silica during heating in air
B: Dehydration of annealed (700°C) and rehydratied
   silica during heating in vacuum
C: Data on unannealed silica
Shaded area: Range of data on a variety of silica

Figure 7.3 Hydroxyl concentration on the silica
            surface versus temperature [58].

Furthermore, all the gel-derived powders have the same type of adsorption-desorption isotherm hysteresis loops as that shown in Figure 7.4 which was obtained from the nitrogen absorption BET measurement of 58S gel-derived powders. deBoer [235] has identified five types of adsorption-desorption isotherm hysteresis loops shown in Figure 7.5 and correlated them with various pore shapes as follows: Type A loops are attributed to cylindrical pores; Type B hysteresis is associated with slit-shaped pores; Type C is produced by wedge-shaped pores with open ends; Type D loops result from wedge-shaped pores with narrow necks at one or both open ends. The Type E hysteresis is attributed to "ink-bottle" pores. Figure 7.4 is typically a Type A hysteresis loop which confirms that the pores of the 58S gel-derived powders with average radius as small as 34 Å are cylindrical with negative curvatures. The hydroxyl groups on the surface have the most hydrogen bonding and are the most difficult to dehydrate [87]. All of these account for the extremely active surface of the gel-derived bioactive powders.

It can therefore be summarized that the bioactive powders derived by sol-gel processing have a high surface area and a large amount of silanol groups. Due to the small negative curvature, these hydroxyl groups are highly hydrogen bonded, active and difficult to eliminate even at high temperature. The polycondensation reaction of these silanol
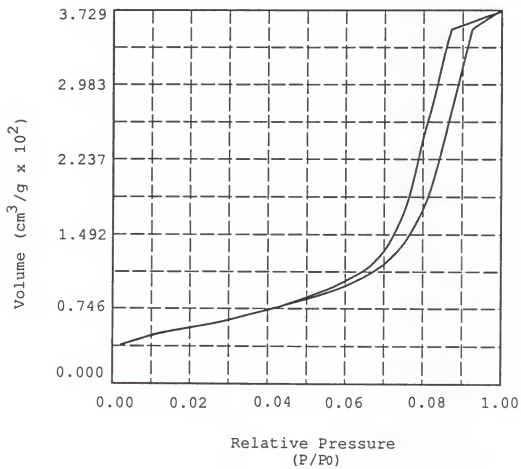
Figure 7.4 Adsorption-desorption isotherms
for 58S gel-derived powders.
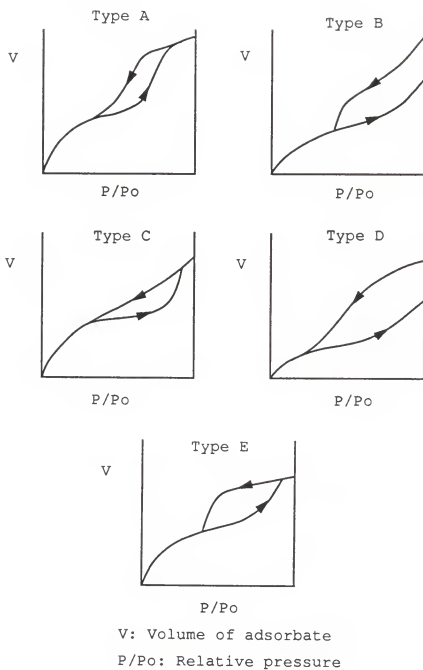
Figure 7.5   de Boer's five types of hysteresis
loops [235].

groups to form Si-O-Si takes place very rapidly. It is an exothermic reaction and occurs due to the presence of a metastable pentacoordinated silica molecule on the surface as an intermediate step in the reaction [236]. It is possible that this metastable state and the loss of water from the condensation reaction are associated with the nucleation and crystallization of hydroxyapatite on the gel surface. It is this layer that forms the bonding with biological moieties and eventually gives rise to tissue bonding and bioactivity.

7.2 Comparison of Melt-Derived Glass powders vs Gel-Derived Glass Powders

Figure 7.6(a) and Figure 7.6(b) show the comparison of FTIR spectra of 45S5 Bioglass® powders and 58S gel-derived powders with various reaction times in tris-buffered solutions at the early stages. The reaction times in tris-buffered solutions for 45S5 Bioglass® powders were 2, 10, 20, 40 and 120 minutes. The curves coded as 2M, 10M, 20M, 40M and 120M respectively in Figure 7.6(a) of 45S5 Bioglass® powders and for 58S gel-derived powders were 2, 10, 20 and 40 minutes (2M, 10M, 20M and 40M) in Figure 7.6(b) of 58S bioactive gel-derived powders. The interpretation of the peaks were given in previous Chapters.

For 45S5 Bioglass® powders, only a very slight single peak at 566 cm^{-1}, characterized as a P-O bonding vibration in
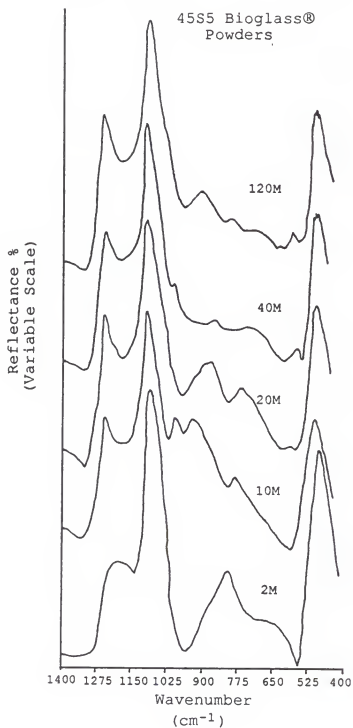
Figure 7.6(a) FTIR spectra for 45S5 Bioglass® powders with various reaction time at early stages.
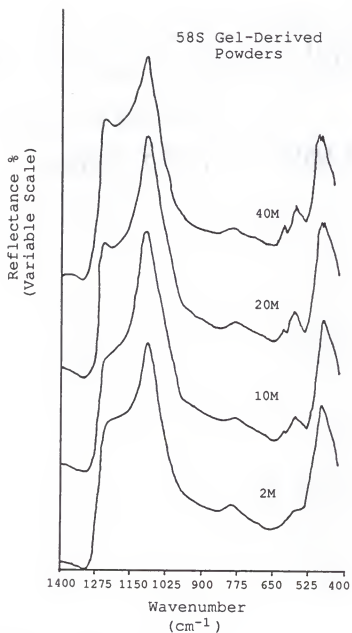
Figure 7.6(b)   FTIR spectra for 58S gel-derived
                powders with various reaction
                time at early stages.

a [PO$_4$] tetrahedra or calcium phosphate complex, can be seen after the samples were immersed in the solution for 20 minutes, curve 20M in Figure 7.6(a). Its intensity slowly increases with the reaction time, curve 40M in Figure 7.6(a). When the samples were reacted for 120 minutes, the single peak splits into two separated peaks at 598 cm^{-1} and 566 cm^{-1}, which are characteristic of hydroxyapatite crystals reported by Fowler [207], indicating that the amorphous calcium phosphate complex on the surface starts converting into the hydroxyapatite crystalline phase by that time. This result is consistent with the ICP data of decreasing phosphorus ion concentrations in the solution for 45S5 Bioglass® powders discussed in Chapter V.

It is surprising that for the gel-derived 58S powders, however, no single peak at 566 cm^{-1} is observed and a pair of characteristic peaks of hydroxyapatite crystals at 566 cm^{-1} and 598 cm^{-1} appears after the samples were reacted in the tris-buffered solution for only 10 minutes in Figure 7.6(b). The characteristic peaks increase their intensities with increasing reaction time which is also equivalent to the fast phosphorus ion takeup from the solutions for 58S gel-derived powders described in Chapter V. The finding suggests that there is a difference not only in the rate but also in the mechanism of the formation of hydroxyapatite surface layer between the melt-derived and the gel-derived powders. The

gel-derived powders have a much higher rate of formation of the hydroxyapatite surface layer than the melt-derived Bioglass® powders. This appears to be because the nucleation and crystallization of hydroxyapatite occur simultaneously on the surface of the gel-derived powders.

7.3 Discussion

The formation of surface hydroxyapatite on the gel-derived powders is a time dependent kinetic phenomenon. As discussed in the Chapter II literature review there are four stages of interfacial reactions that describe the chemical changes occurring on the biomaterial side. Recently, Hench et al. investigated the kinetics of bioactive glass and glass-ceramics [237]. They divided the chemical changes occurring with bioactive glasses or glass-ceramics bonding to bone into six stages:

Stage (1): Ion exchange of Na^{+1} or K^{+1} with H^{+1} or H_3O^{+1} from solution.

Stage (2): Loss of soluble silica of $Si(OH)_4$ to the solution resulting from breakage of Si-O-Si bonds and formation of silanols at the glass solution interface.

Stage (3): Condensation and repolymerization of a SiO_2-rich layer on the surface depleted in alkalis and alkaline earth ions.

Stage (4): Migration of Ca^{+2} and PO_4^{-3} groups to the surface through the SiO_2-rich layer forming a CaO-P_2O_5-rich film on top of the SiO_2-rich layer, followed by growth of the amorphous CaO-P_2O_5-rich film by incorporation of soluble calcium and phosphates from the solution.

Stage (5): Crystallization of the amorphous CaO-P_2O_5 film by incorporation of OH^{-1}, CO_3^{-2} from solution to form a mixed hydroxyl, carbonate apatite layer composed of small crystallites.

Stage (6): Agglomeration and chemical bonding of biological moieties within the growing HA layer leading to incorporation of collagen fibrils produced by osteoblasts or fibroblasts.

These studies lead to a finding that the critical reaction rate in bioactive glass and glass-ceramics is stage (3) which controls the polycondensation of silanol groups that form Si-O-Si bonds on the surface.

The kinetics of bioactive gel-derived powders seems to be different. According to the results in previous Chapters, it is proposed that there may be only five stages of interfacial reactions which can be used to describe the chemical changes occurring on the bioactive gel-derived powders. The five stages are

Stage (1): Very rapid ion exchange of Ca^{+2} with H^{+1} or H_3O^{+1} from solution,

$$Si-O-Ca + H^{+1} + OH^{-1} \rightarrow Si-OH + Ca^{+2} + OH^{-1} \qquad (7.1)$$
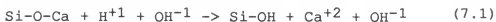
Stage (2): Cation exchange which increases the hydroxyl concentration of the solution and causes very rapid loss of soluble silica in form of $Si(OH)_4$ to the solution and additional silanol (Si-OH) formation at the surface of the materials accompanied by migration of P ions to the solution which also occurs rapidly,

$$2(Si-O-Si) + 2 (OH^{-1}) \rightarrow Si-OH + HO-Si \qquad (7.2)$$

Stage (3): Extremely rapid polycondensation of silanol groups either initially on the surface or created by stage (2) forming a SiO_2-rich surface layer depleted in alkaline earth Ca ions,

$$2(Si-OH) \rightarrow -Si-O-Si- + H_2O \qquad (7.3)$$

Stage (4): Heterogeneous nucleation and crystallization of hydroxyapatite crystals which occurs simultaneously on the surface of the gel powders,

Stage (5): Agglomeration and chemical bonding of biological moieties within the growing of hydroxyapatite

layer leading to incorporation of collagen fibrils produced by osteoblasts.

In general, the rates of all stages are so fast that the hydroxyapatite crystals on the surface of the gel-derived powders (e.g. 58S) were detected by FTIR reflection spectroscopy during the very early stage such as 10 minutes of reaction in the tris-buffered solutions.

The high surface area and the microporous nature of the gel-derived powders facilitate stage (1), the ion exchange, resulting in a very rapid release of calcium ions to the solution as well as a rapid increase in pH.

The loss of silica in form of $Si(OH)_4$ to the solution in stage (2) is completed very fast as can be seen from the large increase of Si ion concentration followed by a stabilized state during the very early stage of reaction shown in Figure 5.14.

Stage (3) is more complicated than the previous stages. A characteristic of the bioactive gel-derived powders as well as bioactive glasses or glass-ceramics is the formation of a silica-rich layer on the surface prior to the migration of Ca^{+2} ions and PO_4^{-3} groups to the surface or corresponding with the development of a hydroxyapatite surface layer both in-vitro and in-vivo. The role of this silica-rich layer in the nucleation and crystallization of the hydroxyapatite film has been a subject of great concern for a long time.

Damen and Ten Cate [238] investigated the effects of silicic acid on calcium phosphate precipitation in vitro. By measuring the decrease in Ca ion concentration in the solutions, it was determined that both silicic acid and silica cause spontaneous precipitation and enhance the growth rate of hydroxyapatite. He concluded that both silicic acid or silica acted as a substrate for hydroxyapatite nucleation. This finding gave support for the idea that polysilicic acid or silica may promote the formation of hydroxyapatite.

It has been established for many years that a critical concentration of biologically fixed silicon is essential for the mineralization of bone [239]. Carlisle has reported observations on the silicon content of bone during mineralization [240]. Utilizing the technique of electron microprobe analysis she showed that in young mice and young chickens there is a relative abundance of silicon in newly mineralizing bone and as mineralizing becomes more complete that the content of silicon and the molar ratio of silicon to calcium decreases. The region of high silicon concentration was observed to move ahead of the mineralization front. These results suggest that silicon may be an important ion in the initiation of bone mineralization.

In light of Carlisle's findings, it seems reasonable to speculate that the bond formed between bone and the bioactive glass or glass-ceramics may be initiated through the silicon

containing gel on the surface on the bioactive glass or glass-ceramics. This gel, containing calcium and phosphorus ions as well as silicon ions, may be so similar in concentration to that of normal bone in osteogenesis that osteoblasts recognize it as a surface on which to lay down collagen and mucopolysaccharides. When the polysaccharides interact with the gel and the collagen fibrils are bonded to the surface, the stability of the gel should be increased and further corrosion should be prevented. The net effect is the incorporation of collagen fibers into the gel which is itself part of the implant surface.

As mentioned earlier, the gel surface is covered by a large amount of silanol groups. Hydrogen bonding occurs quite readily between polar organic groups and the polar silanol surface. Iler has shown that the adsorption of nonionic organic compounds on the surface of silica is dependent on the presence of polar groups such as oxygen and nitrogen in the molecule [87]. According to Iler, it is through the hydrogen bonding that protein molecules are strongly absorbed onto the surface of silica gel. Collagen and glycoproteins, two major organic components of healing bone, are either protein or contain protein. They would hydrogen bond with the silanol surface of the gel. All these findings point out that a SiO_2-rich silica gel surface may be the key to the precipitation or crystallization of hydroxyapatite. It is the

silica gel that stimulates or promotes the formation of hydroxyapatite, through providing heterogeneous nucleation sites.

The bioactive gel-derived powder itself is actually a high SiO_2 content gel with high surface area formed through controlled hydrolysis and condensation reaction of the alkoxides. In gel-derived powders, there are a large amount of active silanol groups initially on the surface either isolated or hydrogen bonded even before an in-vitro reaction or implantation. In other words, it is not necessary to create silanol groups on gel powders through the first and second stage reactions. The supersaturation of silicic acid can be reached very fast as soon as the powders are immersed in the tris-buffered solution (Figure 5.14). In addition, since the tris-buffered solution has a relatively higher pH of 7.2-7.4, further condensation reactions will be greatly accelerated on the surface of the powders resulting in a SiO_2-rich layer with depletion of calcium ions. In this particular case, stage (3) may occur at the same time with stage (1) and (2) and its rate should be very fast.

Since no single characteristic peak at 566 cm^{-1}, assigned to P-O modes in amorphous calcium phosphate in the FTIR spectra, were observed on any bioactive gel-derived powders studied (Section 7.2), during stage (4), simultaneous

nucleation and crystallization of hydroxyapatite crystals on the surface is proposed.

Since in-vivo tests have just started, there is no data available yet to explain stage (5) and whether it is accelerated as expected.

In summary, the very rapid formation of surface hydroxyapatite crystals on these gel-derived bioactive powders is believed to depend on their silica-rich gel nature such as the extremely high surface area terminated with a large amount of silanol groups with a high degree of hydrogen bonding which may give rise to an increased density of potential nucleation sites for hydroxyapatite crystals. It is proposed that the relatively higher pH of the tris-buffered solution accelerates the condensation reaction of the silanol groups on the surface. It is this exothermic polycondensation reaction that may promote the heterogeneous nucleation and crystallization of hydroxyapatite to occur simultaneously, at least for the 58S gel-derived bioactive powders.

8.4 Conclusion

The three component $CaO-P_2O_5-SiO_2$ system gel powders produced by sol-gel processing are very bioactive. FTIR spectra, X-ray diffraction analysis and other techniques confirmed a very rapid formation of a hydroxyapatite layer on

the surface of the powders after exposure to the tris-buffered solutions.

As discussed in Chapter VI, the sol-gel processing of the $CaO-P_2O_5-SiO_2$ gel-derived powders also increases the compositional range of bioactivity by a significant amount. The new compositional field of bioactivity is schematically illustrated in Figure. 7.7. Gel-derived powders containing as high as 90 mol.% SiO_2 with 4 mol.% P_2O_5 and 6 mol.% CaO still show formation of a hydroxyapatite layer within 7 days reaction at 37°C. In contrast, the previous composition limit of bioactivity of all the bioactive glasses and glass-ceramics so far produced was established at 60 %, as shown in Figure 1.1. The important potential advantage of low temperature solution processing to yield new compositions, Table 3.1, has thus been realized.

The mechanism proposed for the enhanced bioactivity and the larger compositional region of bioactivity of gel-derived powders is the increased density of nucleation sites for crystallization of hydroxyapatite on the surface of the gels. The surface of the gels are covered by silanols with active hydrogen bonds. The exothermic polycondensation of silanol groups may promote the formation of hydroxyapatite crystals. The very fast appearance of crystalline hydroxyapatite peaks suggests that nucleation and crystallization of hydroxyapatite crystals occur simultaneously.
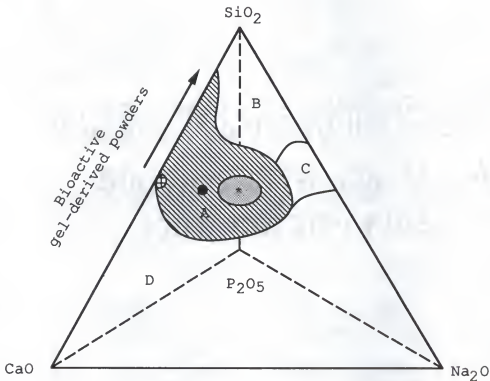
Figure 7.7 New bioactivity composition boundary.

CHAPTER VIII
CONCLUSION AND SUGGESTIONS FOR FUTURE WORK

The recent development of sol-gel processing offers a new approach for the preparation of bioactive gel-glass powders with potential advantages over those of bioactive glass and glass-ceramics made by conventional processing. The objectives of this study fell into two categories. The first objective was to develop a reliable method for preparing the bioactive gel-glass powders in the $CaO-P_2O_5-SiO_2$ system via a sol-gel route. The second one was to study several series of gel-derived powder samples with the intent of developing an understanding of the characteristic features that control the rate of hydroxyapatite formation in-vitro and thereby their bioactivity.

In order to fulfill these objectives, a series of bioactive gel-glass powders were prepared using tetraethylorthosilicate (TEOS), triethyl phosphate and calcium nitrate as precursors and nitric acid as catalyst. The sol-gel processing successfully utilized in the study was as follows: 1) mixing precursors to generate sol, 2) casting, 3) gelation, 4) aging, 5) drying, 6) densification at a relatively low temperatures and 7) milling and screening to

obtain powders with required sizes. The details were described in Chapter III.

The characteristic features of the gel-derived powders were measured using FTIR reflection spectroscopy, X-ray diffraction analysis, thermal analysis and nitrogen absorption BET. The results show that most gel-derived powders exhibit completely amorphous X-ray spectra except 49S and 54S which have relatively lower SiO_2 contents. A very small amount of crystallinity was observed on 49S and 54S gel-derived powders. The interpretation of FTIR spectra for gel-derived powders of various compositions was given in Chapter IV. Basically, the FTIR spectra of these gel-derived powders appear similar to those of melt-derived bioactive glasses. The only difference between the two is a slight shift of the 1095 cm^{-1} stretching vibration peak towards higher frequencies for the gel-derived powders which could in part be due to a certain degree of strain in the Si-O-Si bridging bonds at the surface of the pores. Nitrogen absorption BET data of the gel-derived powders indicate that these powders have very large surface areas, ranging from 200 m^2/g to 650 m^2/g. DTA analysis of 58S gel-derived powders suggests that the gel-derived powders have a tendency to crystallize at high temperatures: a 58S sample starts to crystallize at about 900°C.

Chapter V gave evidence of the bioactivity of the gel-derived glass powders. It has been concluded that the essential condition for glass and glass-ceramics to bond to bone is the formation of the surface hydroxyapatite layer in the body environment. The bioactivity of glasses or glass-ceramics could thus be defined as the ability of a material to form a surface hydroxyapatite in a controlled simulated body fluid. The appearance of characteristic peaks of hydroxyapatite crystals at 566 cm^{-1} and 596 cm^{-1} for most gel-derived powders after only one-hour exposure to tris-buffered solutions indicate the strong bioactivity of the powders. The Si-O-Si rocking vibration peak at 482 cm^{-1} is diminished for the 58S and 54S gel-derived powders and replaced by the peaks at 566 cm^{-1} and 596 cm^{-1} which are well defined as characteristic of hydroxyapatite crystals after only eight hours reaction. It is surprising to find that the peaks at 566 and 596 cm^{-1} never appear separately in the FTIR spectra for gel-derived powders, whenever they appear, even in the very early stages (Figures 5.1, 5.2, 5.3 and also Figure 7.4), they appear as a pair. This shows the strong evidence that the nucleation and crystallization of hydroxyapatite crystals occur simultaneously on the surface of the gel-derived powders. The comparison of the FTIR spectra of gel-derived 58S powders and melt-derived 45S5 Bioglass® indicates that 58S develops hydroxyapatite more

rapidly than 45S5 Bioglass®, suggesting 58S gel-derived powders are more bioactive than 45S5 Bioglass®.

This suggestion was further confirmed by the X-ray diffraction analysis. The X-ray diffraction spectrum of 58S gel-derived powders shows a stronger X-ray diffraction peak at 32° 2θ after only 8 hours reaction than that of 45S5 Bioglass® after exposure to the same tris-buffered solution for 100 hours.

The development of hydroxyapatite on the surface of the materials in-vitro is a time dependent, dynamic phenomenon. The variation of pH and Si, Ca, P and Na ions concentrations of the testing solutions were measured for both gel-derived powders and 45S5 Bioglass® powders as a function of reaction time. The very rapid increase in pH and ion concentrations of the solution for gel-derived powders is consistent with their high bioactivity. It is interesting to observe that silicon ion concentrations increased to about 45 ppm immediately after the sample was put in the testing solution and kept constant for up to 8 hours, suggesting the system reached a supersaturation of silicic acid very rapidly. This is an important clue concerning the fast formation of hydroxyapatite in-vitro and the bonding with bone in-vivo.

The shorter phosphorus takeup time from the solution of the gel-derived 58S powders matches the above discussion of FTIR reflection spectra and the X-ray diffraction spectra.

The comparison of ICP data for the powder and the bulk samples of 45S5 Bioglass® showed the important role of surface area in behavior of the materials. The powder 45S5 Bioglass® samples with a ratio of surface area to volume (SA/V) of 1 to 10 cm^{-1} have more rapid leaching rate of ions than the bulk samples with a ratio of only 0.1 cm^{-1}.

The results of Chapter VI show that the rate of formation of hydroxyapatite on the surface is greatly affected by both the composition and the texture of the gel-derived powders. Varying the SiO_2 content and P_2O_5 content changes the rate of hydroxyapatite formation.

In general, the bioactivity increases with decreasing SiO_2 content, a lower SiO_2 content of the gel-derived powders favors the formation of a hydroxyapatite surface layer. However, gel-derived powders containing as high as 90 mol.% SiO_2 with 4 mol.% P_2O_5 and 6 mol.% CaO still show the formation of a hydroxyapatite surface layer within 7 days at 37°C. In contrast, the SiO_2 compositional boundary of bioactivity of all conventional melt-derived bioactive glasses and glass-ceramics is 60 mol.%. The sol-gel processing increases substantially the compositional range of bioactivity by a significant amount.

When P_2O_5 content increases, liquid-liquid phase separation induced by phosphorus may occur in the system. This may be the reason why it took a longer time for the

development of hydroxyapatite peaks for 68S-8P gel-derived powders with higher P_2O_5 content.

The texture, mainly the surface area, of gel-derived powders plays a secondarily important role for the formation of the hydroxyapatite layer. The surface area of the gel-derived powders can be controlled by changing the heat treatment temperatures. The increasing heat treatment temperature reduces the surface area as well as the surface hydroxyl concentrations resulting in the decrease of the rate of hydroxyapatite formation on the surface of 58S gel-derived powders.

Chapter VII summarizes the study and further discusses the bioactivity of the materials in terms of surface chemistry.

A comparison of FTIR spectra of gel-derived powders and melt-derived Bioglass® powders has been made. The possible mechanisms of the rapid formation of hydroxyapatite layer on the gel-derived powders have been proposed.

The gel-derived bioactive powders are characterized by their microporosity with an extremely large surface area. It is believed that the surface is terminated by a large amount of silanol groups with hydrogen bonding and therefore must be very active chemically. It is the intrinsic porous gel nature, the large surface area, the large coverage of hydroxyl groups on the surface and the extremely fast rate of

the formation of the silanol-rich surface during the reaction that may play the key roles for the development of hydroxyapatite layer in-vitro and the bonding with bone in-vivo. Since the single FTIR peak at 566 cm^{-1} was never observed, the characteristic peaks of hydroxyapatite crystals at 566 and 596 cm^{-1} always appear as a pair, it gives strong evidence that nucleation and crystallization of HA may occur simultaneously for the gel-derived bioactive glass powders.

Thus, sol-gel processing not only increases the rate of hydroxyapatite formation but also extends the compositional range of bioactivity, as described in Chapter VI. It is the first time for 20 years that the compositional boundary for bioactivity is increased from a limit of 60 mol.% SiO_2 up to 90 mol.% SiO_2.

The mechanism proposed for the enhanced bioactivity and the larger compositional region of bioactivity is the increased density of nucleation sites for crystallization of hydroxyapatite and the SiO_2-rich surface nature of the sol-gel derived powders.

In-vivo tests for the gel-derived powders have just started. So far, there is no data available yet.

The results of the in-vitro studies of the gel-derived bioactive glass powders offer an exciting approach for biomaterial science. The need for further basic research to pursue these discoveries is clear.

It is important to correlate the observed in-vitro responses with in-vivo results.

The mechanisms and kinetics for the interfacial reaction which are still uncertain need to be further investigated. Only by a thorough understanding of the mechanisms and kinetics of the surface reactions and their dependence on processing will it be possible to develop better bioactive glass powders with predictable properties and high performance.

The gel-derived bioactive powders, with superior and unique properties, such as the substantially lower processing temperature and the very rapid and controllable bioactivity which can meet different clinical needs, have a variety of potential applications. They can be directly placed in bone-deficient areas and can be also mixed with various types of resorbable polymer carrier systems to form pastes that can fill in the deficiency. The material in either powder or paste form can fill irregular bony wounds and spaces caused by local or systemic disease as a putty or by injection without being shaped clinically or preclinically like bulk materials. Coatings of the powders on substrates is probably another attractive direction. The low temperature processing may make it possible to coat biopolymers such as silicones.

The consensus is that the future for sol-gel derived bioactive materials is bright.

It is hoped that our work will aid in the further development of this promising new type of bioactive materials.

REFERENCES

[1]   D.F. Williams, J. Materials Science, 22 (1987) 3421.

[2]   L.L. Hench and E.C. Ethridge, in Biomaterials, An
        Interfacial Approach, Academic Press, New York
        (1982).

[3]   L.L. Hench, Science, 208 (1980) 826.

[4]   L.L. Hench and J. Wilson, Mater. Res. Symp.
        Proceedings, 55 (1986) 112.

[5]   J.S. Hirschhorn, A.A. McBeath and M.R. Dustoor,
        Biomed. Mater. Symp. No.2, Bioceramics-Engineering in
        Medicine, Wiley, New York (1972) 49.

[6]   R.P. Welsh, R.M. Pilliar and I. Macnab, J. Bone and
        Joint Surgery, 53A (1971) 963.

[7]   J. Galante, W. Rostoker, R. Lueck and R.D. Ray, J.
        Bone and Joint Surgery, 53A (1971) 101.

[8]   E. Lembert, J. Galante and W. Rostoker, Clinical
        Orthapaedics and Related Research, 87 (1972) 303.

[9]   W.W. Kriegel and H. Palmour, eds., Ceramics in Severe
        Environments, Plenum Press, New York (1971).

[10]   S.F. Hulbert, J.C. Bokros, L.L. Hench, J. Wilson and
        G. Heimke, in High Tech Ceramics, P. Vincenzini, ed.,
        Elsevier, Amsterdam (1987) 189.

[11]   L. Smith, Archives of Surgery, 87 (1963) 653.

[12]   R.T. Chiroff, E.W. White, J.N. Webber, and D. Roy,
        J. Biomed. Mater. Res. Symp., 6 (1975) 29.

[13]   R.E. Holmes, R.W. Mooney, R.W.Bucholz, and A.F.
        Tencer, Clin. Orthop. Relat. Res., 188 (1984) 282.

[14]   E.W. White, J.N. Webber, D.M. Roy, E.L. Owen, R.T.
        Chiroff, and R.A. White, J. Biomed. Mater. Res.
        Symp., 6 (1975) 23.

[15]   T. Yamamuro, L.L. Hench, and J. Wilson, eds., Handbook
         of Bioactive Ceramics, V.II, Calcium Phosphate and
         Hydroxylapatite Ceramics. CRC Press, Boca Raton, FL
         (1990).

[16]   S.F. Hulbert, J.R. Matthews, J.J. Klawitter, B.W.
         Sauer, R.B. Leonard, J. Biomed. Mater. Res. Symp., 5
         (1974) 85.

[17]   K.de Groot, A. Tencer, P. Waite, J. Nichols and J.
         Kay, in Bioceramics: Material Characteristics Versus
         In Vivo Behavior, P. Ducheyne and J. E. Lemons, eds.,
         The New york Academy of Sciences, New York, 523 (1988)
         272.

[18]   K.de Groot, in Bioceramics of Calcium-Phosphate, K.de
         Groot ed., CRC Press, Boca Raton, FL (1983) 99.

[19]   L.L. Hench, T.K. Greenlee and W.C. Allen, U.S. Army
         Report No.1, August, University of Florida,
         Gainesville (1970).

[20]   L.L. Hench, T.K. Greenlee and W.C. Allen, U.S. Army
         Report No.2, August, University of Florida,
         Gainesville (1971).

[21]   L.L. Hench, H.A. Paschall and W.C. Allen, U.S. Army
         Report No.3, August, University of Florida,
         Gainesville (1972).

[22]   L.L. Hench, H.A. Paschall and W.C. Allen, U.S. Army
         Report No.4, September, University of Florida,
         Gainesville (1973).

[23]   L.L. Hench, H.A. Paschall, W.C. Allen and G.
         Piotrowski, U.S. Army Report No.5, September,
         University of Florida, Gainesville (1974).

[24]   L.L. Hench, H.A. Paschall, W.C. Allen and G.
         Piotrowski, U.S. Army Report No.6, September,
         University of Florida, Gainesville (1975).

[25]   L.L. Hench, H.A. Paschall, W.C. Allen and G.
         Piotrowski, U.S. Army Report No.7, September,
         University of Florida, Gainesville (1976).

[26]   L.L. Hench, R.W. Petty and G. Piotrowski, U.S. Army
         Report No.8, September, University of Florida,
         Gainesville (1977).

[27]   L.L. Hench, R.W. Petty and G. Piotrowski, U.S. Army
        Report No.9, December, University of Florida,
        Gainesville (1979).

[28]   J. Wilson and D. Nolletti, in Handbook of Bioactive
        Ceramics, T. Yamamuro, L.L. Hench and J. Wilson,
        eds., CRC Press, Boca Raton, FL (1990) 283.

[29]   L.L. Hench and J. Wilson, J. Biomed. Mater. Res., 10
        (1981) 231.

[30]   L.L. Hench and J. Wilson, Science, 226 (1984) 630.

[31]   J. Wilson, G.H. Pigott, F.J. Schosen and L.L. Hench,
        J. Biomed. Mater. Res., 15 (1981) 805.

[32]   J. Wilson, G.E. Merwin, L.W. Rodgers, R.G. Martin and
        D. Spilman, in Biological and Biomechanical
        Performance of Biomaterials, P. Christel, A. Meunier
        and A.J.C. Lee, eds., Elsevier, Amsterdam, 93 (1963).

[33]   A.E. Clark, Ph.D. Dissertation, University of
        Florida, (1974).

[34]   L.L. Hench, in Bioceramics: Material Characteristics
        Versus In Vivo Behavior, P. Ducheyne and J.E. Lemons,
        eds., The New York Academy of Sciences, New York, 523
        (1988) 54.

[35]   M. Ogino, F. Ohuchi and L.L. Hench, J. Biomed. Mater.
        Res., 14 (1980) 55.

[36]   H. Broemer, H. Kaes and E. Pfeil, U.S. Patent No.
        3,981,736 (1976).

[37]   W. Bluethgen, H. Broemer, H. Klaus and K. Deutscher,
        U.S. Patent No. 4,131,597 (1978).

[38]   T. Nakamura, T. Yamamuro, S. Higashi, T. Kokubo and S.
        Itoo, J. Biomed. Mater. Res., 19 (1985) 685.

[39]   T. Kokubo, S. Ito, Z.T. Huang, T. Hayashi and S.
        Sakka, T. Kitsugi and T. Yamamuro, J. Biomed. Mater.
        Res., 24 (1990) 331.

[40]   T. Kokubo, H. Kushitani and S. Sakka, J. Biomed.
        Mater. Res., 24 (1990) 721.

[41]   U. Gross and V. Strunz, J. Biomed. Mater. Res., 19
        (1985) 251.

[42]   U. Gross, J. Brandes, V. Strunz, I. Bab and J. Sela,
       J. Biomed. Mater. Res., 15 (1981) 291.

[43]   T. Kokubo, T. Hayashi, S. Sakka, T. Kitsugi, T.
       Yamamuro, M. Takagi, T. Shibuya, in High Tech
       Ceramics, P. Vincenzini, ed., Elsevier, Amsterdam,
       175 (1987).

[44]   J.B. Grey, M.E. Steen, G.J. King and A.E. Clark,
       American J. Orthodontics, 83, No.4 (1983) 67.

[45]   G.E. Marwin, Annals of Otology, Rhinology and
       Laryngology, 95 (1986) 78.

[46]   J. Wilson, H.R. Stanley and L.L. Hench, in Clinical
       Dentistry, J.W. Clark, ed., Harper and Row,
       Philadelphia, 50 (1981) 1.

[47]   R.Z. LeGeros, Adv. Dental Res., 2 (1988) 164.

[48]   L.C. Chow, Adv. Dental Res., 2 (1988) 181.

[49]   J.N. Kent and M. Jarcho, in Reconstructive
       Preprosthetic Oral and Maxillofacial Surgery, R.J.
       Fonseca and W.H. Davis, eds., Saunders, Philadelphia,
       305 (1986).

[50]   J. Wilson, S. Low, A. Fetner and L.L. Hench, in
       Biomaterials Clinical Applications, A. Pizzoferrato,
       P.G. Marchetti, A. Ravaglioli and A.J.C. Lee, eds.,
       Elsevier, Amsterdam, 223 (1987).

[51]   M. Ramer, J. Wilson, D. Walker and A.E. Clark,
       in Transactions 16th Annual Meeting Society
       for Biomaterials, Charleston, SC, 195 (1990).

[52]   U. Gross and V. Strunz, J. Biomed. Mater. Res., 14
       (1980) 607.

[53]   D.C. Greenspan and L.L. Hench, J. Biomed. Mater. Res.,
       10 (1976) 503.

[54]   T. Kitsugi, T. Yamamuro, T. Nakamura, S. Kotani and T.
       Kokubo, Bioceramics V.1, H. Oonishi, H. Aoki and K.
       Sawai, eds., Ishiyaku Euro Amirica Inc., Tokyo, 169
       (1989).

[55]   R. Roy, J. Amer. Ceram. Soc., 52 (1969) 344.

[56]   J. Zarcycki, in Glass Science and Technology, D.R.
        Uhlmann and N.J. Kreidl, eds., V.2, Academic Press,
        New York 209 (1984) .

[57]   J.L. Woodhead, J. Phys, 47, (1986) C1-3.

[58]   C.J. Brinker and G.W. Scherer, Sol-Gel Science,
        Academic Press, New York (1989).

[59]   C.J. Brinker and G.W. Scherer, J. Non-Cryst. Solids,
        70 (1985) 301.

[60]   E.J.A. Pope and J.D. Mackenzie, J. Non-Cryst. Solids,
        87 (1986) 185.

[61]   U. Gross, R. Kinne, H. Schmitz and V. Strunz, in CRC
        Critical Reviews in Biocompatibility, V.4, D.F.
        Williams, ed., CRC Press, Boca Raton, FL, 155 (1988).

[62]   D.F. Williams ed., Definitions in Biomaterials,
        Elsevier, Amsterdam, 66 (1987).

[63]   L.L. Hench, R.J. Splinter, W.C. Allen and T.K.
        Greenlee, J. Biomed. Mater. Res. Symp., 2 (1971)
        117.

[64]   A.E. Clark, C.G. Pantano, and L.L. Hench, J. Am.
        Ceram. Soc., 59 (1976) 37.

[65]   A.E. Clark, L.L. Hench H.A. Paschall, J. Biomed.
        Mater. Res., 10 (1976) 161.

[66]   C.Y. Kim, A.E. Clark, L.L. Hench, J. Non-Cryst.
        Solids, 113 (1989) 195.

[67]   R. Li, A.E. Clark and L.L. Hench, in Chemical
        Processing of Advanced Material, L.L. Hench and J.K.
        West eds., Wiley, New York, in press.

[68]   L.L. Hench and H.A. Paschall, J. Biomed. Mater. Res.
        Symp., 4 (1973) 25.

[69]   L.L. Hench and A.E. Clark, in Biocompatibility of
        Orthopedic Implants, D.F. Williams, ed., V.2 CRC
        Press, Boca Raton, FL, 129 (1982) .

[70]   G.J. Miller, D.C. Greenspan, G. Piotrowski and L.L.
        Hench, U.S. Army Medical Research and Development
        Command, Report No.7, October, University of Florida,
        Gainesville (1976).

[71]   G. Piotrowski, L.L. Hench, W.C. Allen, and G.J.
       Miller, J. Biomed. Mater. Res. Symp., 6 (1975) 47.

[72]   G. Piotrowski, M.G. Ferrari and R.W. Petty, U.S. Army
       Medical Research and Development Command, Report
       No.8, October, University of Florida, Gainesville
       (1977).

[73]   J.K. West, A.E. Clark, M.B. Hall and G.E. Turner,
       in Handbook of Bioactive Ceramics, V.I, T. Yamamuro,
       J. Wilson and L.L. Hench, eds., CRC Press, Boca Raton,
       FL, 161 (1990).

[74]   H. Broemer, E. Pfeil and K. Kaes, German Patent No.
       2,326,100, (1973).

[75]   B.A. Blencke, H. Broemer and K.K. Deutscher, J.
       Biomed. Mater. Res., 12, (1978) 307.

[76]   T. Kitsugi, T. Yamamuro, T. Nakamura, S. Higashi, Y.
       Rakutari, K. Hyakura, S. Ito, T. Kokubo, M. Takagi and
       T. Shibuya, J. Biomed. Mater. Res., 20 (1986) 1295.

[77]   T. Kokubo, in Handbook of Bioactive Ceramics, V.I T.
       Yamamuro, J. Wilson and L.L. Hench, eds., CRC Press,
       Boca Raton, FL, 41 (1990).

[78]   M.M. Walker, Masters Thesis, University of Florida
       (1977).

[79]   O.H. Andersson, K.H. Rarlsson and K. Kargasrieni,
       J. Non-Cryst. Solids, 119 (1990) 290.

[80]   S. Yoshii, Y. Kakutari, T. Yamamuro, T. Nakamura, T.
       Kitsugi, M. Oka, T. Kokubo and M. Takagi, J. Biomed.
       Mater. Res., 22 (1988) 327.

[81]   S. Yoshii, T. Yamamuro, T. Kitsugi, T. Nakamura, T.
       Kokubo, M. Oka, T. Shibuya and M. Takagi, in Handbook
       of Bioactive Ceramics, V.I, T. Yamamuro, J. Wilson
       and L.L. Hench, eds., CRC Press, Boca Raton, FL, 51
       (1990).

[82]   O.H. Andersson, Ph.D. Dissertation, Department of
       Chemical Engineering, Abo, Akademi, Finland (1990)

[83]   O.H. Andersson and K. Kangosniemi, J. Mater. Sci.,
       Materials in Medicine, in press.

[84]   W. Vogel and W. Holand, Angew, Chem. Int. Ed. Engl.,
       26 (1987) 527.

[85]   W. Vogel, W. Holand, K. Naumann and J. Gummel, J. Non-Cryst. Solids, 80 (1986) 34.

[86]   J. Zarzycki, J. Non-Cryst. Solids, 48 (1982) 105.

[87]   R.K. Iler, The Chemistry of Silica, Wiley, New York (1979).

[88]   T. Graham, J. Chem. Soc., 17 (1864) 318.

[89]   C.B. Hurd, Chem. Rev., 22 (1938) 403.

[90]   S.S. Kisler, J. Phys. Chem., 36 (1932) 52.

[91]   R.H. Ewell and H. Insley, J. Res. NBS, 15 (1935) 173.

[92]   R.M. Barrer and L. Hinds, Nature, 166 (1950) 562.

[93]   R. Roy, J Am. Ceram. Soc., 39, No.4 (1956) 145.

[94]   D.M. Roy and R. Roy, Am. Mineral, 39 (1954) 957.

[95]   G.J. MaCarthy R. Roy and J.M. McKay, J. Am. Ceram. Soc., 54 (1971) 637.

[96]   W. Stober, A. Fink and E. Bohn, J. Colloid Interface Sci. 26 (1968) 62.

[97]   R.M. Dell, in Reactivity of Solids, J.S. Anderson, M.W. Roberts, and F.S. Stone, eds., Chapman and Hall, New York, 553 (1972).

[98]   J.L. Woodhead, Silicates Ind., 37 (1972) 191.

[99]   J.J. Ebelmen, Ann. Chim. Phys., 57 (1846) 331.

[100] J.J Ebelmen, Ann. Chim. Phys., 16 (1846) 129.

[101] D.C. Bradley, R.C. Mehrotra, and D.P. Gaur, Metal Alkoxides, Academic Press, New York (1978).

[102] W.Z. Ostwald, Phys. Chem., 27 (1897) 365.

[103] L. Raykeigh, Philos. Mag., 38 (1919) 738.

[104] D.J. Lloyd, in Colloid Chemistry, J. Alexander, ed., Chemical Catalog Co., New York, 767 (1926).

[105]   H.N. Holmes, in Colloid Chemistry, J. Alexander, ed., Chemical Catalog Co., New York, 796 (1926).

[106]   W. Geffcken and E. Berger, German Patent No. 736 411, May (1939).

[107]   H. Schroeder, Phys. Thin Films, 5 (1969) 87.

[108]   H. Schroeder, Opt. Acta., 9 (1962) 249.

[109]   H. Dislich, Angewandt Chemie, Int. Ed. Engl., 10, No.6 (1971) 363.

[110]   L. Levene and I.M. Thomas, U.S. Patent No. 3,640,093, February (1972).

[111]   E. Wainer, German Patent No. 1,249,832, April (1968).

[112]   H.G. Snowman, U.S. Patent No. 3,795,524, March (1974).

[113]   S. Horikuri, K. Tsuji, Y. Abe, A. Fukui and E. Ichiki, Japanese Patent No. 49-108325, October (1974).

[114]   K.Kamiya, S. Sakka and T. Tatemichi, J. Mater. Sci., 15 (1980) 1765.

[115]   E.M. Rabinovich, D.W. Johnson, J.B. Mac Chesney, and E.M. Vogel, J. Non-Cryst. Solids, 47 (1982) 435.

[116]   E.M. Rabinovich, D.W. Johnson, J.B. Mac Chesney, and E.M. Vogel, J. Am. Ceram. Soc., 66 (198) 683.

[117]   D.W. Johnson, E.M. Rabinovich, J.B. Mac Chesney and E.M. Vogel, J. Am. Ceram. Soc., 66 (1983) 688.

[118]   L.R. McCreight, H,E. Rauch and W.H. Stutton, Ceramic Fibers and Fibrous Composite Materials, Academic Press, New York (1965).

[119]   L.E. Seufer, U.S. Patent No. 3,808,015, April (1974).

[120]   K. Miyahara and N. Nakayama, U.S. Patent No. 4,159,205 (1979).

[121]   M. Leitheiser and H.G. Snowman, U.S. Patent No. 145,383 (1980).

[122]   H. Dislich and P. Hinz, J. Non-Cryst. Solids, 48 (1982) 11.

[123]   N.J. Arfsten, R. Kaufmann and H. Dislich, in
        Ultrastructure Processing of Ceramics, Glasses and
        Composites, L.L. Hench and D.R. Ulrich, eds., Wiley,
        New York, 189 (1984).

[124]   H. Dislich, J. Non-Cryst. Solids, 73 (1985) 599.

[125]   J.D. Mackenzie, J. Non-Cryst. Solids, 42 (1982) 1.

[126]   J.D. Mackenzie, in Ultrastructure Processing of
        Ceramics, Glasses and Composites, L.L. Hench and
        D.R. Ulrich, eds., Wiley, New York, 15 (1984).

[127]   J. Wenzel, in Glass...Current Issue, A.F. Write and
        A.F. Dupuy, eds., Martinus Nijhojj, Dordrecht,
        Netherlands, 224 (1985).

[128]   L.L. Hench, ed., Ultrastructure Advanced Structural
        and Electronic Materials, Noyles, Park Ridge, NJ
        (1984).

[129]   L.L. Hench and D.R. Ulrich, eds., Ultrastructure
        Processing of Ceramics, Glasses and Composites,
        Wiley, New York (1984).

[130]   L.L. Hench and D.R. Ulrich, eds., Science of Ceramic
        Chemical Processing, Wiley, New York (1986).

[131]   D.R. Ulrich, J. Non-Cryst. Solids, 100 (1988) 174.

[132]   J.D. Mackenzie, J. Non-Cryst. Solids, 73 (1985) 631.

[133]   G.W. Scherer, J.Non-Cryst. Solids, 73 (1985) 661.

[134]   J. Wenzel, J.Non-Cryst. Solids, 73 (1985) 693.

[135]   L.L. Hench and J.K. West, Chem. Rev. 90 (1990) 33.

[136]   N.P. Bansal and R.H. Doremus, Handbook of Glass
        Properties, Academic Press, New York, 9 (1986).

[137]   L.L. Hench, S.H. Wang and J.L. Nogues, Multifuctional
        Materials, R.L. Gunshor, ed., SPIE, V.878, Bellingham,
        WA, 76 (1988).

[138]   S.H. Wang, C. Campbell and L.L.Hench in Ultrastructure
        Processing of Advanced Ceramics, J.D. Mackenzie and
        D.R. Ulrich, eds., Wiley, New York, 145 (1988).

[139]   G.F. Wang, Master's Thesis, University of Florida
        (1988).

[140]   W.L. Vasconcelos, Ph.D. Dissertation, University of
        Florida (1989).

[141]   S.Liu and L.L. Hench, in Chemical Processing of
        Advanced Material, L.L. Hench and J.K. West eds.,
        Wiley, New York, in press.

[142]   E. Elias, Master's Thesis, University of Florida
        (1989).

[143]   J.L. Nogues, C. Balaban, W.V. Moreshead and R.S.
        Sheu, in Advanced Ceramics, W.P.E. Longo, S.N.
        Monteiro and J.D. Filho eds., Florida-Brazil
        Institute, Rio de Janeiro, 51 (1989).

[144]   T. Tanaka, Sci. Amer., 244 (1981) 124.

[145]   G. Orcel and L.L. Hench, in Science of Ceramic
        Chemical Processing, L.L. Hench and D.R. Ulrich
        eds., Wiley, New York, 224 (1986).

[146]   L.L. Hench, G. Orcel and J.L. Nogues, in Better
        Ceramics Through Chemistry II, C.J. Brinker, D.E.
        Clark and D.R. Ulrich, eds., Materials Research
        Society, Pittsburgh, PA, 35 (1986).

[147]   R.K. Iler, in Science of Ceramic Chemical Processing,
        L.L. Hench and D.R. Ulrich,eds., Wiley, New York,
        (1986) 3.

[148]   S.A. Khan, E.M. Rabinovich, R.K. Prudhomme, M.J.
        Sammon and N.J. Kopylor, in Better Ceramics Through
        Chemistry III, C.J. Brinker, D,E. Clark and D.R.
        Ulrich, eds., Materials Research Society, Pittsburgh,
        PA, 73 (1988).

[149]   J. Zarzycki, M. Prassas and J. Phalippou, J. Mater.
        Sci., 17 (1982) 3371.

[150]   G.W. Scherer, J. Non-Cryst. Solids, 100 (1988) 77.

[151]   G.W. Scherer, in Better Ceramics Through Chemistry
        III, C.J. Brinker, D.E. Clark and D.R. Ulrich, eds.,
        Materials Research Society, Pittsburgh, PA, 179
        (1988).

[152]   T.K. Sherwood, Ind. Eng. Chem., 21 (1929) 12.

[153]   T.K. Sherwood, Ind. Eng. Chem., 22 (1930) 132.

[154]   T.K. Sherwood, Ind. Eng. Chem., 21 (1929) 976.

[155]   R.B. Keey, Drying Principles and Practice, Pergamon
        Press, New York (1972).

[156]   A.S. Mujumdar, ed., Advances in Drying, Hemisphere,
        New York, V.1 (1980).

[157]   A.S. Mujumdar, ed., Advances in Drying, Hemisphere,
        New York, V.2 (1983).

[158]   F. Moore, Trans. Brit. Ceram. Soc., 60 (1961) 517.

[159]   S. Whitaker, Adv. Heat Transfer, 13 (1977) 119.

[160]   A.R. Cooper, in Science of Ceramic Processing Before
        Firing, G. Onoda and L.L. Hanch, eds., Wiley, New
        York (1978) 261.

[161]   R.W. Ford, Ceramics Drying, Pergamon, New York (1988).

[162]   G.W. Scherer, J. Non-Cryst. Solids, 87 (1986) 199.

[163]   G.W. Scherer, J. Non-Cryst. Solids, 91 (1987) 83.

[164]   G.W. Scherer, J. Non-Cryst. Solids, 91 (1987) 101.

[165]   G.W. Scherer, J. Non-Cryst. Solids, 92 (1987) 122.

[166]   G.W. Scherer, J. Non-Cryst. Solids, 89 (1987) 217.

[167]   T. Kawaguchi, J. Jura, N. Taneda, H. Hishikura and
        Y.J. Kokubu, J. Non-Cryst. Solids, 82 (1986) 50.

[168]   R.K. Dwivedi, J. Mater. Sci. Lett., 5 (1986) 373.

[169]   J. Zarzycki, in Science of Ceramic Chemical
        Processing, L.L. Hench and D.R. Ulrich, eds., Wiley,
        New York, 21 (1986).

[170]   M.J.R. Wilson, Master's Thesis, University of Florida,
        (1989).

[171]   J. Zarzycki, in Glass...Current Issues, A.F. Wright
        and J. Dupuy, eds., Martinus Nijhoff Publishers,
        Boston, 203 (1985).

[172]   M. Yamane and S. Okano, J. Japan Ceram. Soc., 87
        (1979) 434.

[173] C.J. Brinker, K.D. Keefer, G.W. Scherer and C.S. Ashley, J. Non-Cryst. Solids, 48 (1982) 47.

[174] C.J. Brinker, G.W. Scherer and E.P. Roth, J. Non-Cryst. Solids, 72 (1985) 345.

[175] G.W. Scherer, C.J. Brinker and E.P. Roth, J. Non-Cryst. Solids, 72 (1985) 369.

[176] F. Orgaz-orgaz, J. Non-Cryst. Solids, 100 (1988) 115.

[177] M.L. Hair, Infrared Spectroscopy in Surface Chemistry, Dekker, New York (1967).

[178] T. Tseng and J. Yu, J. Mater. Sci., 21 (1986) 3615.

[179] I. Matsuyama, K. Susa, S. Satoh, and T. Suganuma, Ceramic Bull., 63 (1984) 1408.

[180] P.F. James, J. Non-Cryst. Solids, 100 (1988) 93.

[181] D.R. Uhlmann, M.C. Weinberg and G. Teowee, J. Non-Cryst. Solids, 100 (1988) 154.

[182] S.P. Mukherjee, J. Zarzycki, J.M. Badie and J.P. Traverse, J. Non-Cryst. Solids, 20 (1976) 455.

[183] W.G. Klemperer and S.D. Ramamuthi, in Better Ceramics Through Chemistry III, C.J. Brinker, D.E. Clark and D.R. Ulrich eds., Materials Research Society, Pittsburgh, PA, 1 (1988).

[184] S. Wallace, Ph.D. Dissertation, University of Florida, (1991).

[185] L.L. Hench, M. Prassas and J. Phalippou, J. Non-Cryst. Solids, 53 (1982) 183.

[186] M. Prassas, L.L. Hench, J. Phalippou and J. Zarzycki, J. Non-Cryst. Solids, 48 (1982) 79.

[187] M. Prassas, J. Phalippou and L.L. Hench, J. Non-Cryst. Solids, 63 (1984) 375.

[188] R. Li and L.L. Hench, in Better Ceramics Through Chemistry III, C.J. Brinker, D.E. Clark and D.R. Ulrich eds., Materials Research Society, Pittsburgh, PA, 589 (1988).

[189] J. Phalippou, M. Prassas and J. Zarzycki, J. Non-Cryst. Solids, 48 (1982) 17.

[190] C. Zhu, J. Phalippou and J. Zarzycki, J. Non-Cryst.
       Solids, 82 (1986) 321.

[191] G.F. Neilson and M.C. Weinberg, J. Non-Cryst. Solids,
       63 (1984) 365.

[192] M.A. Villegas and J.M. Fernandez Navarro, J.
       Non-Cryst. Solids, 100 (1988) 453.

[193] M. Yamane, J.B. Caldwell and D.T. Moore, J. Non-Cryst.
       Solids, 85 (1986) 244.

[194] W. Holand, E.R. Plumat and P.H. Duvigneaud, J.
       Non-Cryst. Solids, 48 (1982) 205.

[195] S.P. Mukherjee and R.K. Mohr, J. Non-Cryst. Solids,
       66 (1984) 523.

[196] B.E. Yoldas, J. Non-Cryst. Solids, 38/39 (1980) 81.

[197] G. Orcel, Ph.D. Dissertation, University of Florida,
       Florida (1987).

[198] G. Orcel, L.L. Hench, I. Artaki, J. Jones and T.W.
       Zerda, J. Non-Cryst. Solids, 105 (1988) 223.

[199] L.L. Hench and G. Orcel, J. Non-Cryst. Solids, 82
       (1986) 1.

[200] W.G. Klemperer and S.D. Ramamurthi, in Better Ceramics
       Through Chemistry III, C.J. Brinker, D.E. Clark and
       D.R. Urich eds., Materials Research Society,
       Pittsburgh, PA, 1 (1988).

[201] I. Ataki, M. Bradley, T.W. Zerda, J. Jones, G. Orcel
       and L.L. Hench, in Science of Ceramic Chemical
       Processing, L.L. Hench and D.R. Urich, eds., Wiley,
       New York, 73 (1986).

[202] H. Schmidt, A. Kaiser, M. Rudolph and A. Lentz, in
       Science of Ceramic Chemical Processing, L.L. Hench
       and D.R. Urich, eds., Wiley, New York, 87 (1986).

[203] H. Schmidt and H. Scholze, in Glass...Current
       Issues, A.F. Wright and A.F. Dupuy, eds., Martinus
       Nijhojj, Dordrecht, Netherlands, 253 (1985).

[204] M.W. Colby, A. Osaka and J.D. Mackenzie, J. Non-Cryst.
       Solids, 82 (1986) 37.

213

[205] L.D. Warren, A.E. Clark and L.L.Hench, J. Biomed.
       Mater. Res.: Applied Biomaterials, 23 (1989) 201.

[206] L.D. Warren, Master's Thesis, University of Florida
       (1987).

[207] B.O. Fowler, Inorg. Chem., 13, No.1 (1974) 194.

[208] C. Okkerse, in Physical and Chemical Aspects of
       Adsorbents and Catalysts, B.G. Linsen, ed., Academic
       Press, London, 213 (1970).

[209] W.B. Spencer, Masters Thesis, University of
       Pittsburgh (1950).

[210] S. Brunauer, R. Sh. Mikhail and E.E. Bodor, J.
       Colloid and Interface Sci., 24 (1967) 451.

[211] W. Cao, R. Gerhardt and J.B. Watchman, J. Am. Ceram.
       Soc., 71 (1988) 1108.

[212] S.P. Mukherjee, J.F. Cordaro and J.C. Debsikdar,
       Adv. Ceram. Mater., 3 (1988) 463.

[213] C. Duval, Inorganic Thermogravimetric Analysis,
       Elsevier, Amsterdam, 274 (1963).

[214] R.J. Bell and P. Dean, Discussions of the Faraday
       Society, 50 (1970) 55.

[215] P.H. Gaskell, Discussion of the Faraday Society, 50
       (1970) 82.

[216] A. Duran, C. Serna, V. Fornes and J.M. Fernandez
       Navarro, Non-Cryst. Solids 82 (1986) 69.

[217] W.L. Konijnendijk, Phillips Res. Rep. Suppl. 1
       (1975).

[218] F. Gervais, A. Blin, D. Massiot, J.P. Coutures, M.H.
       Chopinet and F. Naudin, J. Non-Cryst. Solids, 89
       (1987) 384.

[219] Y.C. Cheng, Ph.D. Dissertation, University of Florida
       (1991).

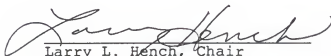[220] X.H. Wang, Ph.D. Dissertation, University of Florida
       (1988).

[221] R.M. Almeida, T.A. Guiton and C,G, Pantano, J.
       Non-Cryst. Solids, 121 (1990) 193.

[222] R.F. LeGeros, G. Bone and R. LeGeros, Calcif. Tissue
       Res., 26 (1978) 111.

[223] A.E. Clark, C.Y. Kim, J. West and L.L. Hench, in
       Handbook of Bioactive Ceramics, V.1, T. Yamamuro,
       L.L. Hench and J. Wilson, eds., CRC Press, Boca Raton,
       FL, 73 (1990).

[224] L.L. Hench, in Stability of Ceramics in the
       Physiological Environment, V.1, D.F. Williams ed.,
       CRC Press, Boca Raton, FL, 67 (1981).

[225] K. Ohura, T. Nakamura, T. Yamamuro, T. Kokubo, Y.
       Ebisawa, Y. Kotoura and M. Oka, J. Biomed. Mater.
       Res., 25 (1991) 357.

[226] E.M. Levin, C.R. Bobbins and H.F. McMurdie eds.,Phase
       Diagram for Ceramists, The American Ceramic Society,
       Columbus, Ohio, 231 (1964).

[227] P.W. McMillan, Glass Ceramics, Academic Press, New
       York (1964).

[228] P.C. Carman, Trans. Faraday Soc., 36 (1940) 964.

[229] A.V. Kiselev, Trans. Faraday Soc. Disc., 52 (1971)
       14.

[230] L.T. Zhuravlev, Langmuir, 3 (1987) 316.

[231] P. Hoffman and E. Knozinger, surf. Sci., 188 (1987)
       181.

[232] R.C. McDonald, J. Phys. Chem., 62 (1958) 1168.

[233] J.J. Fripiat, J. Uytterhoeven, J. Phys. Chem., 66
       (1962) 800.

[234] J.A.G. Taylor and J.A. Hockey, J. Phys. Chem., 70
       (1966) 2169.

[235] J.H. deBoer, The Structure and Properties of
       Porous Materials, Butterworths, London, 68 (1958).

[236] L.P. Davis and L.W. Burggraf, in Ultrastructure
       Processing of Advanced Ceramics, J.D. Mackenzie and
       D.R. Ulrich eds., Wiley, New York, 367 (1988).

[237]   L.L. Hench, O.H. Andersson and G. Latorre, The
        Kinetics of Bioactive Ceramics, in press.

[238]   J.J.M. Damen and J.M. Ten Cate, J. Dental Res., 68
        (1989) 1355.

[239]   E.M. Carlisle, in Silicon Biochemistry, Ciba
        Foundation Symposium, Wiley, New York, 123 (1986).

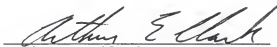[240]   E.M. Carlisle, Science, 167 (1970) 279.

BIOGRAPHICAL SKETCH

Rounan Li was born April 9, 1945, in Shanghai, China. She attended high school at The Third Girls School in Shanghai. She received a Bachelor of Science degree in materials science and engineering in 1968 and a Master of Science degree in materials science and engineering in 1982 in East China University of Chemical Technology. In 1986, she entered the University of Florida to pursue a Doctor of Philosophy in the Department of Materials Science and Engineering.

I certify that I have read this study and that in my opinion it conforms to acceptable standards of scholarly presentation and is fully adequate, in scope and quality, as a dissertation for the degree of Doctor of Philosophy.

Larry L. Hench, Chair
Graduate Research Professor
 of Materials Science and
 Engineering

I certify that I have read this study and that in my opinion it conforms to acceptable standards of scholarly presentation and is fully adequate, in scope and quality, as a dissertation for the degree of Doctor of Philosophy.
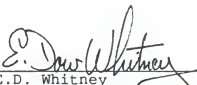
Arthur E. Clark
Associate Professor of
 Materials Science and
 Engineering

I certify that I have read this study and that in my opinion it conforms to acceptable standards of scholarly presentation and is fully adequate, in scope and quality, as a dissertation for the degree of Doctor of Philosophy.

R.T. DeHoff
Professor of Materials
 Science and Engineering

I certify that I have read this study and that in my opinion it conforms to acceptable standards of scholarly presentation and is fully adequate, in scope and quality, as a dissertation for the degree of Doctor of Philosophy.

E.D. Whitney
Professor of Materials
Science and Engineering

I certify that I have read this study and that in my opinion it conforms to acceptable standards of scholarly presentation and is fully adequate, in scope and quality, as a dissertation for the degree of Doctor of Philosophy.

P.H. Holloway
Professor of Materials
Science and Engineering

I certify that I have read this study and that in my opinion it conforms to acceptable standards of scholarly presentation and is fully adequate, in scope and quality, as a dissertation for the degree of Doctor of Philosophy.

C.J. Vierck
Professor of Neuroscience

This dissertation was submitted to the Graduate Faculty of the College of Engineering and to the Graduate School and was accepted as partial fulfillment of the requirements for the degree of Doctor of Philosophy.

August, 1991

Winfred M. Phillips
Dean, College of Engineering

Madelyn M. Lockhart
Dean, Graduate School